ENGINEERING 3D HUMAN NEURAL TISSUE MODELS WITH BIO-INSTRUCTIVE HYDROGELS

By

Kylie Megan Balotin

Dissertation

Submitted to the Faculty of the

Graduate School of Vanderbilt University

in partial fulfillment of the requirements

for the degree of

DOCTOR OF PHILOSOPHY

in

Biomedical Engineering

August 12, 2022

Nashville, Tennessee

Approved:

Ethan Lippmann, Ph.D.

Cynthia Reinhart-King, Ph.D.

Jonathan Brunger, Ph.D.

Angela Jefferson, Ph.D.

Matthew Schrag, Ph.D.

This thesis is dedicated to my family and friends, without whom I could not have completed this work.

ACKNOWLEDGMENTS

There are many people who need to be acknowledged for helping me accomplish the work described in this thesis. First, I would like to thank my thesis advisor, Dr. Ethan Lippmann, for providing guidance and encouragement throughout my PhD studies. I would also like to thank my committee members, Drs. Cynthia Reinhart-King, Angela Jefferson, Matthew Schrag, and Jonathan Brunger for providing feedback on my work and lending their expertise in the fields of biomedical engineering and neuroscience.

I would like to thank the many collaborators who helped me complete the work outlined in this dissertation. Thank you to the members of Dr. Leon Bellan's lab, Dr. Shannon Faley, John Rector, Victoria Vest, and Callie Webber, for allowing me to use the Bellan lab equipment and being patient with me when I asked them questions on how to troubleshoot problems with their confocal microscope. Additionally, thank you to Dr. Vivian and Dr. Alejandra Romero-Morales for their assistance as I helped develop organoid protocols for the Lippmann lab. I would like to thank Dr. Ken Lau and Alan Joey Simmons for their patience and guidance when we began collecting single-cell RNA seq data and the Vanderbilt Technologies for Advanced Genomics (VANTAGE) for their help in collecting the data. Dr. Kevin Ess, Grant Westlake, Dr. Brad Grueter, Jose Zepeda, Dr. Laura Dugan all provided invaluable expertise on electrophysiological assays for assessing the maturity and functionality of my stem cell-derived neurons and access to the necessary equipment to conduct these experiments. Furthermore, I would like to thank the many core facilities at Vanderbilt for teaching me how to use their equipment and all their technical expertise they have provided including the Vanderbilt Cell Imaging Shared Resource (CISR), Vanderbilt Small Molecule NMR Facility, Vanderbilt Institute of Nanoscale Science and Engineering (VINSE), and Vanderbilt's Center for Structural Biology Cryo-Electron Microscopy Facility. I would also like to thank Eli Hootener for creating the original LaTeX template for dissertations, and Haley Adams for reorganizing and updating the document. Outside of the Vanderbilt community, the Chan Zuckerberg Initiative's (CZI) Neurodegenerative Disease Challenge Network was a huge resource as my work developed more computational aspects. I would especially like to thank Drs. Julia Lowndes and Christopher Sifuentes for establishing the CZI Computational Office Hours, which gave me a platform to troubleshoot with other community members, teach about my lab's bioreactors, and learn good coding practices. I appreciate both of their support as I began to relearn how to code and for their help in helping debug code.

I would like to especially thank all the past and present members of the Lippmann lab for their support during my tenure at Vanderbilt. Emma Neal, Jonah Rosch, and Allison Bosworth helped provide so much guidance as I navigated my first few years in graduate school and learned how to do science, and I would have been lost those first few years without all of your support. Additionally, I would like to thank Yajuan Shi, Ketaki Katdare, Lauren Drake, Hyosung Kim, Brian O'Grady, Andrew Kjar, Everett Allchin, Alex Sorets, Lexi Yates, Madison Stiefbold, Daniel Balikov, Corinne Curry, Nick Marinelli, and Kensley Horner for being amazingly supportive labmates. Many thanks are owed to the amazing undergraduates who I have helped train and worked with to complete this work including Robert Weinstein, Colin Fricker, Neelansh Bute, and Kara Poole. It has been an honor to be able to work with and along side all of you, and I can't wait to see what all of you will accomplish over your careers! I hope we will continue to keep in touch over the years to come and continue our lab tradition of celebrating each others' successes. Furthermore, I would like to thank the funding sources that helped support my stipend and research during my time at Vanderbilt including the National Institute of Health, National Science Foundation, and the Chan Zuckerberg Initative. I am grateful to have been supported by the NIH T32 in Environmental Toxicology.

Finally, I'd like to thank my family and friends for their support over the past 5 years. Thank you to my extended family - I always look forward to when we are able to get together and go to escape rooms or play JackBox over the holidays. Times when we are all able to get together have been the highlights of my young adult life, and I cherished these breaks when we were able to coordinate our schedules. To Lauren Beard, Annie Song, and Vincent Nguyen, I am so glad we were all able to keep in touch after high school; you all have brought so much joy and fun to my life, and I am extremely appreciative of the support and encouragement you've given me since we meet in middle and high school. I'd be remiss to not acknowledge my pets in some way - to Foxy, Kobe, Abby, Kat, Sophie, and Kiki, I would like to express my sincerest appreciation for your unwavering love and support. My cats Sophie and Kiki provided so much comfort during my time in graduate school, and I appreciate them for always being by my side whether it was through

napping together in the sun over the weekend or laying on my computer when they think it's time for a work break. To my parents, Drs. Robert Balotin and Ada Wang, and my sister, Lauren Balotin, thank you for your unwavering support of my interests and for always being there to listen to me rant when my experiments failed. I could not have survived without you all providing prospective when I got into experiment ruts and for coming to Nashville whenever you sensed that I needed family close. I cannot wait to explore the Bay Area with my family and could not have succeeded without your support every step of the way.

TABLE OF CONTENTS

LIST OF TABLES

LIST OF FIGURES

LIST OF ABBREVIATIONS

2D Two-dimensional

3D Three-dimensional

α-synuclein alpha synuclein

Aβ Amyloid beta

AAV Adeno-associated virus

AD Alzheimer's disease

AFM Atomic Force Microscopy

aIPs Apical intermediate progenitors

ANOVA Analysis of variance

aRGCs Apical radial glia cells

BBB Blood brain barrier

bIPs Basal intermediate progenitors

BMEC Brain microvascular endothelial cell

BPs Basal progenitors

bRGCs Basal radial glia cells

Cad Cadherin

CNS Central nervous system

CP Cortical plate

DA Dopaminergic

DMF Dimethylformamide

EB Embryoid body

ECM Extracellular matrix

EGFP Enhanced green fluorescent protein

FTIR Fourier-Transform Infrared Spectroscopy

GelMA Methacrylated gelatin

GelMA-Cad Methacrylated gelatin containing N-cadherin peptides

GelMA-Scram Methacrylated gelatin containing scrambled N-cadherin peptides

HA Hyaluronic acid

HAMA Methacrylated hyaluronic acid

HAV Histidine-Alanine-Valine amino acid motif

hPSC Human pluripotent stem cell

iPSC Induced pluripotent stem cell

ISVZ Inner subventricular zone

IZ Intermediate zone

LAP Lithium phenyl-2,4,6-trimethylbenzoylphosphinate initiator

LDN LDN 193189 dihydrochloride

MA Methacrylic anhydride

MEA Microelectrode array

MSN Medium spiny neuron

N-cadherin Neural-cadherin

NBNs Newborn neurons

NMR Nuclear Magnetic Resonance Spectroscopy

NS Not significant

NSCs Neural stem cells

oRG Outer radial glia cells

OSVZ Outer subventricular zone

PD Parkinson's disease

PEG Polyethylene glycol

PEG Polyethylene glycol

PET Positron emission tomography

PFA Paraformaldehyde

PI Propidium iodide

RGD Arginylglycylaspartic acid

SB SB431542

SD Standard deviation

SEM Scanning Electron Microscopy

SVZ Subventricular zone

TEOA Triethanolamine buffer solution

TFF Tangential flow filtration

VZ Ventricular zone

CHAPTER 1

Introduction and Significance

1.1 Motivation

As the United States population ages, the incidence of neurodegenerative diseases has likewise increased (10). While there are treatments to alleviate the symptoms of some disorders, there are currently no treatments able to slow or reverse diseases following onset. The lack of effective treatments or cures may be in part due to the lack of predictive models of the human brain. While animal models are a useful tool for studying the human brain, species differences may impact our ability to translate research results to humans. For example, while certain Alzheimer's disease treatments show efficacy in animal models during pre-clincial trials, these same treatments did not show the same effects, and in some cases were even detrimental to the subjects, during clinical trials (11–14). As a result, there is a need in the field to develop more complex *in vitro* models of the brain to complement our current *in vivo* models in order to better understand and treat neurodegeneration in humans.

1.2 Neuropathology of Neurodegenerative Diseases

Neurodegenerative diseases are characterized by the death of specific populations of neurons over time, often caused by protein aggregation (1). Biomarkers have been difficult to identify for diagnostic purposes (15), and it can be difficult to officially diagnose many of these diseases until postmortem tissue samples are studied (16). It would be extremely useful to the field to develop new models to provide insight to the mechanisms of disease pathology, which might shed light into diagnostic or drugable targets. This section outlines examples of the 4 common neurodegenerative disease types (amyloidoses, tauopathies, synucleinopathies, TDP-43 proteinopathies (1)) that primarily target the brain and the hypothesized disease progression.

1.2.1 Alzheimer's Disease

Alzheimer's disease (AD) is one of the most common neurodegenerative diseases and is characterized by the presence of protein aggregates (extracellular amyloid beta, Aβ, plaques and intracellular phosphorylated tau tangles, p-tau), which are believed to contribute to the progression of this disease (17). There are currently 2 hypotheses of how this disease progresses based on the 2 types of protein aggregates.

The amyloid beta hypothesis involves the improper processing of amyloid precursor protein (APP) (18). The most common form of amyloid beta created during APP processing is amyloid beta 1-40 ($A\beta_{1\text{-}40}$). However, larger peptide sequences of amyloid beta such as amyloid beta 1-42 can also be created, and these

Classification	Example Diseases
Amyloidoses	Alzheimer's Disease, Creutzfeldt-Jakob Disease, Familial British Dementia
Tauopathies	Alzheimer's Disease, Chronic Traumatic Encephalopathy, Corticobasal Degeneration
Synucleinopathies	Parkinson's Disease, Multiple System Atrophy, Lewy Body Disorders
TDP-43 Proteinopathies	Frontotemporal Degeneration, Amyotrophic Lateral Sclerosis, Progressive Muscular Atrophy

Table 1.1: Examples of the 4 common types of neurodegernative diseases (adapted from (1))

peptides are more prone to aggregate and form a variety of structures (19). While it is hypothesized that amyloid beta aggregates play a part in synaptic dysfunction (19–23), it is still unknown what specific structures result in neuronal death and what mechanisms results in amyloid beta inducing synaptic alterations. Additionally, due to the extracellular presence of this protein, reactive glia stimulated by the amyloid beta may result in further synaptic disruptions (19; 21).

The second hypothesis, the tau hypothesis, involves the hyperphosphorylation of tau protein, leading to the accumulation of this protein into neurofibrillary tangles within the neuronal cell bodies, which in turn results in neuronal death (24). Tau protein is critical to the function of neurons as it helps stabilize the microtubule structures that give the neurons their unique elongated shapes (25). This function is disrupted during AD because hyperphosphorylated tau is unable to bind to tubulin and even inhibits the formation of microtubules (26). Like with the amyloid beta hypothesis, the mechanisms in which phosphorylated tau leads to synaptic dysfunction and neuronal death are unknown (24).

1.2.2 Parkinson's Disease

Parkinson's disease (PD) is the second most common neurodegenerative disease and is characterized by the loss of controlled motor skills due to the degeneration of dopaminergic neurons in the substantia nigra, resulting in disrupted communication between the substantia nigra and striatum (27; 28). Alpha-synuclein (α-synuclein) has long been hypothesized to be involved in the death of these dopaminergic neurons, as it is abundantly found in Lewy bodies (a hallmark of PD) (27). Due to the colocalization of α-synuclein with presynaptic terminals and synaptic vesicles, it is believed that this protein plays a role in synaptic transmission (29; 30). During PD progression, α-synuclein misfolding leads to the formation of neurotoxic oligomers and fibrils (27; 29). Currently the mechanisms in which α-synuclein leads to synaptic dysfunction is not well understood. At the presynaptic terminal, this protein can interfere with SNAREs and neurotransmitter

release; at the postsynaptic terminal, this protein may affect the components of the postsynaptic density (31). Additionally, it is not well understood why substrantia nigra dopaminergic neurons are specifically vulnerable to α-synuclein aggregates; it is hypothesized to be due to the long axonal projections or spontaneous electrical activity of this neuronal subtype (31).

1.2.3 Frontotemporal Degeneration

A less studied form of neurodegenerative is frontotemporal dementia, and one form of frontotemporal dementia involves the accumulation of TDP-43 protein (1; 32). This protein is believed to play a role in regulating splicing and trafficking of DNA and RNA and is primarily located in the nucleus (32). It is believed that in response to oxidative stress, TDP-43 aggregates can form, although the mechanisms in which TDP-43 plays a role in oxidative stress response is unknown (33). Furthermore, under stress, TDP-43 protein can relocate to the cytoplasm, where it is able to accumulate and become hyperphosphorylated (32; 33). The protein is also believed to become incorporated in stress granules, but the dynamics between TDP-43 and stress granules are still being studied (33). Studies have also shown that TDP-43 is important to mRNA transport in the neurite projections in neurons, which can then affect synaptic function through unknown mechanisms(34).

1.2.4 Corticobasal Degeneration

During disease progression of the tauopathy cortical basal degeneration, both neurons and glia are affected by tau aggregation (1; 35). Unlike in AD, where both 3R and 4R tau isoforms accumulate, corticobasal degeneration is primarily linked to 4R tau accumulation (35). Additionally, unlike in AD, the accumulation of tau in corticobasal degeneration is not liked with amyloid beta (1). Similar to the other diseases discussed in this section, the specific mechanisms in which tau becomes hyperphorsphoylated in this disease and contributes to synaptic dysfunction completely understood (35). Animal models suggest that tau accumulation can modulate glutamatergic receptor function, although these studies do not distinguish between AD and corticobasal degeneration (36; 37). A common theme in all of the diseases described in this section is that the mechanisms that lead to synaptic dysfunction in the affected neurons still need to be determined, which further emphasizes the need for improved models of neurodegeneration.

1.3 Approach

Human induced pluripotent stem cells (iPSCs) are a promising tool for developing models of the central nervous system. There are published protocols for generating many of the cell types found in the brain including astrocytes, pericytes, brain microvascular endothelial cells, microglia, glutamatergic neurons, in-

terneurons, and dopaminergic neurons (38–52), which can be studied in monocultures or cultures. However, 3D cultures of single-cell suspensions of iPSC-derived neurons typically are not synaptically connected, a feature that is critical to model as electric connectivity is important to neuronal functioning. For example, in Alzheimer's disease, amyloid beta and phosphorylated tau impact synaptic activity, so it is necessary to have functional connectivity in order to observe this behavior *in vitro* (20; 31; 53). While it is possible to differentiate iPSCs into self-organizing 3D brain organoids that are functionally connected, many of these organoids do not properly recapitulate the brain's structure (54). In order to fully study neuronal connectivity in the healthy and diseased brain, proper organization and synaptic functionality are essential(55; 56).

It is well-known that the extracellular matrix (ECM) plays an important role in the maturation of neurons (57). However, this concept has not been explored extensively for 3D cultures of neurons *in vitro*. Stem cell cultures commonly utilize Matrigel scaffolds (decellularized ECM from mouse sarcomas) (58–60; 8), but my lab has observed that it is difficult for 3D suspensions of neurons to mature in this matrix. Furthermore, supply chain shortages during the COVID-19 pandemic has impacted researchers' ability to acquire this material for cell culture use. Methacrylated hyaluronic acid (HAMA) is another common scaffold used for 3D neuronal models as hyaluronic acid makes up a large part of the brain ECM (61; 62). However, this scaffold's viscosity makes it difficult to manipulate and its' low stiffness makes it difficult to create more complex 3D structures. Furthermore, this scaffold lacks RGD-binding domains to promote cell adhesion and survival. In contrast, gelatin (denatured collagen) and methacrylated gelatin (GelMA) contain RGD motifs and have more favorable mechanical properties for developing complex 3D *in vitro* models. GelMA has previously been shown to be compatible with 3D culture of primary neurons (63), but there is little collagen in the brain, suggesting that gelatin and GelMA may lack bio-instructive cues necessary to drive neuronal development into an electrophysiologically mature state.

In order to determine bio-instructive cues that might improve currently existing scaffolds, researchers can look to the known extracellular and cell-cell interactions that are important to cellular maturation and function. Neural-cadherin (N-cadherin) is a calcium dependent cell adhesion molecule that is known to mediate aspects of brain development and maturation. As a Type I cadherin, the histidine-alanine-valine (HAV) motif at the first extracellular domain is believed to be important for cell-cell contacts (64). While the human cortex develops, N-cadherin is expressed by radial glia, which helps facilitate the radial migration of neural progenitors to the proper cortical layer (65–68). Furthermore, N-cadherin is believed to play a role in synapse formation and function (69–72). When N-cadherin is used for supporting 2D stem cell-derived neuronal cultures, the neurons formed an increased number of neurite projections when compared to neurons on gelatin and poly-L-lysine. Additionally, in 2D, this effect has shown to be modulated by the density of N-cadherin, where lower densities result in increased neurite growth (73; 74). These studies have shown

that neurons in low concentrations of N-cadherin also have higher amounts of MAP2 (dendritic marker) and neurofilament (axonal marker) than neurons on higher levels of N-cadherin, indicating increased maturity of neurons in low levels of N-cadherin (73).

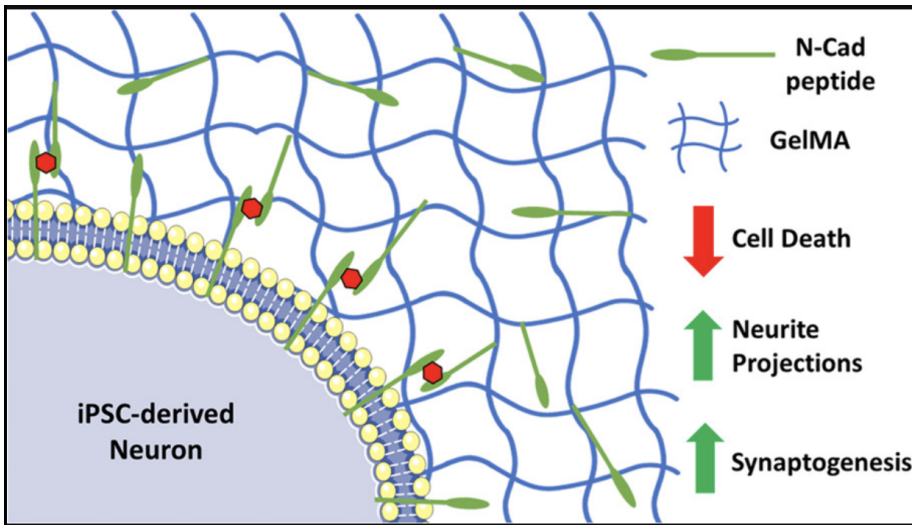

Figure 1.1: Scaffolds functionalized with N-cadherin peptides will support 3D stem cell-derived neuronal cultures (2).

1.4 Innovation

While N-cadherin has been used as a substrate to grow 2D stem cell-derived neuronal cultures (73–75) and conjugated to HAMA to improve chondrogenesis from mesenchymal stem cells (64), there have been no *in vitro* studies examining the effects of N-cadherin on 3D neuronal cultures. Due to N-cadherin's role in brain development, the presence of this molecule in 3D stem cell models may improve the maturation of the neurons and correct the connectivity issues traditionally observed. The creation of GelMA-Cad through the conjugation of N-cadherin peptides to methacrylated gelatin is the first demonstration of using this type of bioinstructive hydrogel for 3D iPSC-derived neuronal cultures. These neurons are able to form functional synapses in 3D, allowing for research on the mechanisms of synaptic dysfunction during neurodegeneration (Fig. 1.1). The use of stem cells as the source for the cell types needed for the model also provide the framework for creating isogenic models to study how specific mutations can lead to disease pathology as well as the ability to create the necessary cell types from the same human patient (i.e. the same genetic background). Furthermore, the use of gelatin as the scaffold background provides the potential for more complex brain structures.

1.5 Specific Aims

To overcome the issues of creating predictive human models of the brain, this dissertation details the work of the following aims. The studies conducted for this thesis demonstrate the utility of bio-instructive scaffolds for improving 3D *in vitro* brain models, and these models will serve as vital resources for understanding neurodegenerative disease mechanisms and for developing future therapeutics.

1.5.1 Aim 1: Develop a 3D synaptically connected model of single-cell suspensions of iPSC-derived neurons.

One major limitation to 3D iPSC-derived neuronal cultures is the difficulty in creating synaptic connections among the neurons. Due to N-cadherin's role in neuronal development and maturation, we hypothesized that creating a scaffold containing this molecule will promote the development of functional synapses in 3D. First, we functionalized GelMA with N-cadherin peptides and confirmed the functionalization with nuclear magnetic resonance and Fourier transform infrared spectroscopy. We also assessed the mechanical properties of this new hydrogel, which we coined GelMA-Cad, using atomic force microscopy, rheometry, and scanning electron microscopy. Then we embedded iPSC-derived cortical glutamatergic neurons into GelMA-Cad and control hydrogels (including but not limited to Matrigel and GelMA). We used live confocal imaging to assess neurite growth and synaptic activity over time and immunostaining to assess the formation of functional synapses. We demonstrate that addition of N-cadherin cues to hydrogel scaffolds results in synaptically connected 3D single-cell neuronal suspensions.

1.5.2 Aim 2: Improve cortical laminar organization and maturation of iPSC-derived cortical forebrain organoids.

Brain organoids are emerging as a promising tool for studying the human brain as they are self-organizing multicellular models. However, existing human cortical brain organoid differentiation protocols do not properly recapitulate cortical laminar organization, limiting it's utility in studying diseases that affect neuronal connections. We hypothesized that the presence of N-cadherin may help tackle this issue. In this aim, I demonstrate that gelatin scaffolds functionalized with N-cadherin peptides improve cortical organization of organoids by providing cues to support radial glia projections and to guide neurogenesis. The N-cadherin peptide guides the development of the cortical plate throughout brain organoid development, which I assessed using immunohistochemistry and whole organoid tissue clearing. Additionally, I used synaptic tracing assays to demonstrate that conjugation of N-cadherin peptides to scaffolds results in improved maturation of cortical organoids. These results show biofunctionalized gelatin results in more reproducible organoid structures that have improve cortical architecture.

1.6 Outline

This dissertation outlines the development of two 3D *in vitro* models of the human brain using iPSCs and a biofunctionalized hydrogel. Chapter 2 provides a review of current models of the human brain and scaffolds that have been used to build 3D neuronal models. Chapters 3 and 4 describe the development and optimization of the hydrogel, GelMA-Cad, to improve 3D single-cell suspensions of iPSC-derived neurons. Chapter 5 demonstrates the utility of using GelMA-Cad to improve the reproducibility and structure of iPSC-derived cortical brain organoids. Finally, Chapter 6 provides conclusions for the work provided in this thesis as well as future directions for research in this field of study. Each research chapter will include a short introduction and methods section in addition to the results and discussion.

CHAPTER 2

Background

2.1 Current Models of the Human Brain

In order to study neurodegeneration in the human brain, it is critical that researchers have tools that can properly recapitulate the human brain structure and function. There are 3 primary methods of studying brain tissue in research labs: *in vivo* animal models, *ex vivo* tissue extracted from animals or patients, and *in vitro* cellular models. This section will describe the currently available models and technologies, and the pros and cons of each method.

2.1.1 *In Vivo* Models of the Human Brain

In vivo animal model systems play an extremely important role to our understanding of the human brain and neurodegenerative disease. Since it can be difficult to conduct research studies on humans, particularly on live patients, animals are studied in order to determine the mechanisms in which the normal brain operates and how brain functions are disrupted during disease. Additionally, drug screening is performed on animal models prior to moving to clinical trials in order to decrease the potential risks to the human subjects.

There are several important animal models used to study the neuropathology of neurodegenerative diseases, such as Alzheimer's disease, Parkinson's disease, and frontotemporal dementia, that span a large variety of species from drosophila to non-human primates (11; 76–96). These models can be used to study complex interactions between the brain and other organs. For example, animal models have been used to study gut-brain interactions in Parkinson's disease (97), which can be more difficult to study in *in vitro* models. This aspect also allows researchers to look at systemic affects of administering a drug during drug development studies. Animal models already incorporate cell types found in the brain (and other organs), so researchers do not need to go out of their way to make sure critical cell types are incorporated into their model. If researchers are interested in specific cell types, methods exist to help researchers identify and manipulate those cells (98). Additionally, animal models like rodents or non-human primates allow researchers to study symptoms of neurodegenerative diseases such as memory, learning, and other signs of cognitive impairment (88; 92), which is not possible to study using *in vitro* models.

However, there are some considerations that need to be taken into account when it comes to animal models. First, animal models can be extremely expensive, especially for higher order species, and more time consuming than *in vitro* models (16). As a result, this may not be the preferred first model to study when conducting pilot studies or quickly trying to screen for possible drug targets. Second, there are species

differences between model organisms and humans. For example, the mouse brain is much smaller than the human brain and doesn't have the exact same architecture as the human brain (Fig. 2.1). Additionally, there can be genetic differences between the animal models and human patients that can make it difficult to translate research into effective therapeutics (99). Third, many of the neurodegnerative disease models in animals present an extremely aggressive model of the disease. For example, some mouse AD models that are based on FAD mutations result in the overproduction of amyloid beta plaques (16). This is also true for mouse models where young mice are studied rather than aged mice (16). These genetic mutation-based models usually only account for rare heritable forms of neurodegenerative diseases rather than spontaneous forms of the disease, and as a result, the results of these experiments may not be applicable for the majority of the patient population. Furthermore, some of the commonly used Parkinson's disease animal models use toxins to induce parkinsonian symptoms (i.e. motor deficits) (83), which may not reflect the larger human patient population. It is believed that these limitations to model organisms lead to the high failure rate of clinical trials for neurodegenerative disease therapeutics (16). Despite these limitations, animal models have contributed significantly to the field of neurodegenerative disease research.

2.1.2 *Ex Vivo* Models of the Human Brain

Ex vivo tissue models are typically created from tissue explants removed from animal models, or humans if the researchers are lucky enough to be able to get live tissue. The benefits of using this type of model is that the researcher has greater access to the cell types being studied (100). This model type retains the architecture of the organ, which allows the researchers to study complex systems that retain the tissue's connectivity and cell composition (101). However, these tissue slices can be difficult to culture and can lose function over time (100). Additionally, the process of removing the tissue can cause damage and death to the cells, which can alter the function of those cells (102; 103). Furthermore, since these tissues typically come from animals, *ex vivo* model preparation can be costly and time-consuming and can require advanced expertise (100). With the advances in methods of studying *in vivo* and *in vitro* models, *ex vivo* studies have become less common (100; 102).

2.1.3 *In Vitro* Models of the Human Brain

2.1.3.1 Two Dimensional Models

Two dimensional (2D) models refers to the cells laying in a relatively flat manner, with little to no differences to cell culture in the z-axis.

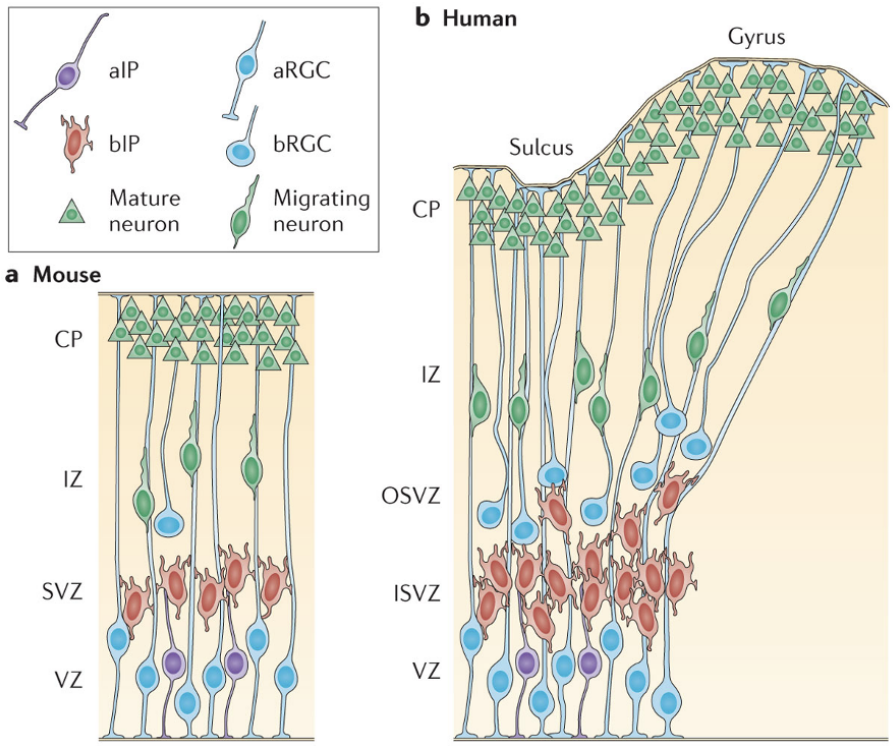

Figure 2.1: The mouse cortex lacks the outer subventricular zone (OSVZ) that is found in the human cortex. This results in a smaller mouse cortex because mice do not have the extra neural progenitors found in the OSVZ. aIP = apical intermediate progenitor; aRGC = apical radial glia cells; bIP = basal intermediate progenitors; bRGC = basal radial glia cells; VZ = ventricular zone; SVZ = subventricular zone; ISVZ = inner subventricular zone; OSVZ = outer subventricular zone; IZ = intermeidate zone; CP = cortical plate Reprinted with permission from Tao Sun et. al: Springer Nature: Nature Reviews Neuroscience (3).

2.1.3.1.1 Monocultures

Traditional 2D *in vitro* models are monocultures in which only one cell type is used to create this model. These models tend to be more reproducible, are typically simpler to study, and can be easier to scale up (101). As a result, 2D monocultures are a popular with high-throughput screens. While these models have provided new insights into the mechanisms of cellular function, monocultures do not completely recapitulate the complexity of human tissues in terms of the cell types present and the 3D ECM-cell interactions (100).

2.1.3.1.2 Co-Cultures

It is also possible to incorporate multiple cell types into 2D cultures. It is known that other cell types like astrocytes can help support the maturation of neurons, so researchers can incorporate astrocytes to encourage maturation in iPSC-derived neurons (52). This idea can also be used to increase the blood-brain barrier properties of endothelial cells by incorporating supporting cell types like astrocytes and pericytes (43; 104). Some Organ-on-a-Chip models (discussed in Section 2.1.3.2.1) also fall into the 2D co-culture category. Like

with 2D monocultures, 2D co-cultures do not completely recapitulate the complexity of a 3D organ.

2.1.3.2 Three Dimensional Models

Three dimensional (3D) models refers to cell cultures that cultured in the x, y, and z-planes. These models come in a variety of forms, but all of them usually require some sort of scaffold to help support the cells. Current scaffolds that are commonly used for brain 3D models are discussed in Section 2.2.

2.1.3.2.1 Organ-on-a-Chip

Organ-on-a-chips typically utilize microfluidic technology to engineer tissue-like structures that can incorporate static or perfusable conditions. One benefit to this type of model is that multiple organ-on-a-chip devices can be connected in order to simulate the organ connectivity found in animals and humans (105; 106). Furthermore, it is possible to create co-culture systems in a single chip, which can model the cell-cell interactions observed in a human organ. For example, the neurovascular-unit-on-a-chip typically incorporates at least neurons, astrocytes, and brain microvascular endothelial cells (107–109). Some of the chips incorporate 3D components, which add an the additional layer of complexity in the systems (108; 110). However, the technical expertise to build the microfluidic chips, the high cost of commercial microfluidic chips, and the specialized equipment sometimes needed to run the organ-on-a-chip systems can be a huge barrier to the wide spread use of organ-on-a-chip technology (110; 111). Additionally, the surface effect of small volumes of fluid must be taken into consideration when designing an organ-on-a-chip experiment (110). Furthermore, while perfusion can mimic the vascular networks of the human body, these model systems currently lack the ability to model the circulating immune system or endocrine system (105).

2.1.3.2.2 Cell Suspensions and Co-Cultures

Advances in cell culture sources and biomaterials has lead to the increased development of 3D cultures (100). These 3D models can range from single-cell suspensions of a single cell type (2) to co-culture systems (112). These models incorporate a lot of the complexity missing in 2D *in vitro* cultures as it incorporates more complex cell-cell and cell-ECM interactions. One consideration for this type of model is the matrix scaffold needed to support the 3D systems; Section 2.2 discusses some common scaffolds used for neuronal models. Depending on the chosen scaffold, it can be easy to produce 3D models and scale up the cultures for high-throughput screens (101). Additionally, many 3D brain models do not currently incorporate a blood-brain barrier, which can play a role in neurodegenerative disease progression (100). The lack of a vasculature system can also make it difficult to connect these 3D brain models to other organ models, so these models cannot be used for systemic studies. Additionally, researchers might need to consider matrix remodeling and

degradation when culturing the models long term as a changing scaffold might result in the model collapsing (101).

2.1.3.2.3 Organoids

Newer to the 3D*in vitro* modeling toolbox, organoids are cellular structures that aim to recreate the architecture of an organ. As opposed to spheroid cultures, which are traditionally monoculture assemblies, organoids typically have at least 2 different cell types present in the structures. Protocols have been published that generate different organoid brain regions including the midbrain, hippocampus, and forebrain (113), and these structures are particularly exciting because they (at least partially) recreate the architecture of the human brain and are able to model cell-cell and cell-matrix interactions (114). Brain organoids have been used to model diseases such as Alzheimer's disease (115–121), frontotemporal dementia (122; 123), Parkinson's disease (124; 125), and Zika-induced microcephaly (121; 126; 127).

However, there are still a few limitations to organoid models. First, organoid differentiation protocols can produce heterogeneous structures, which limits the reproducibility of organoid experiments (101). Furthermore, as the organoids expand in size, nutrient/waste exchange can be impaired, creating a necrotic core at the center of the organoid and reducing the stem cell population that would have created the more superficial layers (54). Additionally, the organoids do not always fully recreate the architecture of the human brain. For example, cortical brain organoids do not have proper laminar organization. Unlike in the human brain, where all the cortical layers form distinct populations, the cortical neuron populations are largely intermixed in organoid models (54). There is currently no universal protocol that can make all the brain regions within a single brain organoid; if additional brain regions are needed for disease modeling, researchers typically create 2 separate organoids that relate to specific brain regions and fuse the organoids at a later time point (128). This can introduce additional reproducibility issues. Furthermore, current organoid protocols lack certain cell types including brain microvascular endothelial cells, pericytes, microglia, and oligodendrocytes (54).

2.2 Current Scaffolds Used for Neuronal Models

As 3D human models become more utilized and more complex, the development of biomaterials that are able to support brain cell types has become an important research area. This section will describe a selection of commonly used scaffolds for neuronal modeling.

2.2.1 Matrigel

Matrigel is a commonly used scaffolds for stem cell cultures. This biomaterial is derived from mouse sarcoma ECM (129). Neurons grown on Matrigel coated plates have good cell viability and can mature over

long term culture (2; 47; 129). Furthermore, this is a commonly used scaffold for cortical brain organoids, and these organoids can be cultured long term and form mature cortical structures (6; 8; 130). However, this hydrogel can be extremely expensive, and the quick crosslinking properties of this matrix at room temperature can make it difficult to manipulate (2). Matrigel batches can also be heterogeneous, making it difficult to reproduce results from models that utilize this scaffold (2; 101).

2.2.2 Hyaluronic Acid

One major component of the human brain ECM is hyaluronic acid (HA), and as a result, this is a commonly used scaffold for 3D *in vitro* neuronal models (57; 101). Neural stem cells that have been embedded in HA are able to mature into neurons provided that the cell density is high effect to support differentiation (131). Additionally, studies with HA demonstrate that softer hydrogels promote neurogenesis while stiffer hydrogels promote astrogenesis (131). However, HA does not naturally contain cell binding domains, so researchers have to either conjugate binding domains (ex: RGD), conjugate cell adhesion molecules, or mix with hydrogels that have these binding domains (ex: gelatin) (2; 101).

2.2.3 Decellularized Brain Extracellular Matrix

Decellularized brain extracellular matrix is brain tissue that has been modified to remove all cellular material so that only the extracellular matrix is left (132). As a result, this scaffold is believed to be left with components that should support neuronal cultures such as glycoaminoglycans, which is another large component of the brain ECM. This type of scaffold can be generated from a variety of species including rats, pigs, cows, and (if the researcher is able to obtain tissue) humans (132–135). Neural stem cells cultured on this scaffold differentiate into neurons (132; 133), and organoids embedded into decellualrized brain scaffolds demonstrate enhanced neurogenesis (135).

However, the steps to completely remove cellular components of the brain tissue can be time and labor intensive, and the results can be heterogeneous in terms of the composition of the remaining extracellular matrix (132; 135). Furthermore, the resulting extracellular matrix does not exactly match the composition of the human brain (135). Finally, it can be difficult to obtain tissue to make the decellularized matrix.

2.2.4 Gelatin

Gelatin is primarily denatured collagen and is a relatively cheap scaffold to purchase. Gelatin naturally contains RGD cell binding motifs that support cell survival. Additionally, methacrylated gelatin has been previously been shown to be compatible with 3D culture of primary neurons (63), and gelatin can be used as a surface coating to support stem cell-derived neurospheres (75). Gelatin has favorable mechanical properties

for creating complex 3D structures as it can support its own weight, unlike the previous scaffolds described in this section.While collagen is not a large component of the brain parenchyma ECM, we have shown that gelatin can be biofunctionalized to help support stem cell-derived neuronal maturation in 3D, potentially making up for the lack of specific biological cues found naturally in gelatin (2). When designing experiments using gelatin as the scaffold base, it is important to take into account the hydrogel stiffness necessary to support the desired cell type, crosslinking method (can contribute to hydrogel degradation properties over long term cultures, porosity of the hydrogel, maximum potential size of the model), and whether bioinstructive cues are needed to support the model's cell types.

CHAPTER 3

Development of an N-Cadherin Biofunctionalized Hydrogel to Support the Formation of Synaptically Connected Neural Networks

Text adapted from:

O'Grady BJ*, **Balotin KM***, Bosworth AM, McClatchey PM, Weinstein RM, et al. Development of an N-Cadherin Biofunctionalized Hydrogel to Support the Formation of Synaptically Connected Neural Networks. ACS Biomater Sci Eng. 2020; 6(10):5811–5822 *with permission from the American Chemical Society*.

3.1 Summary

In vitro models of the human central nervous system (CNS), particularly those derived from induced pluripotent stem cells (iPSCs), are becoming increasingly recognized as useful complements to animal models for studying neurological diseases and developing therapeutic strategies. However, many current three-dimensional (3D) CNS models suffer from deficits that limit their research utility. In this work, we focused on improving the interactions between the extracellular matrix (ECM) and iPSC-derived neurons to support model development. The most common ECMs used to fabricate 3D CNS models often lack the necessary bioinstructive cues to drive iPSC-derived neurons to a mature and synaptically connected state. These ECMs are also typically difficult to pattern into complex structures due to their mechanical properties. To address these issues, we functionalized gelatin methacrylate (GelMA) with an N-Cadherin (Cad) extracellular peptide epitope to create a biomaterial termed GelMA-Cad. After photopolymerization, GelMA-Cad forms soft hydrogels (on the order of 2 kPa) that can maintain patterned architectures. The N-cadherin functionality promotes survival and maturation of single-cell suspensions of iPSC-derived neurons into synaptically connected networks as determined by synaptic tracing and electrophysiology. Immunostaining reveals a pronounced increase in presynaptic and postsysnaptic marker expression in GelMA-Cad relative to Matrigel, as well as extensive colocalization of these markers, thus highlighting the biological activity of the N-cadherin peptide. Overall, given its ability to enhance iPSC-derived neuron maturity and connectivity, GelMA-Cad should be broadly useful for *in vitro* studies of neural circuitry in health and disease.

3.2 Background

Neurodegenerative diseases are estimated to affect 30 million people worldwide (10). Aging is the number one risk factor for neurodegeneration, and disease incidence is expected to increase concurrently with an increasingly aged population worldwide. These diseases (e.g. Alzheimer's disease, Parkinson's disease,

Huntington's disease, amyotrophic lateral sclerosis, and multiple sclerosis) all have different region-specific presentation and cell-cell communication, making it difficult to understand the mechanisms underlying their onset and propagation and thereby hampering the development of effective treatments. As an example, clinical trials for Alzheimer's disease have had a high failure rate since 2010 and currently available drugs can only alleviate symptoms but do not reverse neural tissue damage (136). These failures occur despite many candidate therapeutics having efficacy in various mouse models. As such, there has been a growing interest in developing human in vitro models for studying neurodegeneration (62; 137–141) and reducing the attrition rate in therapeutic development.

Recent advancements in three-dimensional (3D) neural tissue models, particularly those constructed from human pluripotent stem cell (hPSC)-derived progenies (including human embryonic stem cells and induced pluripotent stem cells (iPSCs)), have generated much excitement for their ability to mimic the structure and function of human brain regions (8; 62; 142). Such models typically consist of neurons and varying mixtures of supporting cells (e.g., glia and vascular components) embedded in a hydrogel formed from extracellular matrix (ECM) components. Currently, a wide variety of ECMs are available for constructing neural tissue models (143). Historically, the majority of early models have utilized Matrigel, an ECM composite derived from Engelbreth–Holm–Swarm mouse sarcoma tumors that consists of many proteins (type IV collagen, laminin, etc.) and growth factors

Despite their utility toward fabricating complex neural tissue structures from hPSCs, existing ECMs have some known shortcomings for neural cell culture. Many ECM platforms lack appropriate bioinstructive cues to promote cell–cell or cell–ECM interactions that facilitate neuronal maturation. Of the aforementioned materials, only the components of Matrigel (e.g., laminin) and HA have physiological relevance to brain ECM; HA in particular has been shown to support hPSC-derived NPC maturation into neurons that exhibit enhanced neurite projection with synaptic vesicles and electrophysiological activity (61). However, Matrigel and HA are difficult to handle due to their viscosity, and both materials have a very low elastic modulus, meaning that they collapse under their own weight and cannot be molded into more complex macrostructures. These factors limit the fabrication of topographic features, such as vasculature or perfusion channels. Synthetic hydrogels may overcome these issues by incorporating custom functional groups that enable tuning of the mechanical and rheological properties, but they can be prohibitively difficult to fabricate and require more extensive chemical modification to recapitulate tissue-specific biochemical cell–ECM interactions (144). Moreover, the majority of natural and synthetic ECMs are relatively expensive, which can further limit their widespread use.

Herein, we focused on engineering an ECM material to overcome some of these challenges. Our goal was to produce a material that would: (1) facilitate neuron survival and maturation within 3D tissue con-

structs through biophysical cues, (2) exhibit ideal mechanical properties to promote neuron outgrowth while also supporting macropatterned features, and (3) be relatively easy to synthesize at low cost and therefore widely accessible. We ultimately produced a biomaterial termed GelMA-Cad, which consists of methacrylated gelatin (GelMA, a well-characterized biomaterial capable of being photopatterned (145–147)) conjugated with a peptide from an extracellular epitope of N-cadherin (Cad) that has previously been used for cartilage tissue engineering (64). Using this bioinstructive material, we form hydrogels with physiological stiffness that can not only maintain photopatterned features, but additionally facilitate iPSC-derived glutamatergic neuron survival and extension of neurite processes (as compared to GelMA, Matrigel, and various other negative controls). Moreover, relative to Matrigel, GelMA-Cad supports enhanced formation of synaptically connected neural networks, as measured by immunocytochemistry, electrophysiology, and viral synaptic tracing. We suggest that GelMA-Cad will aid the construction of 3D neural tissue models to study human disease biology and augment drug screening assays.

3.3 Methods

3.3.1 Cell Culture

CC3 iPSCs (148) were maintained in Essential 8 (E8) medium on standard tissue culture plates coated with growth-factor reduced Matrigel (VWR). At 60-70% confluency, the cells were replated using Versene (Thermo Fisher) as previously described (149).

Stem cells were differentiated into cortical glutamatergic neurons using a previously described protocol (47) with some modifications (Fig. 3.1). iPSCs were washed once with PBS and dissociated by incubation with Accutase (Thermo Fisher) for 3 minutes. Following collection by centrifugation, the cells were replated onto Matrigel-coated plates at a density of 2.5 x 10^2 cells/cm^2 in E8 medium with 10 μM Y27632 (Tocris). The next day, the medium was changed to Essential 6 (E6) medium (149) supplemented with 10 μM SB431542 (Tocris) and 0.4 μM LDN1931189 (Tocris) for 5 days as previously described (46). Over the next 5 days, the medium was gradually transitioned from E6 medium to N2 Medium (DMEM/F12 basal medium (Thermo Fisher) and 1x N2 supplement (Gibco)) supplemented with 10 μM SB431542, and 0.4 μM LDN1931189 (46). On the 11th day of the differentiation protocol, the resultant neural progenitors were dissociated by incubation with Accutase for 30 minutes and passed onto Matrigel in Neuron Medium with 10 μM Y27632. Neuron Medium was made by miaxing a 1:1 ratio of N2 Medium and B27 Medium (Neurobasal Medium (Thermo Fisher), 200 mM Glutamax (Gibco), and 1X B27 supplement (Gibco)) (47). The cells received fresh Neuron Medium every day for the next 20 days and then a media change every 3-4 days afterward. Glutamatergic neurons were used for experiments between days 70 and 100 of differentiation.

For the synaptic tracing experiments described below, a small population of glutametergic eurons were

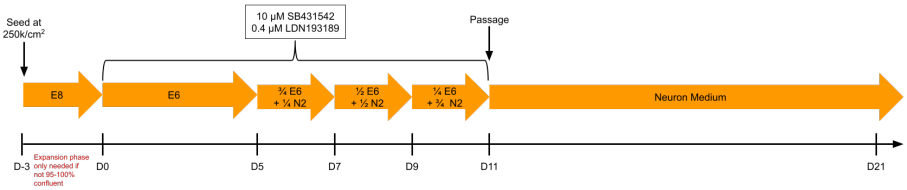

Figure 3.1: Cortical Glutamatergic Neuron Differentiation Protocol (47).

transduced with an adenoassociated virus (AAV) encoding enhanced green fluorescent protein (EGFP) under the control of the human synapsin promoter, which was a gift from Dr. Bryan Roth (Addgene plasmid 50465). Two weeks before use, the neurons were dissociated with Accutase and replated onto Matrigel-coated plates at a density of 2.5 x 10^2 cells/cm^2 in Neuron Medium with 10 µM Y27632. The following day, the medium was replaced, and the AAV was added at a MOI of 5,000. Fresh medium was added to the cells 24 hours after to remove any residual virus and normal media changes were resumed thereafter.

3.3.2 GelMA Synthesis and Characterization

Methacrylated gelatin (GelMA) was synthesized as described previously (150). Type A procine skin gelatin (Sigma) was mixed at 10% (w/v) into DI water (sourced from an in-house Continental Modulab ModuPure reagent grade water system) at 60°and stirred until fully dissolved. Methacrylic anhydride (MA, Sigma) was slowly added to the gelatin solution and stirred at 50°for 3 hours. The solution was then centrifuged at 3,500*g* for 3 minutes, and the supernantant was collected. Following a 5x dilution with additional warm (40°C) UltraPure water (Thermo Fisher) to stop the reaction, the mixture was dialyzed against DI water for 1 week at 37 °using a 12-14 kDa cutoff dialysis tubing (Fisher) to remove salts and methacrylic acid. The pH of the solution was then adjusted to 7.25-7.45 by adding 1.0 M HCl or 1.0 M NaOH as measured with a Thermo Fisher Scientific Orion Star pH meter. The resulting GelMA solution was lyophilized for 3 days using a Labconco lyophilizer and stored at -20°.

3.3.3 Peptide Conjugation

Peptides were conjugated to GelMA as previously reported (64) with slight modifications (Fig. 3.2). Briefly, GelMA was reconstituted in triethanolamine buffer (TEOA, Sigma) to create a 10% (w/v) solution and stirred at 37°for 2 hours until fully dissolved. The pH of the solution was then adusted to 8.0-8.5 by adding 1.0 M HCl or 1.0 M NaOH. Scrambled (Ac-AGVGDHIGC, to make GelMA-Scram) or N-cadherin

mimic (Ac-HAVDIGGGC, to make GelMA-Cad) peptides (GenScript) were added to the GelMA/TEOA buffer to form a 0.1% (w/v) solution. The cystine residue at the C-terminal end of the peptides permited a Michael-type addition reaction with GelMA (64). The solution was stirred at 37°for 24 hours. GelMA-Cad/Scram that was dialyzed against DI water using a 6-8 kDa cutoff dialysis tubing (Spectrum) for 1 week at 37°(2). The pH of the dialyzed hydrogel was then adjusted to 7.35-7.45 by adding 1.0 M HCl or 1.0 M NaOH, and the solution was lyophilized and stored at -20°. Hydrogel was stored for up to 6 months in the freezer.

3.3.4 Nuclear Magnetic Resonance Spectroscopy

Conjugation was routinely verified through ^{1}H-NMR using a Bruker 500 Hz NMR spectrometer set to 37°for the prescence of the amino acid valine. The degree of functionalization of the methacrylic side chains to the gelatin backbone was determined by taking the integral of the lysine peak (2.8-3.0 ppm) of gelatin, normalizing the GelMA spectra to the integral of the gelatin aromatic amino acid (7.2-7.4 ppm), and calculating the percent degree in the lysine peak (151; 152). The degree of functionalizatio of the peptides to GelMA was calculated by normalizing the integral of the valine peak (3.5 ppm) to the integral of the gelatin aromatic amino acid.

3.3.5 Fourier-Transform Infrared Spectroscopy

198 mg potassium bromide (Sigma) was added to 2 mg of lyophilized gelatin, GelMA, GelMA-Cad, or GelMA-Scram and crushed using a mortar and pestle. The crushed samples were transferred to a 13 mm Specac evacuable pellet press die and compressed into a thin disc using a Specac manual hydraulic press. An additional disc was made of only potassium bromide for calibration. The samples were stored in a dry container overnight and analyzed the following day using a Bruker Tensor 27.

3.3.6 Atomic Force Microscopy

GelMA, GelMA-Scram, and GelMA-Cad were reconstituted and polymerized into hydrogel discs, as described in the cell seeding section below. A Bruker Dimension Icon Atomic Force Microscope was used to measure hydrogel stiffness. 0.01 N/M Novascan probes containing a 4.5 μm polystyrene bead ((PT.PS.SN.4.5.CAL) were used to measure 3 distinct 5 x 5 μm^2 areas of each hydrogel. Three hydrogel disc replicates of each sample were utilized, with a total of 576 stiffness measurements per sample. For each individual force curve, a first-order baseline correction was performed, and the Hertzian model was used to calculate Young's modulus. For tool calibration, polyacrylamide hydrogels were prepared as previously reported (153) and measured prior to GelMA and its derivatives.

3.3.7 Rheological Characterization

The stiffness of GelMA, GelMA-Cad, and GelMA-Scram was measured using an AR-G2 (TA Instruments) strained-controlled rheometer equipped with 20 mm parallel plates. The hydrogels were loaded on the lower plate and photo-cross-linked for 8 seconds with 25 mW/cm^2 UV light using a ThorLabs UV Curing LED System. Immediately following UV exposure, the top plate was lowered to a gap of 0.8 mm. The cross-linking was recorded with a time sweep oscillatory test under cotnraint amplitude of 1% and at a constant frequency of 1 Hz. Three independent replicates were performed for each hydrogel condition.

3.3.8 Scanning Electron Microscopy

Lyophilized GelMA, GelMA-Cad, and GelMA-Scram were reconstituted into PBS to form 10% (w/v) solutions with a 0.05% lithium phenyl-2,4,6-trimethylbenzoylphosphinate (LAP) initiator (Sigma). 30 µL of each solution was added to a Ted Pella pin mount and cross-linked by an 8 second exposure with 25 mW/cm^2 UV light. These pin mounts were stored in a Ted Pella mount storage tube and placed in a -80 °freezer overnight. The following day, the samples were transferred to a Labconco lyophilizer for an additional 2 days and stored at room temperature until used. To characterize the internal microstructures of GelMA, GelMA-Cad, and GelMA-Scram, the dried samples were observed using a scanning electron microscope (Zeiss Merlin) at an accelerating voltage of 2 kV. ImageJ software was used to quantify pore sizes, where the mean diameter of each pore was considered the average pore size.

3.3.9 Fabrication and Seeding of Hydrogels

GelMA, GelMA-Scram, and GelMA-Cad were reconstituted in Neurobasal Medium to make a 10% (w/v) solution with 0.05% LAP initiator. iPSC-derived neurons were detached from 12-well plates via a 5 minute incubation with Accutase and centrifuged for collection. The glutamatergic neurons were mixed with a reconstituted hydrogel/initator solution to achieve a density of 2 x 10^3, 2 x 10^4, 2 x 10^5 cells/mL depending on the experiment. Once the solutions were prepared they were mixed thoroughly with a P1000 pipette to break up any cell clumps. Next, 100 µL of the cell suspension was added to RainX-treated glass slides and covered with 12 mm diameter coverslips (Carolina) to form discs. These discs were then exposed to 25 mW/cm^2 UV light for 8 seconds and set aside for 10 minutes at room temperature. Hydrogel discs were then removed from the glass slides and transferred to a 12-well plate with 1 mL of Neuron Medium per well.

GelMA-Cad and GelMA were mixed to create a 2:1 ratio (66% GelMA-Cad concentration) and 1:3 ratio (33% GelMA-Cad concentration) and were seeded with glutamatergic neurons at a density of 2 x $10^{5.}$ cells/mL (2).

For some control experiments, GelMA was mixed with soluble peptide rather than via covalent coupling;

here, soluble peptides were reconstituted in dimethyl sulfoxide (DMSO, Sigma) to create a 10 mg/mL solution. Then the peptides were added to GelMA/initator/neuron solution (2 X 10^5 cells/mL) to create a 50 µg/mL peptide concentration.

To embed the neurons in Matrigel, 1 mL of Matrigel aliquots was thawed on ice. Once thawed, the neurons were embedded at a density of 2 x 10^5 cells/mL, and 100 µL of the solution was added directly onto the coverslips in a 12-well plate. The plate containing the Matrigel discs was placed in an incubator at 37°to cross-link for 30 minutes. After the Matrigel was fully cross-linked, 1 mL of Neuron Medium was added to each of the wells.

For all experiments involving hydrogels, once the neurons were encapsulated, the media was changed every 3 days until the cells were used.

3.3.10 Live/Dead Cell Imaging

To assess long-term cell viability, hydrogel discs were incubated with CytoCalcein Violet 450 (AAT Bioquest) and propidium iodide (PI, Thermo Fisher) for 1 hour. The staining was performed at 48 hours, 72 hours, 5 days, and 10 days following embedding. The hydrogel discs were imaged using a Zeiss 710 confocal microscope, and cell viability was quantified using ImageJ. Following imaging, 1 mL of Neuron Medium was added to each well to dilute any remaining Calcein/PI from the hydrogels.

3.3.11 Neurite Projection Quantification

Raw data were exported in a 16-bit TIF format and imported into MATLAB 2017 for quantification using a custom image analysis script. Briefly, the images were smoothed using a 3 x 3 pixel smoothing filter to mitigate image noise, and in-focus neurite segments were identified by isolating the regions at least 5% brighter than the mean pixel intensity in the surrounding 50 pixel radius (154). Cell bodies and neurites were distinguished by successive erosion of the resulting binary mass. The erosion radius at which the total cell mass declined most steeply was used to define the radius required to erode neurites while sparing cell bodies. Following segmentation of neurites and cell bodies, algorithms previously developed for analysis of mitochondrial networks (4) were used to measure the average length and width of each neurite segment. Code can be found in Section 3.7.1.

3.3.12 Synaptic Tracing

Hydrogel discs were fabricated as described above with wild-type glutamatergic neurons densities of 2 x 10^5 cells/mL. Prior to cross-linking the hydrogels, separate neurons transduced with synapsin-driven EGFP were dissociated from plates via a 5 minute incubation with Accutase and then added to the center of the

hydrogel disc at a density of 2 x 10^3 cells/mL glutamatergic neurons (as shown in Fig. 3.12). After cross-linking, the hydrogel discs were placed in 1 mL of Neuron Medium and stored in an incubator at 37°until imaging. The formation of synaptic connections was visualized by the spread of the EGFP fluorescence across the neuronal cultures using a Zeiss LSM 710 confocal microscope. On day 21, calcein was added to visualize live cells. Colocalization of EGFP and calcein was quantified using Zeiss Zen Black software.

3.3.13 Immunofluorescence

After 2 weeks of culture, neurons embedded in hydrogels were fixed in 4% PFA (Sigma) for 20 minutes and then washed 3 times with PBS. A solution of 5% goat serum and 0.03% Triton X-100 (Thermo Fisher) was then added to the hydrogels overnight on a rocking platform at room temperature. The hydrogels were then incubated overnight with 4,6-diamidino-2-phenylindole (DAPI) or fluorescently conjugated primary antibodies: βIII tubulin Alexa Fluor 647 (Abcam ab190575), PSD-95 Alexa Fluor 488 (Novus Biologicals NB300556AF488), and/or synaptophysin Alexa Fluor 555 (Abcam ab206870). The hydrogels were then imaged using a 40x objective on a Zeiss LSM 710 confocal microscope. The number of PSD-95 and synaptophysin puncta was quantified using the cell counter plugin on ImageJ. Colocalization of the two markers was quantified using Zeiss Zen Black software.

3.3.14 Electrophysiology

The neurons in GelMA-Cad or Matrigel hydrogels were recorded in a bath consisting of 140 mM NaCl, 2.8 mM KCl, 2 mM $CaCl_2$, 2 mM $MgCl_2$, 10 mM *N*-(2-hydroxyethyl)piperazine-N'-ethanesulfonic acid (HEPES), and 10 mM $_{D\text{-}}$glucose. Sharp glass microelectrodes were prepared from borosilicate glass with a Sutter P97 pipette puller and filled with extracellular solution to reach a resistance of 6-8 Ω. The recording electrode was placed near the edge of the hydrogel disc. Extracellular field potential recordings were performed in a recording chamber placed on the stage of a Zeiss Axioscope upright microscope. The electrical activity was recorded with an Axon Multiclamp 700A amplifier. Data recording and analysis were performed with Axon pClamp software.

3.4 Results

3.4.1 Synthesis and Characterization of GelMA Functionalized with N-Cadherin Peptide

GelMA was chosen as a base material due to its ease of handling and robust mechanical properties (after cross-linking) compared to ECMs such as Matrigel and HA. Meanwhile, N-cadherin functionality was chosen for the role of this cell adhesion molecule in neurite growth during neurogenesis (65–68; 75; 155). The extracellular peptide epitope of N-cadherin chosen for this study has previously been used to functionalize

methacrylated HA to support chondrogenesis from mesenchymal stem cells (64), but 3D scaffolds fabricated with this peptide have not been used to support neural cultures. To generate the GelMA-Cad scaffold, porcine gelatin was first functionalized with methacrylic anhydride to create the GelMA backbone that could be cross-linked when exposed to the photoinitiator LAP and UV light (Fig. 3.2) (150).

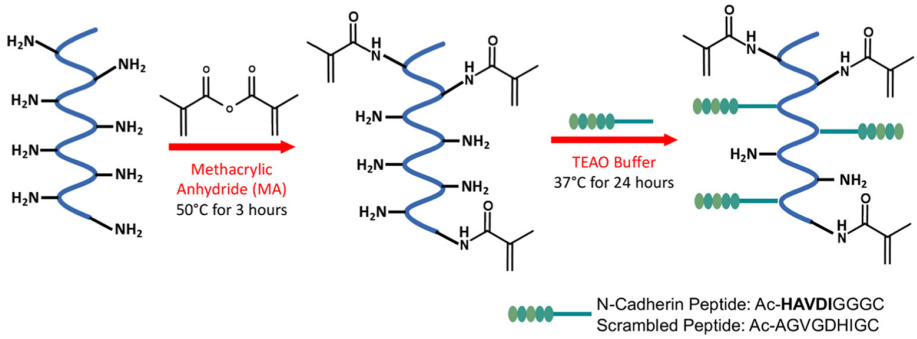

Figure 3.2: Synthesis Scheme for GelMA and GelMA-Cad/Scram. The conventional method for synthesizing GelMA uses methacrylate anhydride (MA) to introduce a methacryloyl substitution group on the reactive primary amine group of amino acid residues. GelMA was then dissolved in TEOA buffer with the N-cadherin or N-cadherin-scrambled peptide for Michael-type addition to the reactive primary amine groups.

This modification was confirmed through the presence of methacrylic side-chain protons (5.45 and 5.7 ppm) using ^{1}H-NMR (Fig. 3.3A), where a 77.5±8.4% degree of functionalization was achieved. GelMA was then functionalized with the first extracellular epitope of N-cadherin (HAVDIGGGC) or an N-cadherin-scrambled peptide (AGVGDHIGC), which is referred to as GelMA-Cad and GelMA-Scram, respectively. The conjugation of these peptides to the scaffold was also confirmed via ^{1}H-NMR through the presence of valine protons (3.5 ppm), which are no present in the gelatin or GelMA spectra (Fig. 3.3A). Based on the NMR spectra, 39.4±12.7% and 38.2±19.2% degrees of functionalization were achieved for GelMA-Cad and GelMA-Scram, respectively. Additionally, Fourier-transform infrared (FTIR) spectroscopy was employed to further validate successful functionalization. The FTIR transmittance spectra showed a noticeable decrease in the PO_4 peaks (1,000 cm^{-1}) compared to GelMA (Fig. 3.3B), likely due to the peptide conjugation. Collectively, these data suggest that GelMA was properly synthesized and functionalized.

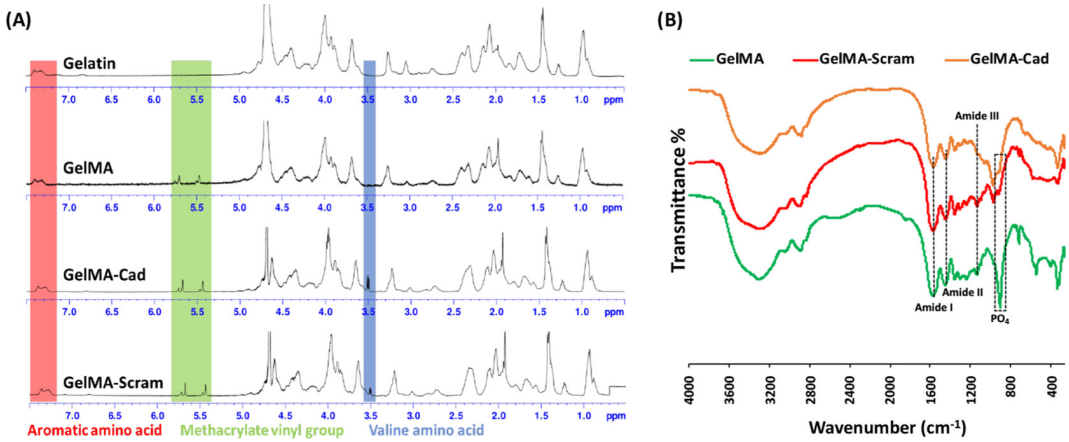

Figure 3.3: Assessment of biomaterial functionalization. (A) NMR spectra of gelatin, GelMA, GelMA-Cad, and GelMA-Scram. Successful conjugation of MA to the gelatin backbone was assessed by peaks at 5.5 and 5.7 ppm, and N-cadherin/scram peptide addition was assessed by the valine peak at 3.5 ppm. (B) FTIR spectra were used to confirm the congjuation of the peptide to the backbone of GelMA due to the decrease in the following relevant bands: 1000 cm^{-1} (PO_4 stretching) and 1250, 1540, and 1640 cm^{-1} (NH bending).

3.4.2 Mechanical and Physical Properties of Cross-Linked Hydrogels

The microporous structures of cross-linked hydrogels were confirmed by scanning electron microscopy (SEM). Porous network structures are commonly observed in hydrogels and are important for nutrient diffusion, cell integration, and removal of waste products, and the degree of chemical substitution has an inverse relation to pore size upon cross-linking (156; 157). The average pore size diameters of GelMA, GelMA-Cad, and GelMA-Scram were measured at 42.8±0.2, 43.1±0.2, and 42.4±0.2 μm, respectively (Fig. 3.5A). Next, to determine the local stiffness of GelMA, GelMA-Cad, and GelMA-Scram, atomic force microscopy (AFM) was performed. Polyacrylamide hydrogels (0.8 and 13 kPa) were produced and measured by AFM (153) to validate that the tool was properly calibrated (Fig. 3.5B). After cross-linking with LAP and UV light, GelMA, GelMA-Cad, and GelMA-Scram exhibited stiffness values of approximately 1–5 kPa (Fig. 3.5B), which resembles the stiffness of the native brain tissue (158; 159). Despite its relatively low elastic modulus, GelMA-Cad is stiff enough to maintain patterned architectures: when it was cross-linked around silicone tubing, followed by manual extraction of the tubing, a straight, a perfusable channel remained in the GelMA-Cad (Fig. 3.4A), whereas Matrigel collapses and the perfusion channel does not remain patent (Fig. 3.4B). Thus, similar to GelMA (150; 160), GelMA-Cad can be patterned into more complex macrostructures. To determine bulk stiffness, cross-linked hydrogels were measured by rheometry, where the stiffness of GelMA, GelMA-Scram, and GelMA-Cad was determined to be 1.3±0.03, 1.4±0.03, and 2.1±0.04 kPa, respectively (Fig. 3.5C). Overall, the average local and bulk stiffness measurements are in good agreement, and these measurements confirm that the hydrogels all have similar physical and mechanical properties, such that differences in neuron behavior can likely be attributed to peptide functionalization.

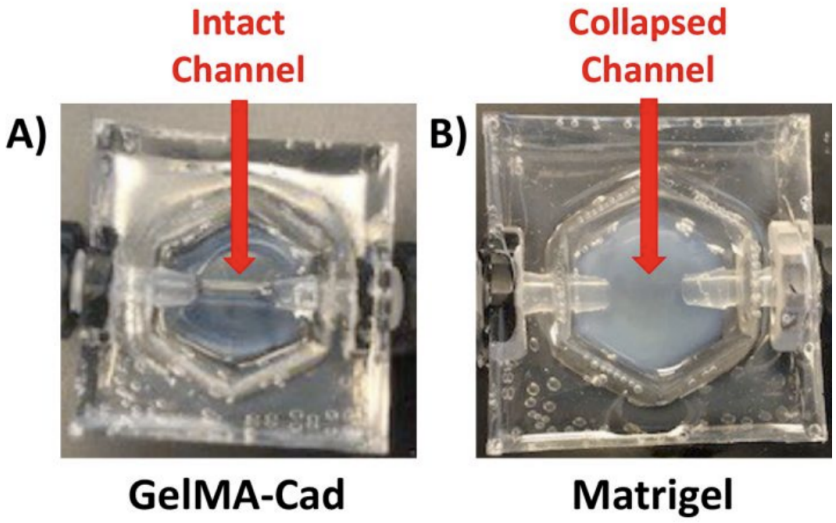

Figure 3.4: GelMA-Cad can support molded structures. A) PDMS mold with crosslinked GelMA-Cad with showing an intact channel that can be perfused. B) PDMS mold with crosslinked Matrigel showing a collapsed channel.

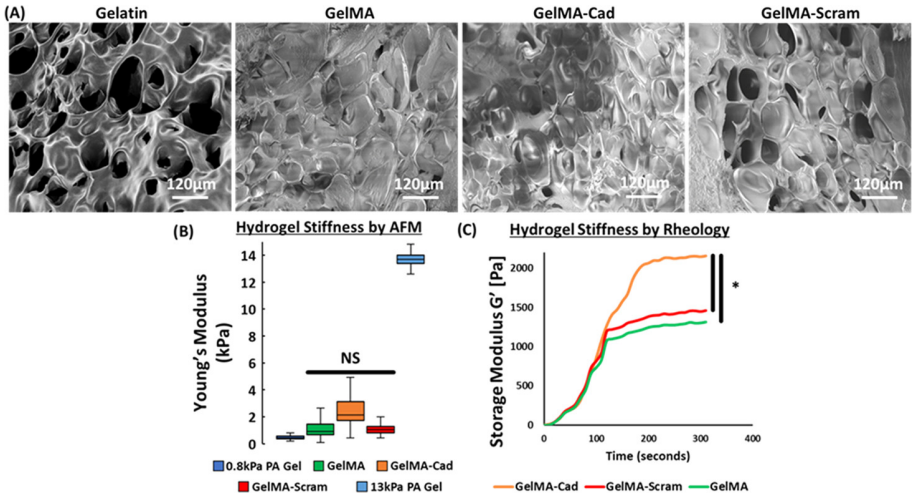

Figure 3.5: Physical properties and cross-linking kinetics of hydrogels characterized using SEM, AFM, and rheology. A) SEM images of the hydrogels fabricated from gelatin, GelMA, GelMA-Cad, and GelMA-Scram. B) AFM measurements of Young's modulus values for GelAM, GelMA-Cad, and GelMA-Scram. Stiffness data in the main text are presented as mean ±standard deviation (SD) from 3 individually prepared hydrogels. Statistical significance was calculated from one-way analysis of variance (ANOVA) with Tukey's post hoc test (NS = not significant). C) Cross-linking kinetics of GelMA, GelMA-Scram, and GelMA-Cad evaluated by rheology. Stiffness data from the 300 second endpoint are presented in the main text as mean ±SD from 3 individually prepared hydrogels. Statistical significance was calculated using unpaired Student's t-test calculations between GelMA-Cad and the 2 control hydrogels (*$p<0.0001$).

3.4.3 GelMA-Cad Hydrogels Support Survival and Outgrowth of iPSC-Derived Glutamatergic Neurons

To assess the ability of the hydrogels to support human neuron survival and outgrowth, human iPSCs were differentiated into highly pure populations of cortical glutamatergic neurons and cultured for 70–100 days before use. This early time point was chosen to ensure that the neurons were relatively immature, such that the effects of hydrogel encapsulation on maturation could be more easily judged. Furthermore, the neurons were dissociated into single-cell suspensions rather than more commonly used aggregates so that we could better assess the effects of hydrogel encapsulation on survival. The neurons were first embedded into Matrigel, GelMA-Cad, GelMA-Scram, or GelMA. As a negative control for physical conjugation of the peptides to the hydrogels, the neurons were also embedded in GelMA with either soluble N-cadherin peptide or soluble scrambled peptide. Using calcein and propidium iodide dyes to mark live and dead cells, respectively, we determined that neurons embedded in GelMA and GelMA-Scram (both conjugated and soluble peptide), as well as Matrigel with the soluble peptide, died within 4 days (Fig. 3.6A and 3.7).

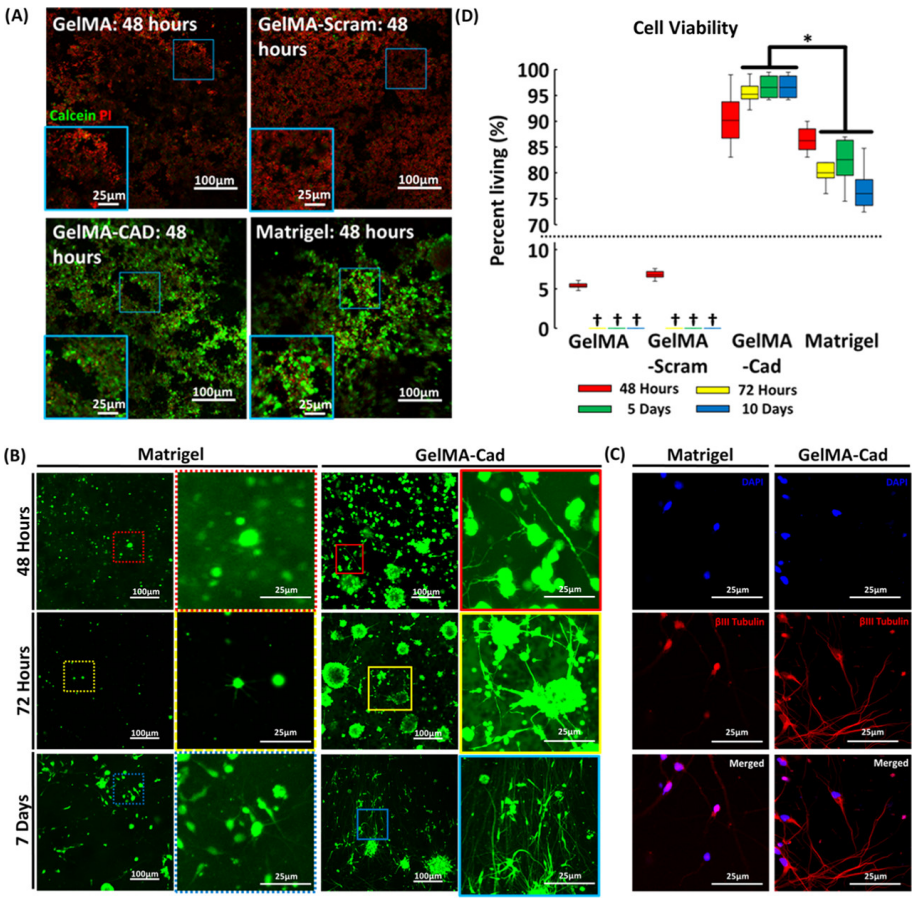

Figure 3.6: Live/dead staining of the iPSC-derived neurons embedded in various hydrogels. (A) Representative images of the hydrogels that were labeled after 48 hours with calcein (green) and propidium iodide (PI, red) to visualize the live and dead cells, respectively. The insets are provided for higher magnification. (B) Representative images of Matrigel and GelMA-Cad hydrogels labeled at various time points with calcein. The insets are provided for higher magnification. (C) Neurons in Matrigel and GelMA-Cad were immunolabeled with βIII tubulin (red) and DAPI (blue) to confirm neural identity and morphological observations. (D) Full quantifcation of cell viability, using calcein and PI, for all conditions and time points. Data are presented as mean ±SD from 3 biological replicates, with 5 images assessed per replicate. †is used to highlight values that fall below 5%. Statistically significant differences in the viability were calculated between GelMA-Cad and Matrigel at later time points using a one-way ANOVA with Tukey's post hoc test (*$p<0.005$).

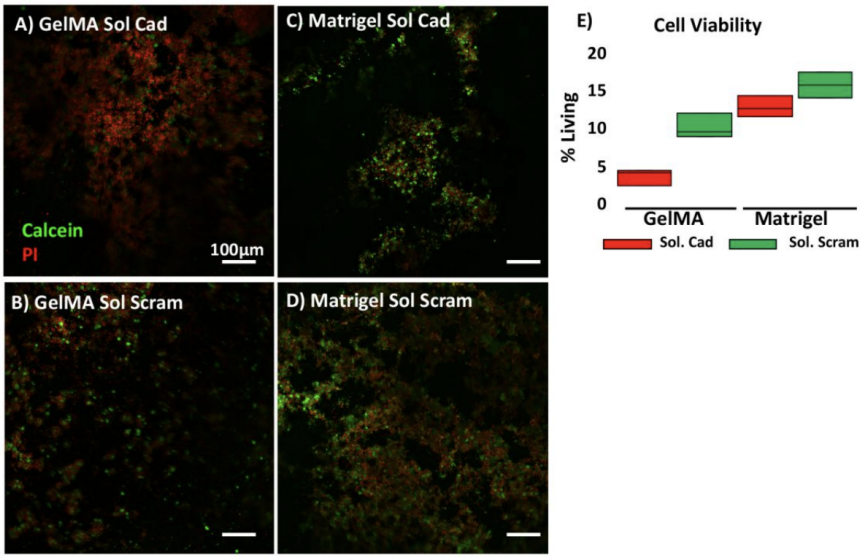

Figure 3.7: Soluble peptides in hydrogels do not support neuron viability. A-D) Representative images of neurons in GelMA and Matrigel hydrogels with soluble peptides. Calcein is used to visualize live cells and propidium iodide (PI) is used to visualize dead cells. Scale bars are the same for all images. E) Quantification of cell viability. Mean ±SD was calculated from 3 biological replicates, with 3 confocal z-stack images (200 μm depth) quantified per replicate.

Next, we monitored neurite projections from single-cell suspensions of the neurons embedded in either Matrigel or conjugated GelMA-Cad (referred to solely as GelMA-Cad from hereon) after 5 and 10 days using calcein. Neurite length and width are frequently employed as measures of neuron health and connectivity (161–165) and so we quantified Z-stack images of neurites using a custom MATLAB script (4). On day 5, relative to Matrigel, individual neurons embedded in GelMA-Cad exhibited significantly higher average neurite length (28.0 ±1.6 vs 14.1 ±2.6 μm; $p < 0.05$), where as average neurite width was not significantly different between GelMA-Cad and Matrigel (4.0 ±0.2 vs 3.7 ±0.2 μm) (Fig. 3.8. However, on day 10, relative to Matrigel, individual neurons in GelMA-Cad exhibited significantly higher average neurite length (67.2 ±3.2 vs 35.3 ±7.1 μm; $p<0.05$) and average neurite width (6.8 ±0.2 vs 3.9 ±0.2 ; $p<0.05$).

To determine if peptide concentration in the hydrogel affected neurite width and length, the cells were embedded in a 2:1 ratio hydrogel of GelMA-Cad/GelMA (66%) and 1:2 GelMA-Cad/GelMA (33%) (Fig. 3.9A-B). After 5 days, the cells were stained with calcein and again quantified for neurite length and width. In the 66% GelMA-Cad/GelMA hydrogels, the average neurite length and width were not significantly different compared to the average neurite length and width in the GelMA-Cad hydrogels (24.7 ±2.1 and 3.9 ±0.2 μm) (Fig. 3.9C-D). However, the cells embedded in 33% GelMA-Cad hydrogels exhibited significantly lower average length (17.5 ±2.4 μm; $p < 0.05$), whereas the average neurite width was not significantly different from the GelMA-Cad and 66% hydrogels (3.8 ±0.3 μm) (Fig. 3.9C-D). To determine if cell density affected

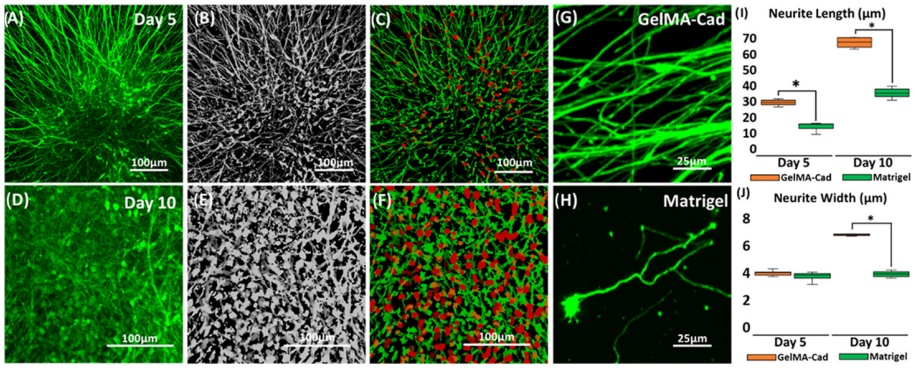

Figure 3.8: Quantification of neurites in the iPSC-derived neurons embedded in Matrigel and GelMA-Cad. Panels A-C demonstrate the quantification of neurites in GelMA-Cad on day 5, and panels D and E demonstrate the quantification of the neurites in GelMA-Cad on day 10. The neurons are stained with calcein (green) and imaged with a confocal microscope (A,D). Using custom MATLAB code as described in ref. (4), a mask is applied (B, E) and cell soma and neurites are identified (C, F), where red corresponds to the soma and green corresponds to neurite extension, which can then be measured and averaged across an image. G, H) Example of high resolution images of neurites in GelMA-Cad and Matrigel, where differences in neurite length and thickness can be observed. I, J) Full quantification of neurite length and width. Data are presented as mean ±SD from seven biological replicates, with four images quantified per biological replicate. Statistical significance was calculated using the Student's unpaired t-test (*$p<0.05$).

behavior in the hydrogel, seeding densities of $2x10^3$, $2x10^4$, and $2x10^5$ cells/mL were tested, followed by quantification of neurite length and width again at day 5 post embedding (Fig. 3.10). Here, the lengths (29.4 ±1.3, 27.4 ±1.6, 28.1 1.5 µm, respectively) and widths ((3.9 ±0.2, 3.9 ±0.2, 3.8 ±0.3 µm, respectively; Fig. 3.10) of neurites were not significantly different in the GelMA-Cad hydrogels as a function of cell density. Thus, these results demonstrate that GelMA-Cad is an effective hydrogel for enhancing survival and maturation of the singularized human iPSC-derived neurons by morphometric parameters regardless of the initial cell seeding density.

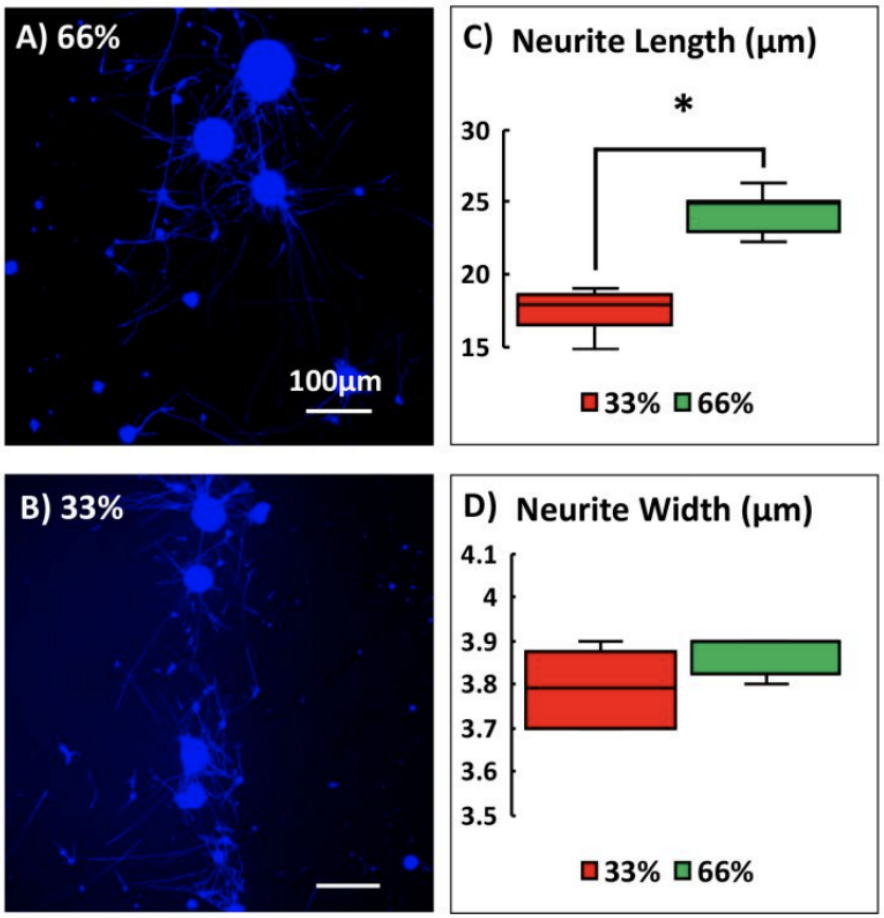

Figure 3.9: Influence of peptide density on neuron physical properties. A-B) Representative images of calcein-labeled neurons embedded in hydrogels with decreased amounts of N-cadherin peptide. The percentages in panels A and B refer to the ratio of GelMA-Cad to GelMA as detailed in the main text. Scale bars are the same for both images. C-D) Quantification of neurite length and width. Mean ±SD was calculated from 3 biological replicates, with 2 confocal z-stack images (100 µm depth) assessed per replicate. Statistical significance was calculated using the student's unpaired t-test (*p <0.05). The difference in neurite widths was not statistically significant.

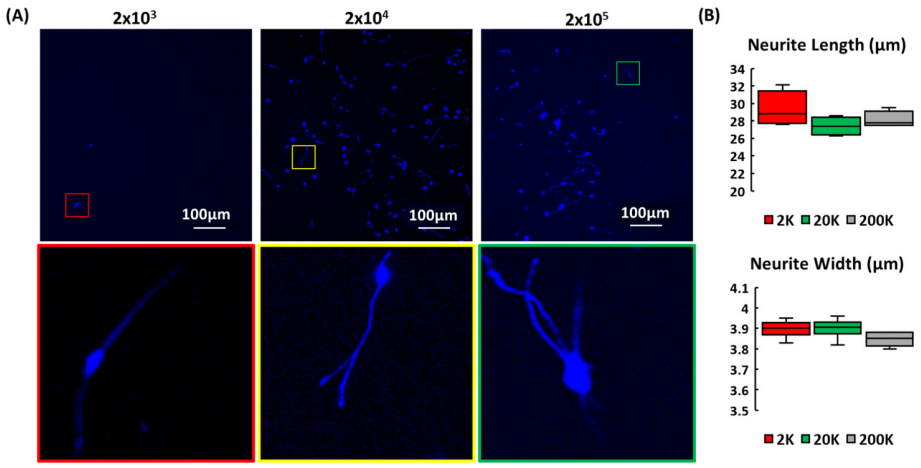

Figure 3.10: Influence of cell density on the neuron physical properties in GelMA-Cad. A) Representative images of the calcein-labeled neurons embedded in GelMA-Cad hydrogels at various cell densities. The numbers above each figure are the corresponding density (cells/mL). The scale bar is the same for all images. An inset is provided to highlight the morphology for each density. B) Quantification of neurite length and width. Mean ±SD was calculated from three biological replicates, with two confocal z-stack images (200 µm depth) assessed per replicate. No significant differences were measured as calculated using a one-way ANOVA with Tukey's post hoc test.

3.4.4 iPSC-Derived Glutamatergic Neurons Form Synaptically Connected Networks in GelMA-Cad Hydrogels

The increased length and width of neurites in GelMA-Cad suggested that the neurons are being conferred with improved functional properties, which we sought to validate with additional metrics including immunostaining, electrophysiological recordings, and viral synaptic tracing. First, we fixed and immunostained embedded neurons for synaptophysin (a presynaptic terminal marker) and PSD-95 (a postsynaptic terminal marker). The neurons embedded in GelMA-Cad expressed both markers 21 days after embedding (average of 492 synaptophysin puncta and 423 PSD-95 puncta per 75 μm^3), and there was an average colocalization of 87.3 ±1.3 %, which indicates the formation of active synapses (Fig. 3.11A). The neurons embedded in Matrigel had substantially lower expression of synaptophysin and PSD-95 (average of 82 puncta and 28 puncta per 75 μm^3, respectively), with only 13.3 ±3.3% colocalization of the presynaptic and postsynaptic markers (Fig. 3.11A), indicating a lower number of functional synapses. Next, to initially assess synaptic connectivity, we measured the electrical activity of the embedded neurons through extracellular field potential measurements. Action potentials were readily measured within the neurons embedded in GelMA-Cad (Fig. 3.11B, red line), but only minimal activity was observed in the Matrigel-embedded neurons (Fig. 3.11B, black line), thus providing evidence that the N-cadherin peptide improves functional maturity.

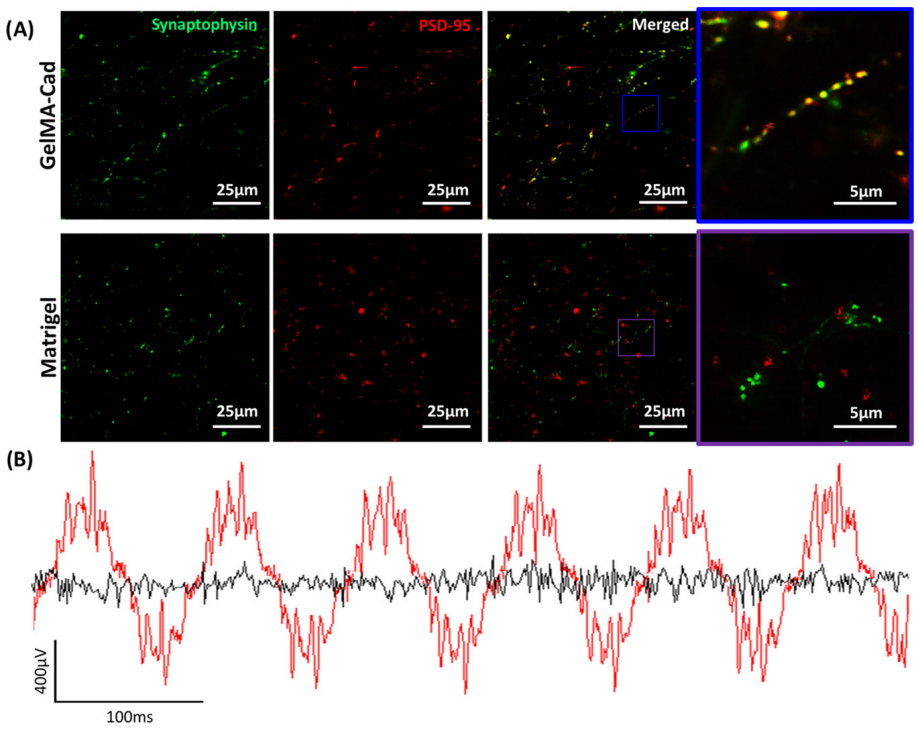

Figure 3.11: Assessment of synaptic connectivity of the iPSC-derived neurons in Matrigel or GelMA-Cad by immunostaining and electrophysiology. (A) Immunostaining of synaptophysin (green) and PSD-95 (red) in the neurons that were embedded in each hydrogel for 21 days. An inset is provided to highlight pronounced differences. Tex images from 3 biological replicates were used for quantification, and statistical significance was calculated using the Student's unpaired t-test. (B) Extracellular field potential measurements for the neurons embedded in GelMA-Cad (red) and Matrigel (black) for 21 days. Voltage traces are representative of 5 biological measurements.

Finally, we conducted synaptic tracing experiments by transducing iPSC-derived neurons with an adeno-associated virus (AAV) encoding EGFP under the control of the human synapsin promoter (where synapsin is a presynaptic terminal marker). Wild-type neurons were mixed with the hydrogel precursor, and prior to cross-linking the hydrogels, a small population of AAV-transduced neurons (1:100 ratio of the transduced to nontransduced neurons) was injected into the center (Fig. 3.12). The spread of the EGFP signal could thus be monitored over time to demonstrate functional synaptic connections. Limited EGFP spread was observed after 7 days, which is consistent with Figure 3.8, demonstrating that neurite length and width are still increasing at this early time point. However, after 21 days, EGFP had propagated to many neurons within the GelMA-Cad hydrogels, whereas sparse EGFP spread was observed in Matrigel (Fig. 3.12). Calcein dye was added to each hydrogel to show that the neurons in Matrigel were alive but not synaptically connected. Quantification of EGFP and calcein colocalization further highlighted this outcome (89 ±0.3% colocalization in GelMA-Cad vs 21 ±0.2% colocalization in Matrigel; $p < 0.0001$). Therefore, only the neurons in the GelMA-Cad hydrogels were able to propagate the virus through functional synapses across the entire tissue

construct. Overall, these data strongly suggest that GelMA-Cad facilitates the maturation of the iPSC-derived neurons on a functional level.

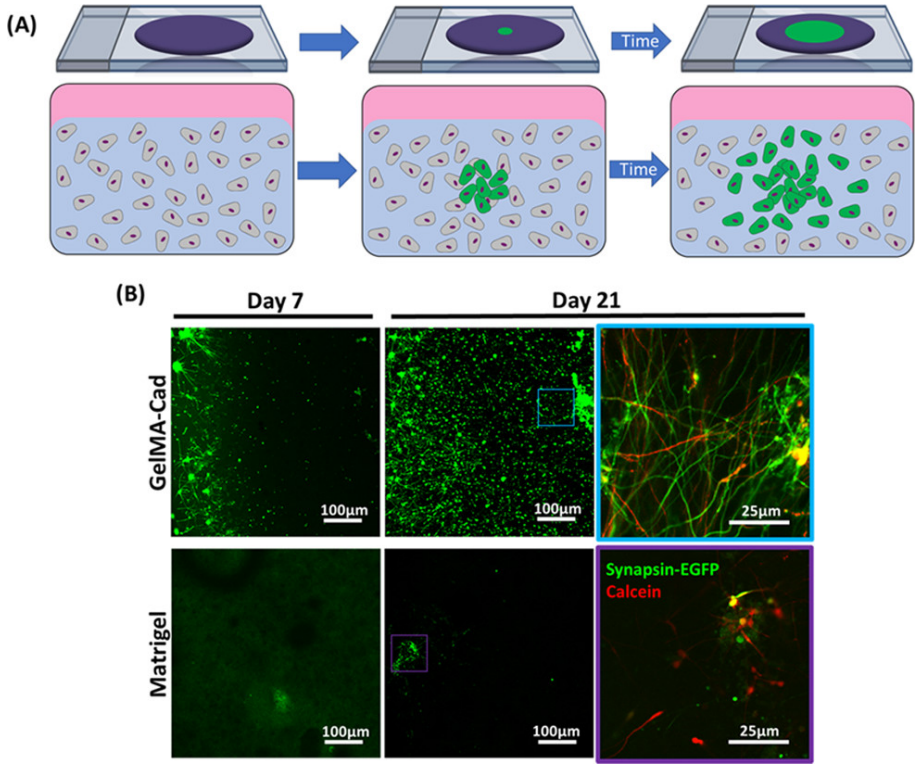

Figure 3.12: Assessment of the synaptic connectivity of the iPSC-derived neurons in Matrigel or GelMA-Cad by viral tracing. (A) Schematic depicts the experimental approach, where the wild-type neurons were uniformly mixed in a hydrogel and a small population of AAV-transduced neurons was injected into the center. (B) Representative images of EGFP on day 7 and day 21. Calcein (red) was added on day 21 to verify cell viability and is shown in the insets. Colocalization of EGFP and calcein was quantified on day 21 in compressed z-stacks imaged across 6 biological replicates (1 image per replicate). A Student's unpaired t-test was used to assess statistical significance.

3.5 Discussion

In native tissues, cells are surrounded by a complex ECM that presents both physical and biochemical cues for tissue development, migration, and proliferation (166). In the brain, the neurons are encased in a soft ECM comprised of various proteins and glycosaminoglycans (GAGs). Many ECMs, as described earlier, have been tested for their ability to support 3D in vitro cultures of neural cells. Several studies have focused on the effect of ECM stiffness and composition on the differentiation of NPCs to terminally differentiated progenies (167; 168), but relatively fewer have examined functional maturation and integration of neurons, particularly those derived from hPSCs. hPSC-derived neurons are notoriously difficult to mature in two-dimensional (2D) without extended culture times or co-culture with astrocytes (164; 169), though more success has been observed in 3D assembly (9). In particular, hydrogels comprised of methacrylated HA

can facilitate the maturation of iPSC-derived neurons to an electrophysiologically active state (61), which is perhaps unsurprising given that HA is the most abundant GAG in the brain tissue. Yet, as mentioned previously, HA has limitations that make it less attractive for either large-scale work or applications requiring patterned structures.

Our approach to these challenges was to use a relatively simple ECM material (GelMA, a well-established biomaterial known to support primary neural cells in 3D matrices (150)) and append it with a biophysical cue to mimic cell–cell communication in the developing and adult brain. N-cadherin was chosen for several reasons. From a biomaterials perspective, the N-cadherin extracellular epitope had already been incorporated into HA gels and shown to be bioactive for cartilage tissue engineering, so it was straightforward to incorporate this epitope into GelMA. Moreover, tethering of an N-cadherin peptide to a solid support had previously been shown to improve neuronal survival and neurite outgrowth of stem cell-derived neurons in 2D cultures (73–75), suggesting relevance for our work in 3D scaffolds. From a biochemical perspective, N-cadherin expression is important for the outgrowth of the neurites on astrocyte monolayers, and given that hPSC-derived neurons are typically cultured on 2D monolayers of astrocytes to facilitate electrophysiological maturation (72), we suspected that GelMA-Cad could partially replace the synaptogenic role of astrocyte co-culture. Cadherins also regulate dendritic spine morphology (71) and N-cadherin-mediated interactions are specifically required for maintenance of dendrites (70), which is particularly interesting because we observed an especially pronounced increase in the expression of postsynaptic terminal markers on the neurons in GelMA-Cad relative to Matrigel. Thus, we believe that GelMA-Cad may specifically enhance synapse formation in iPSC-derived neurons by facilitating postsynaptic terminal maturation. This is a key difference between the GelMA-Cad hydrogels and most other ECM-based hydrogels used for neural tissue engineering (170), which typically seek to mimic key cell–ECM interactions rather than replace key cell–cell interactions.

One confounding variable in our study is that the stiffnesses of the GelMA-Cad and control hydrogels were not perfectly matched. Our rheology measurements suggest that bulk GelMA-Cad hydrogels are 50% stiffer than the controls. These measurements contrast somewhat with the localized stiffness measurements performed by AFM, where the average stiffnesses are similar to the rheology measurements, but the differences are not statistically significant. In general, we would expect AFM to detect more subtle differences in stiffness at the nanoscale, which may be more representative of the stiffness that the neurons would sense within the hydrogel. Furthermore, because Matrigel hydrogels are softer than GelMA and GelMA-Scram (previously measured at 20–300 Pa by rheology and 443 Pa by AFM (171; 172)), we believe that the Cad peptide has a greater impact on neuron survival and maturation compared to the hydrogel mechanics. Overall, because the stiffness of GelMA-Cad should be tunable through the degree of photopolymerization, we expect to address this limitation in future studies where hydrogel mechanics can be more similarly matched between

all conditions.

It is also possible that the gelatin backbone of GelMA-Cad augments neuron health and survival. Gelatin-based hydrogels can be neuroprotective and promote neurite outgrowth through integrin activation and integrin-dependent MAPK signaling (70). Gelatin also improves in vivo outcomes in dissected nerve regeneration, particularly through increased axonal migration (173–175). Recent work has further shown that GelMA alone can support dissociated primary mouse neurons to create a synaptically connected neural network on the micron scale (63). This finding contrasts somewhat with our observations of neuron death in GelMA and GelMA-Scram. However, beyond the obvious species differences, we note that this prior study utilized neurons that had already matured in vivo. Thus, the primary neurons may have been competent enough to form neural networks in GelMA because they already expressed the requisite synaptic machinery, rather than requiring de novo expression of this machinery in the hPSC-derived neurons developing from a more embryonic-like state. Furthermore, our study utilized neurons that were enzymatically dissociated into single-cell suspensions, whereas these primary neuron suspensions were manually dissociated and therefore were likely to retain crucial cell–cell interactions during encapsulation. Our observation of ubiquitous cell death of single-cell neuron suspensions in GelMA and GelMA-Scram at lower densities (1 x 10^7 cells/mL in the aforementioned study (63) versus 2 x 10^5 cells/mL in this study) supports the notion that these cell–cell interactions are key for survival. Likewise, the ability of GelMA-Cad to support the survival of the singularized neurons at low encapsulation densities, followed by robust neurite outgrowth, suggests that the peptide epitope in GelMA-Cad also supports cell adhesion and recapitulates crucial cell–cell interactions in addition to its ability to promote synaptic connectivity. It is possible that addition of other peptide epitopes, such as the well-characterized IKVAV found in laminin (176) or Arg-Gly-Asp (RGD) adhesion motifs (to augment the endogenous RGD motifs found in gelatin), could further enhance the properties of GelMA-Cad.

3.6 Conclusion

Overall, our work provides an exciting scaffolding material for future efforts devoted to assembling complex neurovascular tissue structures. If N-cadherin signaling is a general mechanism for synaptic integration, we speculate that multiple iPSC-derived neuronal cell types could be patterned into complex architectures that would be subsequently directed by the ECM to form relevant neural circuitry. The inclusion of iPSC-derived astrocytes and microglia could further be used to study synaptic pruning and remodeling under healthy and diseased conditions. Then, given the mechanical integrity of GelMA-Cad hydrogels, various micropatterning approaches could be used to generate perfusable channels seeded with endothelial and mural cells, ultimately resulting in functional vasculature throughout the human neural networks. The bioactivity of GelMA-Cad, coupled to its relatively low cost and ease of synthesis, should make it attractive for the aforementioned

applications, as well as other situations throughout bioengineering and neuroscience.

3.7 Appendix

3.7.1 Neurite Quantification Code

Function files for MATLAB code used for quantification (Figs. 3.13,3.14, 3.15, 3.16, 3.17, 3.18). This code inputs RGB .TIFF files of each image in a slice and outputs a table of the neurite measurements and cell counts.

`detect, segment, measure, export_data`

Figure 3.13: master.m

```
clear
directory=uigetdir;
files=dir(directory);
[~, name] = fileparts(directory);
sm=ones(3)/9;
s=ones(50)/(50^2);
comp=[];
z=0;
zmax=0;
for o=1:length(files)
    if length(files(o).name)>4
        if strcmp(files(o).name(end-3:end),'.tif')
            zmax=zmax+1;
        end
    end
end
stack=[];
for o=1:length(files)
    if length(files(o).name)>4
        if strcmp(files(o).name(end-3:end),'.tif')
            z=z+1;
            raw=imread([directory,'/',files(o).name]);
            f=double(raw(:,:,2));
            f=conv2(f,sm,'same');
            f=f-min(f(:));
            f=f/max(f(:));
            fs=conv2(f,s,'same');
            fp=f-fs;
            fp=fp(51:end-50,51:end-50);
            err=[];
            fc=fp>0.05;
            fc=double(bwareaopen(fc,10));
            stack(:,:,end+1)=fc;
            if z==1
                comp=fc*(z+zmax/10)/(zmax*1.5);
                maxint=f;
            else
                comp(fc(:)>0)=fc(fc(:)>0)*(z+zmax/10)/(zmax*1.5);
                maxint(f(:)>maxint(:))=f(f(:)>maxint(:));
            end
            imshow(comp), title('Detecting Neurons'), pause(0.01)
        end
    end
end
binstack=comp;
```

Figure 3.14: export_data.m

```
bins=10:10:100;
ao=bins*0;
for i=1:length(bins)
    ao(i)=mean(orientation(logical((radius<bins(i)).*(radius>(bins(i)-10)))));
end
plot(bins,ao)
```

Figure 3.15: map_orientation.m

```
clear
directory=uigetdir;
files=dir(directory);
[~, name] = fileparts(directory);
sm=ones(3)/9;
s=ones(50)/(50^2);
comp=[];
z=0;
zmax=0;
for o=1:length(files)
    if length(files(o).name)>4
        if strcmp(files(o).name(end-3:end),'.tif')
            zmax=zmax+1;
        end
    end
end
stack=[];
for o=1:length(files)
    if length(files(o).name)>4
        if strcmp(files(o).name(end-3:end),'.tif')
            z=z+1;
            raw=imread([directory,'/',files(o).name]);
            f=double(raw(:,:,2));
            f=conv2(f,sm,'same');
            f=f-min(f(:));
            f=f/max(f(:));
            fs=conv2(f,s,'same');
            fp=f-fs;
            fp=fp(51:end-50,51:end-50);
            err=[];
            fc=fp>0.05;
            fc=double(bwareaopen(fc,10));
            stack(:,:,end+1)=fc;
            if z==1
                comp=fc*(z+zmax/10)/(zmax*1.5);
                maxint=f;
            else
                comp(fc(:)>0)=fc(fc(:)>0)*(z+zmax/10)/(zmax*1.5);
                maxint(f(:)>maxint(:))=f(f(:)>maxint(:));
            end
            imshow(comp), title('Detecting Neurons'), pause(0.01)
        end
    end
end
binstack=comp;
```

Figure 3.16: detect.m

```
[x,y,z]=size(stack);
temp=permute(stack,[3,2,1]);
temp=sum(temp);
temp=permute(temp,[3,2,1]);
imshow(temp), title('Identifying Cell Bodies'), pause(0.01)
ss=sum(stack(:));
r=1;
tst=1;
while sum(tst(:))>0
    tst=stack;
    for i=1:z
        tst(:,:,i)=imerode(tst(:,:,i),strel('disk',r));
        tst(:,:,i)=imdilate(tst(:,:,i),strel('disk',r));
    end
    temp=permute(tst,[3,2,1]);
    temp=sum(temp);
    temp=permute(temp,[3,2,1]);
    imshow(temp), title('Identifying Cell Bodies'), pause(0.01)
    ss(end+1)=sum(tst(:));
    r=r+1;
end
dss=-diff(ss);
[~,mi]=max(dss);
r=mi+1;
tst=stack;
for i=1:z
    tst(:,:,i)=imerode(tst(:,:,i),strel('disk',r));
    tst(:,:,i)=imdilate(tst(:,:,i),strel('disk',r));
end
bodies=tst.*stack;
for j=1:5
    for i=1:z
        if i>1
            bodies(:,:,i)=bodies(:,:,i)+bodies(:,:,i).*bodies(:,:,i-1);
            bodies(bodies(:)>1)=1;
        end
        if i<z
            bodies(:,:,i)=bodies(:,:,i)+bodies(:,:,i).*bodies(:,:,i+1);
            bodies(bodies(:)>1)=1;
        end
    end
end
axons=stack-bodies;
for i=1:z
    axons(:,:,i)=bwareaopen(axons(:,:,i),50);
    axons(:,:,i)=imdilate(axons(:,:,i),strel('disk',2));
    axons(:,:,i)=imerode(axons(:,:,i),strel('disk',2));
end
comp=[];
for i=1:z
    if i==1
        comp(:,:,1)=bodies(:,:,i)*(i+z/10)/(z*1.5);
        comp(:,:,2)=axons(:,:,i)*(i+z/10)/(z*1.5);
        comp(:,:,3)=0;
    else
        rp=bodies(:,:,i);
        ru=find(rp(:)>0);
        temp=comp(:,:,1);
        temp(ru)=rp(ru)*(i+z/10)/(z*1.5);
        comp(:,:,1)=temp;
        gp=axons(:,:,i);
        gu=find(gp(:)>0);
        temp=comp(:,:,2);
        temp(gu)=gp(gu)*(i+z/10)/(z*1.5);
        temp=temp-0.5*comp(:,:,1);
        temp(temp(:)<0)=0;
        comp(:,:,2)=temp;
    end
    imshow(comp), title('Segmenting Image'), pause(0.1)
end
colstack=comp;
```

Figure 3.17: segment.m

```
L=[];
W=[];
A=[];
N=[];
radius=[];
orientation=[];
alength=[];
plane=[];
xs=zeros(x);
ys=zeros(y);
for i=1:x
    for j=1:y
        xs(i,j)=i;
        ys(i,j)=j;
    end
end
for i=1:z
    slice=axons(:,:,i);
    spots=bodies(:,:,i);
    if i==1
        orsh=spots*(i+z/10)/(z*1.5);
    else
        temp=orsh(:,:,1);
        temp(spots(:)==1)=spots(spots(:)==1)*(i+z/10)/(z*1.5);
        orsh(:,:,1)=temp;
    end
    ib=bwconncomp(spots);
    N(i)=ib.NumObjects;
    ib.xc=[];
    ib.yc=[];
    for b=1:ib.NumObjects
        ib.xc(b)=mean(xs(ib.PixelIdxList{b}));
        ib.yc(b)=mean(ys(ib.PixelIdxList{b}));
    end
    ia=bwconncomp(slice);
    se=edge(slice);
    me=sum(se(:))/ia.NumObjects;
    ma=sum(slice(:))/ia.NumObjects;
    mean_length=(me+sqrt(me^2-16*ma))/4;
    mean_width=ma/mean_length;
    L(i)=mean_length;
    W(i)=mean_width;
    A(i)=sum(slice(:));
    lines=bwmorph(slice,'skel',Inf);
    lraw=lines;
    ints=bwmorph(lines,'branchpoints');
    ints=imdilate(ints,strel('disk',1));
    lines=lines-ints;
    lines(lines<0)=0;
    lines=bwareaopen(lines,10,8);
    il=bwconncomp(lines,8);
    com=xs*0;
    for l=1:il.NumObjects
        x0=xs(il.PixelIdxList{l}(1));
        y0=ys(il.PixelIdxList{l}(1));
        x1=xs(il.PixelIdxList{l}(end));
        y1=ys(il.PixelIdxList{l}(end));
        xd=x0-x1;

        yd=y0-y1;
        xc=mean(xs(il.PixelIdxList{l}));
        yc=mean(ys(il.PixelIdxList{l}));
        rs=((xc-ib.xc).^2+(yc-ib.yc).^2).^0.5;
        [rm,mi]=min(rs);
        com(il.PixelIdxList{l})=2*rm/x;
        xr=xc-ib.xc(mi);
        yr=yc-ib.yc(mi);
        thetar=abs(atan(yr/xr))*180/pi;
        thetad=abs(atan(yd/xd))*180/pi;
        radius(end+1)=rm;
        orientation(end+1)=abs(thetar-thetad);
        alength(end+1)=length(il.PixelIdxList{l});
        plane(end+1)=i;
    end
    if i==1
        orsh(:,:,2)=lines*(i+z/10)/(z*1.5);
    else
        temp=orsh(:,:,2);
        temp(lines(:)==1)=lines(lines(:)==1)*(i+z/10)/(z*1.5);
        orsh(:,:,2)=temp;
    end
    if i==1
        orsh(:,:,3)=com;
    else
        temp=orsh(:,:,3);
        temp(com(:)==1)=com(com(:)==1);
        orsh(:,:,3)=temp;
    end
    orsh(:,:,3)=0;
    imshow(orsh), title('Skeletonizing Axon Network'), pause(0.1)
end
skelstack=orsh;
```


Figure 3.18: measure.m

CHAPTER 4

Examining the Effects of N-Cadherin density and Scaffold Stiffness on 3D Stem Cell-Derived Neuronal Models

4.1 Summary

Extracellular cues are known to be important to the development of the human brain. One important cue is N-cadherin signaling from cell-cell contacts. Previous *in vivo* and *in vitro* studies have shown that reduction of N-cadherin signaling promotes neurogenesis, which reduces the stem cell pool and increases the neuronal population. In a previous study, we developed a novel hydrogel in which N-cadherin peptides are conjugated to methacrylated gelatin (termed GelMA-Cad), and we showed that GelMA-Cad can support synaptically connected stem cell-derived neurons in 3D. In this study, we build on this previous study to examine the effects of N-cadherin density on 3D neuronal cultures. Induced pluripotent stem cell-derived glutamatergic neurons were embedded in hydrogels with varying amounts of N-cadherin peptide conjugation. We measured the neurite width and lengths over at 1 and 2 weeks, and found that the lowest N-cadherin presence results in the longest and widest neurites after 2 weeks of culture. However, when we stained the neurons for pre- and post-synaptic markers, all the neurons form similar amounts of functional synapses after 2 weeks. Overall, this study demonstrates that while N-cadherin presence can affect neurite projections of embedded neurons, the cells retain their functionality in all iterations of GelMA-Cad hydrogels.

4.2 Background

The brain extracellular matrix (ECM) is known to be important to the development and function of the brain. Early studies show that ECM stiffness can affect the differentiation of stem cells into different cell types (177). Additionally the components of the ECM can influence cell differentiation and maturation. For example, in the brain, the components of the ECM will change around synapses in order to support the function of the synapses (57). Furthermore, cell-cell adhesion molecules, such as N-cadherin, can influence the cell fates of the surrounding cells. N-cadherin is known to be expressed in the neuroepithelium during development, where it plays a variety of roles including supporting structural integrity, influencing cell migration, and contributing to synapse development (178). This molecule also plays an important role in maintaining neural progenitors through the regulation of β-catenin signaling (179). In one study, N-cadherin knockdown reduced the differentiation of cortical neural precursors in rat primary cultures and mice (179). When N-cadherin expression is reduced, β-catenin signaling is also reduced; since this signaling pathway regulates exit from the cell cycle, the reduction of β-catenin signaling influences cell differentiation. The researchers

found that reduction of β-catenin signaling increased cell migration in the cortex and neuronal differentiation. When the N-cadherin/β-catenin signaling is restored, the progenitor population was rescued (179).

The utilization of N-cadherin *in vitro* may help researchers build better stem cell-derived models by influencing the populations they are interested in studying and further elucidating the role of N-cadherin on neuronal maturation. The use of N-cadherin to coat surfaces to support neuronal cultures has been well established in 2D *in vitro* cultures (73–75) One study of 2D stem cell-derived neuronal cultures demonstrated that reduction of N-cadherin coating on tissue culture plates supports neurogenesis and neurite projections (73). Furthermore, the neurons in lower N-cadherin presence had higher expressions of MAP2 protein, which the researchers use as an approximation of neuronal maturation (73; 74). These studies further emphasize the interplay between N-cadherin expression and neuronal differention from progenitors. However, the influence of N-cadherin density has not been studied in 3D *in vitro* neuronal cultures, which have an additional layer of complexity when compared to 2D cultures.

In a previous study, we demonstrated that N-cadherin peptides can be conjugated to methacrylated gelatin (GelMA) in order to create a novel, bio-instructive biomaterial, coined GelMA-Cad (2). This study showed that single-cell suspensions of induced pluripotent stem cell (iPSC)-derived cortical glutamatergic neurons can form synaptically connected networks in GelMA-Cad, which addresses a major limitation of 3D iPSC-derived neuronal models. In this paper, we describe how the GelMA-Cad synthesis protocol can be altered to increase the conjugation efficiency of N-cadherin to GelMA. Additionally, we further investigate how scaffold stiffness and N-cadherin density affect 3D iPSC-derived neuronal cultures, which can help provide a framework for understanding how to manipulate GelMA-Cad to support the desired 3D neuronal models.

4.3 Methods

4.3.1 Cell Culture

CC3 iPSCs (148) were maintained in Essential 8 (E8) medium on standard tissue culture plates coated with growth-factor reduced Matrigel (VWR). At 60-70% confluency, the cells were replated using Versene (Thermo Fisher) as previously described (149).

Stem cells were differentiated into cortical glutamatergic neurons using a previously described protocol (47) with some modifications (Fig. 3.1). iPSCs were washed once with PBS and dissociated by incubation with Accutase (Thermo Fisher) for 3 minutes. Following collection by centrifugation, the cells were replated onto Matrigel-coated plates at a density of 2.5 x 10^2 cells/cm^2 in E8 medium with 10 μM Y27632 (Tocris). The next day, the medium was changed to Essential 6 (E6) medium (149) supplemented with 10 μM SB431542 (Tocris) and 0.4 μM LDN1931189 (Tocris) for 5 days as previously described (46). Over the next 5 days, the medium was gradually transitioned from E6 medium to N2 Medium (DMEM/F12 basal

medium (Thermo Fisher) and 1x N2 supplement (Gibco)) supplemented with 10 μM SB431542, and 0.4 μM LDN1931189 (46). On the 11th day of the differentiation protocol, the resultant neural progenitors were dissociated by incubation with Accutase for 30 minutes and passed onto Matrigel in Neuron Medium with 10 μM Y27632. Neuron Medium was made by miaxing a 1:1 ratio of N2 Medium and B27 Medium (Neurobasal Medium (Thermo Fisher), 200 mM Glutamax (Gibco), and 1X B27 supplement (Gibco)) (47). The cells received fresh Neuron Medium every day for the next 20 days and then a media change every 3-4 days afterward. Glutamatergic neurons were used for experiments between days 70 and 100 of differentiation.

4.3.2 GelMA Synthesis and Characterization

Methacrylated gelatin (GelMA) was synthesized as described previously (150). Type A procine skin gelatin (Sigma) was mixed at 10% (w/v) into DI water (sourced from an in-house Continental Modulab ModuPure reagent grade water system) at 60°and stirred until fully dissolved. Methacrylic anhydride (MA, Sigma) was slowly added to the gelatin solution and stirred at 50°for 3 hours. The solution was then centrifuged at 3,500*g* for 3 minutes, and the supernantant was collected. Following a 5x dilution with additional warm (40°C) UltraPure water (Thermo Fisher) to stop the reaction, the mixture was dialyzed against DI water for 1 week at 37 °using a 12-14 kDa cutoff dialysis tubing (Fisher) to remove salts and methacrylic acid. The pH of the solution was then adjusted to 7.25-7.45 by adding 1.0 M HCl or 1.0 M NaOH as measured with a Thermo Fisher Scientific Orion Star pH meter. The resulting GelMA solution was lyophilized for 3 days using a Labconco lyophilizer and stored at -20°.

4.3.3 Peptide Conjugation

Peptides were conjugated to GelMA as previously reported (64) with slight modifications (Fig. 3.2). Briefly, GelMA was reconstituted in triethanolamine buffer (TEOA, Sigma) to create a 10% (w/v) solution and stirred at 37°for 2 hours until fully dissolved. The pH of the solution was then adusted to 8.0-8.5 by adding 1.0 M HCl or 1.0 M NaOH. N-cadherin mimic (Ac-HAVDIGGGC) peptides (GenScript) were added to the GelMA/TEOA buffer to form a 0.1% (w/v) solution. The cystine residue at the C-terminal end of the peptides permited a Michael-type addition reaction with GelMA (64). The solution was stirred at 37°for 24 hours. GelMA-Cad was dialyzed using a Tangential Flow Filtration (TFF) system. Briefly, the hydrogels were diluted in MilliQ UltraPure water and stirred at 37°. The resulting solution was pumped through a 2 kDa TFF filter (Satorius) using a peristaltic pump (Cole Parmer) for 5 hours. Additional MilliQ water was added to the diluted hydrogel solution every hour to facilitate filtering.

The pH of the dialyzed hydrogel was then adjusted to 7.35-7.45 by adding 1.0 M HCl or 1.0 M NaOH, and the solution was lyophilized and stored at -20°. Hydrogel was stored for up to 6 months in the freezer.

4.3.4 Nuclear Magnetic Resonance Spectroscopy

Conjugation was routinely verified through ^{1}H-NMR using a Bruker 500 Hz NMR spectrometer set to 37°for the prescence of the amino acid valine. The degree of functionalization of the methacrylic side chains to the gelatin backbone was determined by taking the integral of the lysine peak (2.8-3.0 ppm) of gelatin, normalizing the GelMA spectra to the integral of the gelatin aromatic amino acid (7.2-7.4 ppm), and calculating the percent degree in the lysine peak (151; 152). The degree of functionalizatio of the peptides to GelMA was calculated by normalizing the integral of the valine peak (3.5 ppm) to the integral of the gelatin aromatic amino acid.

4.3.5 Atomic Force Microscopy

GelMA, GelMA-Scram, and GelMA-Cad were reconstituted and polymerized into hydrogel discs, as described in the cell seeding section below. A Bruker Dimension Icon Atomic Force Microscope was used to measure hydrogel stiffness. 0.01 N/M Novascan probes containing a 4.5 µm polystyrene bead ((PT.PS.SN.4.5.CAL) were used to measure 3 distinct 5 x 5 µm^2 areas of each hydrogel. Three hydrogel disc replicates of each sample were utilized, with a total of 576 stiffness measurements per sample. For each individual force curve, a first-order baseline correction was performed, and the Hertzian model was used to calculate Young's modulus. For tool calibration, polyacrylamide hydrogels were prepared as previously reported (153) and measured prior to GelMA and its derivatives.

4.3.6 Fabrication and Seeding of Hydrogels

GelMA-Cad was reconstituted in Neurobasal Medium to make a 10% (w/v) solution with 0.05% LAP initiator. iPSC-derived neurons were detached from 12-well plates via a 5 minute incubation with Accutase and centrifuged for collection. The glutamatergic neurons were mixed with a reconstituted hydrogel/initator solution to achieve a density of 2 x 10^3, 2 x 10^4, 2 x 10^5 cells/mL depending on the experiment. Once the solutions were prepared they were mixed thoroughly with a P1000 pipette to break up any cell clumps. Next, 100 µL of the cell suspension was added to each well of a glass bottom 24-well plate. These hydrogels were then exposed to 25 mW/cm^2 UV light for 16 seconds and set aside for 20 minutes at room temperature. 1 mL of Neuron Medium was then added to each well.

GelMA-Cad was mixed with GelMA to create a 1:2 ratio (2X GelMA-Cad), 1:2 ratio (1X GelMA-Cad), 2:7 ratio (0.66X GelMA-Cad), and 1:8 ratio (0.33X GelMA-Cad). These hydrogels were seeded with glutamatergic neurons at a a density of 2 x $10^{5\cdot}$ cells/mL.

To embed the neurons in Matrigel, 1 mL of Matrigel aliquots was thawed on ice. Once thawed, the neurons were embedded at a density of 2 x 10^5 cells/mL, and 100 µL of the solution was added directly onto

the coverslips in a 12-well plate. The plate containing the Matrigel discs was placed in an incubator at 37°to cross-link for 30 minutes. After the Matrigel was fully cross-linked, 1 mL of Neuron Medium was added to each of the wells.

For all experiments involving hydrogels, once the neurons were encapsulated, the media was changed every 3-4 days until the cells were used.

4.3.7 Live/Dead Cell Imaging

To assess long-term cell viability, hydrogel discs were incubated with CytoCalcein Violet 450 (AAT Bioquest) and propidium iodide (PI, Thermo Fisher) for 1 hour. The staining was performed at 48 hours, 72 hours, 5 days, and 10 days following embedding. The hydrogel discs were imaged using a Zeiss 710 confocal microscope, and cell viability was quantified using ImageJ. Following imaging, 1 mL of Neuron Medium was added to each well to dilute any remaining Calcein/PI from the hydrogels.

4.3.8 Neurite Projection Quantification

Raw data were exported in a 16-bit TIF format and imported into MATLAB 2017 for quantification using a custom image analysis script. Briefly, the images were smoothed using a 3 x 3 pixel smoothing filter to mitigate image noise, and in-focus neurite segments were identified by isolating the regions at least 5% brighter than the mean pixel intensity in the surrounding 50 pixel radius (154). Cell bodies and neurites were distinguished by successive erosion of the resulting binary mass. The erosion radius at which the total cell mass declined most steeply was used to define the radius required to erode neurites while sparing cell bodies. Following segmentation of neurites and cell bodies, algorithms previously developed for analysis of mitochondrial networks (4) were used to measure the average length and width of each neurite segment. Code can be found in Section 3.7.1.

4.3.9 Immunfluorescence

After 2 weeks of culture, neurons embedded in hydrogels were fixed in 4% PFA (Sigma) for 20 minutes and then washed 3 times with PBS. A solution of 5% goat serum and 0.03% Triton X-100 (Thermo Fisher) was then added to the hydrogels overnight on a rocking platform at room temperature. The hydrogels were then incubated overnight with 4,6-diamidino-2-phenylindole (DAPI) or fluorescently conjugated primary antibodies: βIII tubulin Alexa Fluor 647 (Abcam ab190575), PSD-95 Alexa Fluor 488 (Novus Biologicals NB300556AF488), and/or synaptophysin Alexa Fluor 555 (Abcam ab206870). The hydrogels were then imaged using a 40x objective on a Zeiss LSM 710 confocal microscope. Colocalization of the two markers was quantified using Zeiss Zen Black software.

4.4 Results

4.4.1 Using Tangential Flow Filtration Improves Conjugation Efficiency of Hydrogels

In a previously published paper (2), we demonstrated that 2 sequential Michael-type addition reactions can be used to create GelMA hydrogels biofunctionalized with N-cadherin peptides. We also compared GelMA-Cad to other scaffolds and showed that GelMA-Cad can greatly improve 3D iPSC-derived neuronal cultures. However, the synthesis of this hydrogel can be time consuming as it can take up to a week to move through the process of conjugating the N-cadherin peptide to GelMA and filtering the resulting solution through dialysis. This dialysis step removes any unconjugated peptide and byproducts of the Michael-type addition reaction out from the hydrogel solution. The original sythesis protocol of GelMA-Cad involved manually replacing the DI water to promote osmosis and filtering. By switching to a tangential flow filtration system (TFF), which uses a peristaltic pump to actively filter the hydrogel solution (180), the dialysis time can be shortened from 1 week to just 4 hours, shortening the peptide conjugation protocol to 1 day. Furthermore, when the conjugation efficiencies were confirmed through ^{1}H NMR spectroscopy, we found that TFF dialysis results in 3 times as much peptide conjugated to GelMA-Cad than the original synthesis protocol (Fig. 4.1A). Futhermore, when the hydrogels were measured with AFM, we confirmed that increased peptide conjugation did not significantly affect the stiffness of the hydrogels (Fig. 4.1B). Henceforth, we will refer to the peptide density achieved with TFF dialysis as 3X GelMA-Cad and the peptide density achieved achieved with the original, manual dialysis as 1X GelMA-Cad. All other GelMA-Cad conditions represented the N-cadherin density created when diluted with 3X GelMA-Cad and GelMA as described in the Methods section.

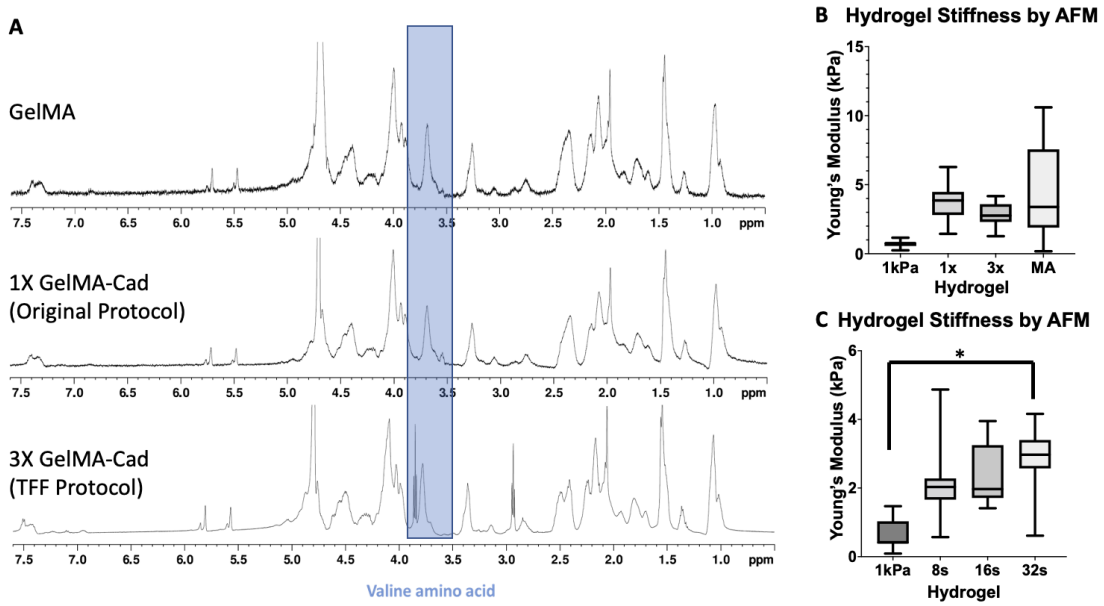

Figure 4.1: Tansgential flow filtration (TFF) increases peptide conjugation A) NMR spectra of gelatin, GelMA, GelMA-Cad synthesis with manual dialysis (1X GelMA-Cad, original protocol), and GelMA-Cad with TFF dialysis (3X GelMA-Cad). Successful conjugation of MA to the gelatin backbone was assessed by peaks at 5.5 and 5.7 ppm, and N-cadherin/scram peptide addition was assessed by the valine peak at 3.5 ppm. The area under the peak represents the amount of conjugation. AFM measurements comparing synthesis protocols (B) and hydrogel stiffness (UV crosslinking times, C). There was no significant difference among the different GelMA-Cad synthesis protocols or hydrogel crosslinking times. Statistical significance was calculated using a one-way ANOVA with posthoc Tukey test (*p $<$0.05).

4.4.2 N-cadherin peptide density plays a role in neuronal maturation in 3D

After confirming that TFF dialysis significantly increases the conjugation efficiency of the GelMA-Cad synthesis protocol, we began to test the effects of increased peptide density on iPSC-derived cortical glutamatergic neurons. We first assessed the neurite lengths and widths at 1 week and 2 weeks after embedding the neurons (Fig. 4.2, 4.3). Interestingly, while 1X GelMA-Cad resulted in the longest observed neurite lengths at the end of 1 week, it did not result in the longest neurites at the end of 2 weeks (Figure 4.2). The lowest density of N-cadherin tested, 0.33X GelMA-Cad, resulted in the longest neurites at 2 weeks postembedding, as well as the widest neurites over both time points (Fig. 4.3). This matches previous 2D neuronal studies, which found that the lower concentrations of N-cadherin resulted in longer neurite projections from iPSC-derived neurons (73; 74).

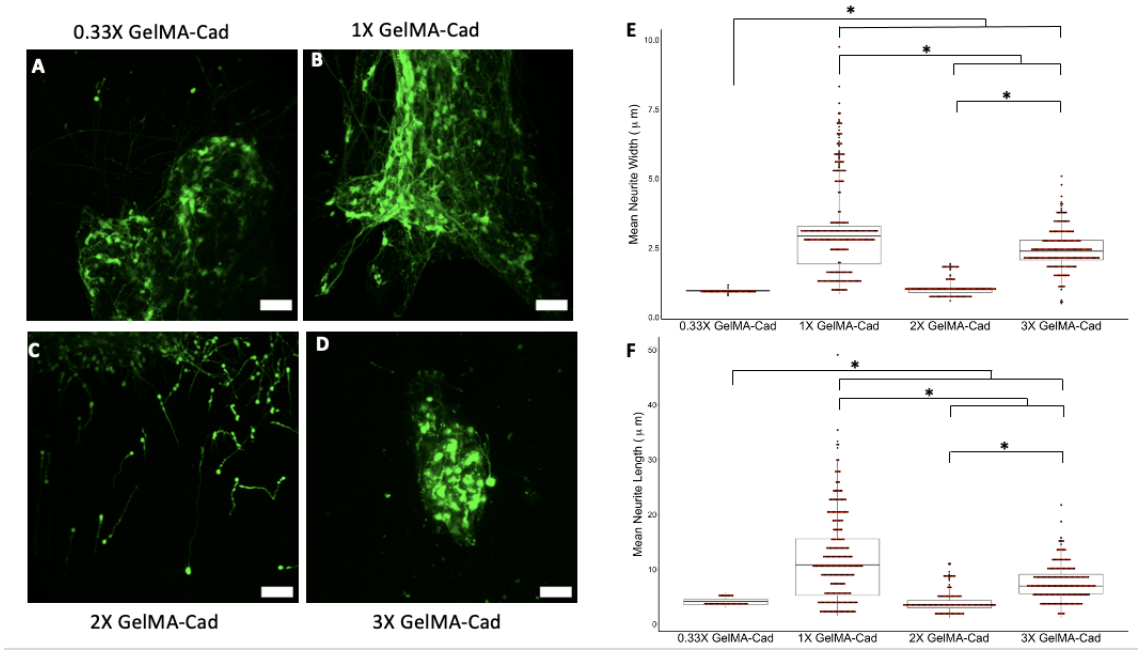

Figure 4.2: Influence of peptide density on neuron physical properties after 1 week. A-D) Representative images of calcein-labeled neurons embedded in 0.33X GelMA-Cad, 1X GelMA-Cad, 2X GelMA-Cad, and 3X GelMA-Cad, respectively. Scalebars are the same for all images. E-F) Quantification of neurite length and width. Mean ±SD was calculated from 3 biological replicates, with 4 confocal z-stack images assessed per replicate. Statistical significance was calculated using a one-way ANOVA with posthoc Tukey test (*p $<$0.05). Scale bar represents 50 μm.

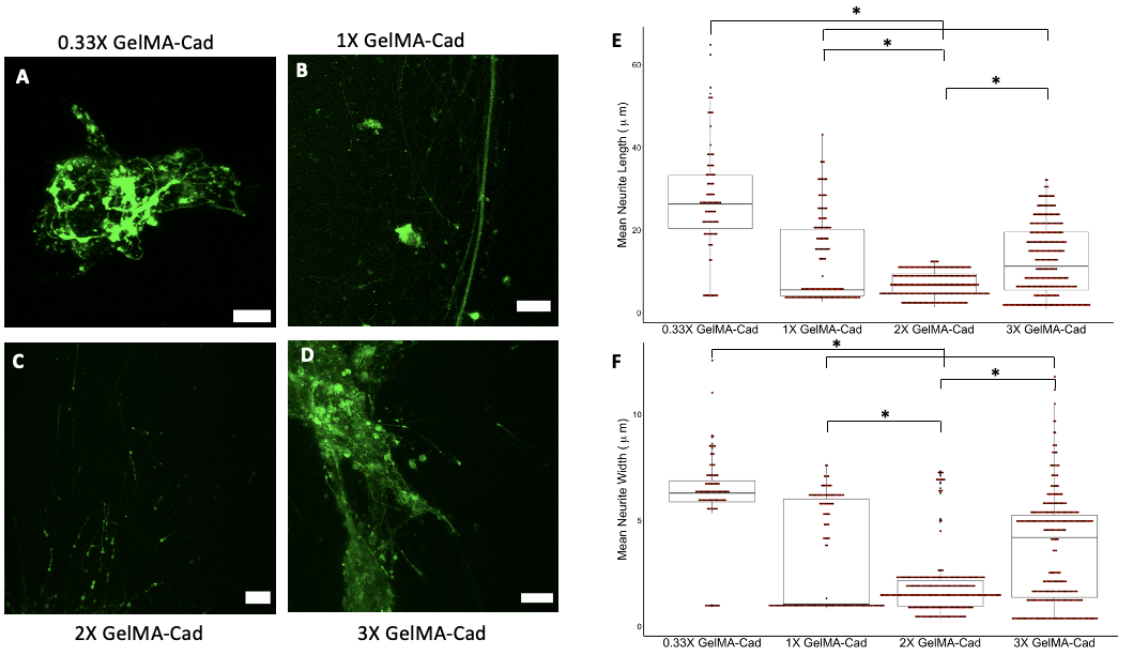

Figure 4.3: Influence of peptide density on neuron physical properties after 2 weeks. A-D) Representative images of calcein-labeled neurons embedded in 0.33X GelMA-Cad, 1X GelMA-Cad, 2X GelMA-Cad, and 3X GelMA-Cad, respectively. Scalebars are the same for all images. E-F) Quantification of neurite length and width. Mean ±SD was calculated from 3 biological replicates, with 4 confocal z-stack images assessed per replicate. Statistical significance was calculated using a one-way ANOVA with posthoc Tukey test (*p $<$0.05). Scale bar represents 50 μm.

We then assessed the colocalization of the presynaptic marker, Synaptophysin, and the post synaptic marker, PSD-95, in order to gain information about the maturity and functionality of the embedded neurons (Fig. 4.4). The higher the amount of colocalization of the markers, the more functional synapses are found in the neuronal cultures. We did not observe significant differences in the amount of colocalization when we compared 0.33X GelMA-Cad, 1X GelMa-Cad, 2X GelMA-Cad, and 3X GelMa-Cad (57.2±28.7%, 84.2±26.7%, 69.8±26.5%, and 61.5±31.2%, respectively) (Fig. 4.4). However, we did observe greater variability in the amount of colocalization in the 0.33X GelMA-Cad and 3X GelMA-Cad conditions. These results suggest that the embedded neurons will form functional synapses in all iterations of the GelMA-Cad hydrogel.

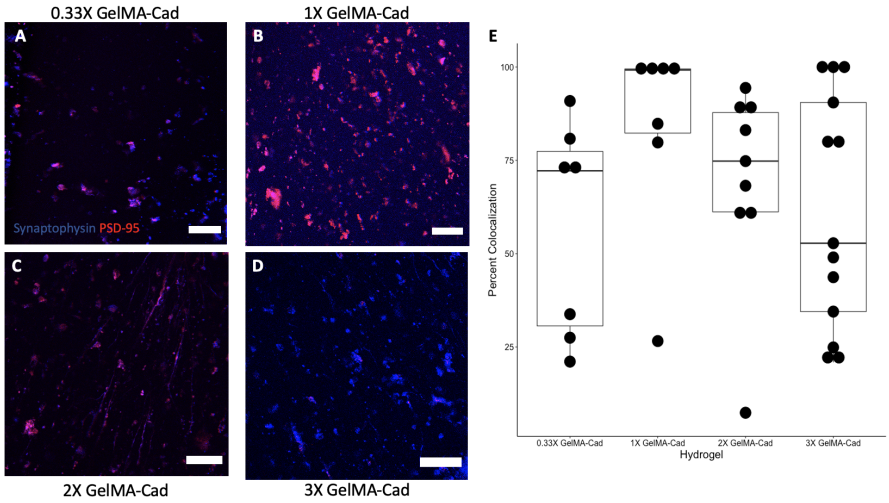

Figure 4.4: Influence of peptide density on neuron synaptic connectivity. A-D) Representative images of neurons embedded in hydrogels with decreased amounts of N-cadherin peptide labeled with the presynaptic marker, Synaptophysin, and the postsynaptic marker, PSD-95. The percentages in panels A and B refer to the ratio of GelMA-Cad to GelMA as detailed in the main text. Scale bars are the same for all images. C-D) Quantification of colocalization of Synaptophysin and PSD-95. Mean ±SD was calculated from 3 biological replicates, with 2 confocal z-stack images assessed per replicate. Statistical significance was calculated using a one-way ANOVA with posthoc Tukey test (*p $<$0.05). The difference colocalization was not statistically significant. Scale bar represents 50 μm.

4.5 Discussion

We have previously shown that GelMA-Cad can be used to create 3D synaptically connected neuronal models. However, there were still questions about whether the originally published protocol resulted in the most optimal hydrogel conditions to support iPSC-derived neuronal maturation. As a result, we altered the dialysis filtration system to incorporate a tangential flow filtration system. This switch resulted in 3 times more N-cadherin peptide conjugated to GelMA and allowed us to test a wider range of N-cadherin peptide densities while significantly cutting down the time it takes to prepare GelMA-Cad.

Other studies that examined the effects of N-cadherin densities on 2D stem cell-derived neuronal cultures found that lower densities of N-cadherin resulted in greater neurite projection lengths than higher densities (73; 74), which we were able to confirm in our 3D neuronal cultures. The lowest N-cadherin condition hydrogel, 0.33X GelMA-Cad, resulted in the longest neurite lengths after 2 weeks of 3D culture and the widest neurites throughout the culture. One limitation to these previously studied 2D models is that the researchers did not examine the synaptic connectivity of the neurons in order to determine the functionality of the neurons; instead the researchers used MAP2, a dendritic marker, expression and glial marker expression (GFAP, OLIG2) to approximate neuronal maturation (73; 74). We used the colocalization of the synaptic markers Synaptophysin and PSD-95 in order to assess the functionality of the 3D neuronal cultures. Interestingly,

we found that there was no significant differences in the colocalization of these markers, suggesting that the neurons form a similar amount of functional synapses no matter what density of N-cadherin is present. This suggests that at least after 2 weeks of 3D culture, N-cadherin density plays a larger role in neurite growth than synapse development. With this information, it may be interesting to see if certain neuronal subtypes respond better in certain N-cadherin densities than others. For example, midbrain dopaminergic neurons in the substantia nigra have long axonal projections that connect them to the striatum. It would be interesting to see if this neuronal subtype is able to form longer neurite projections in lower N-cadherin densities than higher densities, as this would result in a model that better recapitulates the human midbrain.

4.6 Conclusion

This paper builds on the work described previously by examining the effects of N-cadherin presence and hydrogel stiffness on 3D single-cell suspension of iPSC-derived neurons. The results of this study demonstrate that certain aspects of neurons can be modulated by N-cadherin density such as neurite length and width, although neurons in all N-cadherin densities tested result in synaptically connected cells. This data demonstrates that bio-functionalized gelatin is a useful resource for creating 3D neuronal networks. Future work will focus on using this information for 3D culture of other neuronal subtypes such as dopaminergic neurons and medium spiny neurons in order to create more human-like predictive models of neurological diseases.

CHAPTER 5

Improving Reproducibility and Maturation of iPSC-Derived Cortical Organoids with an N-Cadherin Biofunctionalized Hydrogel.

5.1 Summary

While induced pluripotent stem cell (iPSC)-derived cortical brain organoids are emerging as a promising tool for modeling the human brain, there are still a couple limitations preventing the widespread use of this model system. One limitation is the heterogeneity of current organoid cultures, where multiple cortical buds can form within a single organoid. Additionally, cortical organoids do not have proper cortical laminar organization. We hypothesized that these limitations might be due to the lack of biological cues within the scaffolds organoids are grown in. In a previous study, we were able to conjugate N-cadherin peptides to a gelatin backbone, which resulted in improved maturation of single-cell suspensions of iPSC-derived cortical glutamatergic neuron. In this project, we examined how gelatin scaffolds with N-cadherin peptides can improve cortical organoid models. Through circularity measurements, immunostained sectioned organoids, and immunostained tissue cleared organoids, we were able to show that organoids grown in these scaffolds result in more reproducible organoid structures with a single cortical bud. Furthermore, these organoids can be cultured long term to form larger superficial cortical layers than what has been observed in previously published organoid papers. Finally, we conducted synaptic tracing assays to show that there is greater neuronal maturation of the organoids grown in gelatin scaffolds with N-cadherin cues. The results of this study corrects some of the limitations of using cortical organoid models, which makes this system more useful for modeling the human cortex.

5.2 Background

5.2.1 Human cortical development

During development, the human cortex forms in an ”inside-out” manner (65–68). Following the formation of the neural tube during human development, the neuroepithelial cells at the prosencephalon differentiate into the cells found in the forebrain (181). At the ventricle, the neuroepithelial cells first develop into radial glia progenitor cells, which are able to self-renew and differentiate into intermediate progenitor cells (182; 183). The radial glia at the ventricle project out into the extracellular matrix, and the intermediate progentor cells form the subventricular zone, which is the major source of progenitor cells in the human brain, particularly for the later born neurons in the cortex (183). The neural progenitors are able to move up the radial glia tracks during the development of the cortical plate (181; 183). The neural progenitors fill in each individual

cortical layer before moving onto the next layer, beginning with the deepest Layer IV and building on top of each layer up to the most superficial Layer I (181). During early forebrain cortical development, there are 2 migration patterns that the neural progenitors follow: radial migration along the radial glia tracks and lateral migration to fill in each cortical layer (181). Following neurogenesis, radial glia progenitors migrate in the cortex and differentiate into astrocytes (182). Figure 5.1 represents a schematic of cortical development (5).

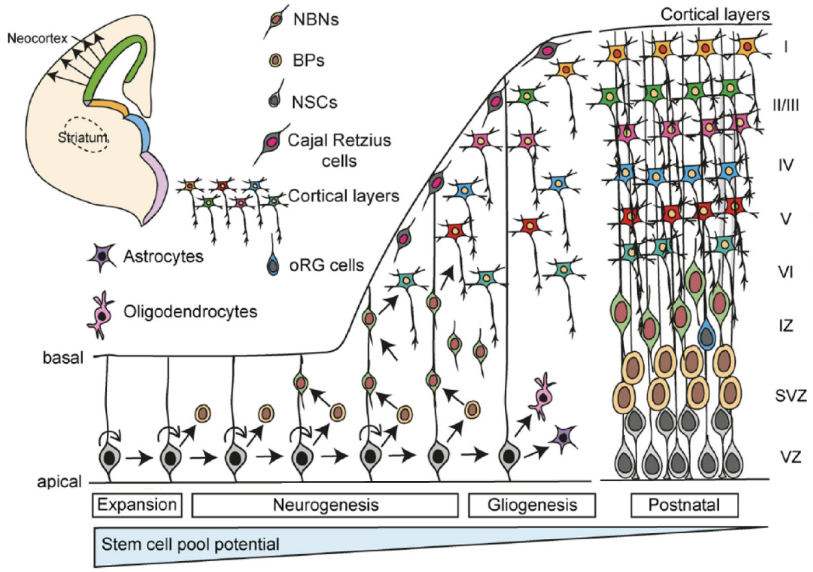

Figure 5.1: Simplified schematic of mouse cortical development. From the ventricular zone (VZ), radial glia (oRG) will project into the extracellular matrix. Radial glia can either self-renew or differentiate into the neural progenitors (NSCs, BPs) found in the subventrical zone (SVZ) and intermediate zone (IZ). These progenitors are a large source of the neurons found in the cortex. Neural progenitors will migrate along the radial glia tracks to each cortical layer, where the cells differentiate into neurons (NBNs). The first layer formed is Layer VI, and each subsequent cortical layer forms on top of the previous layer. After neurogenesis, the radial glia differentiate into the glial cell types found in the cortex (astrocytes and oligodendrocytes). The human cortex follows a similar process of development with some additional progenitor zones. Adapted with permission from the Journal of Experimental Neuroscience (5).

5.2.1.1 Role of N-cadherin in cortical development

The role of the developing brain's extracellular matrix (ECM) has been well studied (184; 57). Different components of the ECM, such as laminin and Reelin, can influence neuronal migration and cerebral folding (185; 186). Furthermore, extracellular cell adhesion molecules like N-cadherin, also affect cortical development (187; 188). In one study where N-cadherin signaling is disrupted in a mouse model, the mice were unable to develop distinct cortical layers (65). The authors of this study found that this disruption affected cortical development as early as ventricle zone formation, which in turn affected the following laminar organization of the mice brains (65). Additionally, another study demonstrated that N-cadherin is needed for

neural progenitor migration up the radial glia tracks (67). The perceived importance of N-cadherin is further supported by our understanding of diseases such as Miller-Dieker syndrome, where the disturbance of N-cadherin signaling pathways is associated with cortical development disorders (189).

5.2.2 Cortical brain organoid models

Human induced pluripotent stem cells (iPSC)-derived cortical organoids are emerging as a promising tool for studying human brain development and neurological diseases (8; 6; 130; 7; 113; 190). These structures are 3D self-organizing models that contain many of the cell types involved in cortical development including radial glia, neural progenitors, neurons, and astrocytes (8; 130; 7).

5.2.2.1 Limitations to current cortical organoid differentiation protocols

There are several limitations to cortical organoid models. One limitation is the lack of proper cortical laminar organization. In the normal human brain, the cortical layers are distinct populations of neurons that are separated from each other (5). While it is possible to get basic separation among the ventricular zone, the deep cortical neurons, and the superficial cortical neurons (8; 130; 7; 113; 9; 191), the majority of the cortical neuron populations are intermixed in current organoid models (113; 56). Furthermore, current organoid models are not able to grow beyond about 4 mm in diameter, as the organoids often form a necrotic core at their center, limiting the potential to grow outward and develop distinct superficial cortical layers. This is due to the increasing difficulty for nutrient/waste exchange in the organoids even when spinning bioreactors are incorporated (113; 190; 192). These organoids are often heterogeneous strucutres, as they are either grown without a scaffold to guide development (7; 9) or grown in Matrigel (8; 6; 130). As a result it can be difficult to replicate organoid studies. The development of hydrogel scaffolds with bio-instructive cues to guide cortical development may help address this issue.

This paper describes how gelatin scaffolds functionalized with N-cadherin peptides (2) can help guide iPSC-derived brain organoid development. This hydrogel improves the reproducibility of the organoid structures when compared to Matrigel. Additionally, the organoids embedded in functionalized gelatin show greater early cortical laminar patterning and increased presence of superficial layers. The functionality of the organoids was assessed with synaptic tracing assays, which showed increased cortical neuron connectivity in organoids embedded in gelatin functionalized with N-cadherin.

5.3 Methods

5.3.1 Cell Culture

CC3 iPSCs (148) were maintained with E8 medium on standard tissue culture plates coated with growth-factor reduced Matrigel (VWR). Cells were passaged with Versene (Thermo Fisher) at 60-70% confluency as previously described (149). Cortical brain organoids were generated using a previously published protocol (6) with slight modifications (Fig. 5.2). Differentiation media was created using the Stemcell Technologies STEMdiff Cerebral Organoid and Cerebral Organoid Maturation kits. Prior to use, AggreWell800 24-well plates (Stemcell Technologies) were washing using AggreWell rinsing solution (Stemcell Technologies). iPSCs were washed with PBS (Thermo Fisher) and dissociated from plates by incubation with Accutase (Thermo Fisher) for 3 minutes. Following collection by centrifugation, the cells were plated into AggreWell plates at a cell density of 2.7 x 10^6 cells/well (9 X 10^3 cells/microwell) in Embryoid Body (EB) Formation Medium with 10 µM Y27632 (Tocris). On day 2 of the differentiation protocol, the medium was replaced with EB Formation Medium supplemented with 10 µM SB431542, and 0.4 µM LDN1931189 (46) in order to induce neuralization. On day 4, the organoids were removed from the AggreWell plate, filtered with a 37 µm cell strainer (Stemcell Technologies) and replated onto 6-well low attachment plates (Thermo Fisher) in EB Formation Mediium supplemented with 10 µM SB431542, and 0.4 µM LDN1931189. The following day, the medium was changed to Induction Medium with 10 µM SB431542, and 0.4 µM LDN1931189.

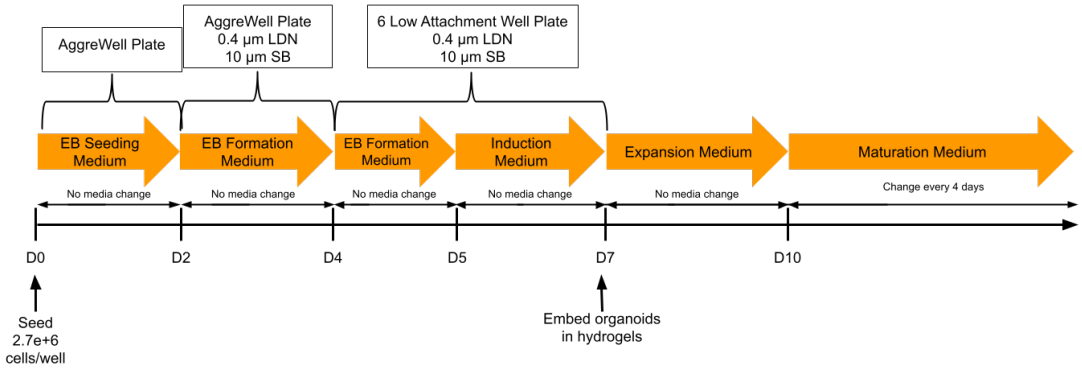

Figure 5.2: Cortical Brain Organoid Differentiation Protocol (6; 7)

5.3.2 Hydrogel Synthesis and Characterization

5.3.2.1 GelMA, GelMA-Cad, and GelMA-Scram

GelMA, GelMA-Cad, and GelMA-Scram were synthesized as previously described (2). Briefly, Type A procine skin gelatin (Sigma) was dissolved into DI water, sourced from an in-house Continental Modu-

lab ModuPure reagent grade water system, at 60°C to create a 10% (w/v) solution. Methacrylic anhydride (Sigma) was stirred into the gelatin solution for 3 hours at 50°C. The solution was then centrifuged at 3,500*xg* for 3 minutes, and the supernatant was collected and diluted in UltraPure water (Thermo Fisher). The mixture was dialyzed against DI water for 1 week at 37°C using a 12-14 kDa cutoff dialysis tubing (Fisher). The pH of the solution was adjusted to 7.35-7.45 and lyophilized for 3 days with a Labconco lyophilizer and stored at -20°C. The lyophilized GelMA was reconstituted in triethanolamine buffer (Sigma) to create a 10% (w/v) solution and stirred at 37°C until fully dissolved. The pH of the solution was adjusted to 8.0-8.5. Scrambled (Ac-AGVGDHIGC, to make GelMA-Scram) or N-cadherin mimic (Ac-HAVDIGGGC, to make GelMA-Cad) peptides (GenScript) were added to the GelMA/TEOA buffer to form a 0.1% (w/v) solution and stirred at 37°C for 24 hours. The resulting solutions were dialyzed using a Tangential Flow Filtration (TFF) system. Briefly, the hydrogels were diluted 5x in MilliQ UltraPure water and stirred at 37°C. The resulting solution was pumped through a 2 kDa TFF filter (Satorius) using a peristaltic pump (Cole Parmer) for 5 hours. Additional MilliQ water was added to the diluted hydrogel solution every hour to facilitate filtering. The pH of the dialyzed hydrogel was then adjusted to 7.35-7.45 before lyophilization and storage at -20°C.Conjugation were confirmed using 1H NMR using a 500 Hz Bruker NMR machine.

5.3.2.2 GelCad

To make the GelCad hydrogel, gelatin was dissolved into PBS at 50°C to make a 4.2% (w/v) solution before lowering the temperature to 37°C and adjusting the pH of the solution to 5-6 using 1M HCl. In a separate beaker, dimethylformamide (DMF, Thermo Fisher) and PBS were mixed in a 2:3 ratio. Carboxy-N-cadherin peptide ((GenScript, sequence HAVDIGGGCE with caboxylated N-terminus), EDC (Sigma), and NHS (Sigma) were mixed with the PBS/DMF solution to make a 0.32%, 0.32%, 4.8% (w/v) peptide activation solution solution, respectively. The peptide solution was allowed to react for 30 minutes at room temperature before adding it dropwise to the gelatin solution to react for 2.5 hours at 37°C. A second 2:3 DMF/PBS solution was created and combined with 3-(4-hydroxyphenyl)propionic acid (HPA), EDC, and NHS to make a 0.32%, 0.32%, 0.48% (w/v) HPA activation solution. The peptide solution was allowed to react for 30 minutes at room temperature before adding it dropwise to the gelatin solution to react for 3 hours at 37°C. After the reaction has completed, adjust pH to 8-9 using 1M sodium hydroxide. The conjugated gelatin solution was filtered with DI water in a 1:2 ratio using tangential flow filtration. Filtration was run until four times the volume of the gelatin solution was reached with DI water. The filtered solution was lyophilized for five days, pulverized, and stored at -20°C. Conjugation of HPA and Carboxy-N-cadherin (Cad) were confirmed using 1H NMR using a 400 Hz Bruker NMR machine.

5.3.3 Hydrogel Fabrication and Organoid Seeding

GelMA, GelMA-Cad, and GelMA-Scram, GelCad were reconstituted in Neurobasal Medium to make a 10% (w/v) solution. A 0.05% (w/v) LAP photoinitator was added to GelMA, GelMA-Cad, and GelMA-Scram hydrogels. Microbial transglutaminase (mTG, Moo Gloo) was reconstituted to make a 10% (w/v) solution in UltraPure water.

Day 7 iPSC-derived organoids were collected and centrifuged for 2 minutes. The supernatant was removed, and the organoids were resuspended in 100 µL Stemcell Technologies Cerebral Organoid Base 2 Medium. 10 µL of the resuspended organoids (approximately 15-20 organoids) was added to 500 µL of each hydrogel. 100 µL per well (24-well glass bottom plate, Cellvis) of GelMA, GelMA-Cad, and GelMA-Scram was crosslinked using 25 mW/cm^2 UT light for 16 seconds using a Thor Labs UV light source. GelCad was mixed with 0.3% (w/v) mTG, and 100 µL per well of each solution was plated into a 24-well glass bottom plate. These plates were placed in an incubator at 37°C to crosslink for 1 hour. After the hydrogels were fully cross-linked, 1 mL Expansion Medium (Stemcell Technologies Cerebral Organoid Base Medium 2 supplemented with Supplements C and D) was added to each of the wells.

All experiments that assed the influence of N-cadherin peptide density, GelMA-Cad and GelAM were mixed to create a 33% and 66% GelMA-Cad solution (2). The hydrogels were crosslinked as described above. For experiments that assessed the influence of hydrogel stiffness, GelMA-Cad was crosslinked using 25 mW/cm^2 UV light exposure for 8 seconds, 16 seconds, and 32 seconds.

To embed the organoids in Matrigel, 500 µL Matrigel aliquots were thawed on ice. Once thawed, 10 µL of the resuspended organoids were added to the Matrigel aliquot, and 100 µL per well was added to a 24-well glass bottom plate. Organoids were gently pushed away from each other, and the plate was placed in an incubator at 37 °C to crosslink for 1 hour. After the Matrigel was fully crosslinked, 1 mL Expansion Medium was added to each of the wells.

Organoid medium was changed to Maturation Medium (Stemcell Technologies Cerebral Organoid Base Medium 2 supplemented with Supplement E) on Day 10, and the medium was changed every 4 days until the organoids were pulled for experiments.

5.3.4 Live Organoid Imaging

To assess organoid cell viability during the first month following embedding, the hydrogels were incubated with CytoCalcein AM (AAT Bioquest) for 1 hour. The organoids were imaged using a Zeiss 710 confocal microscope and processed using ImageJ. Fresh Maturation Medium was added to each well to dilute any remaining Calcein from the hydrogels.

5.3.5 Circularity Measurements

Starting on Day 10 of the organoid differentiation protocol, embedded organoids were imaged with an EVOS microscope. The circularity of the organoids were measured using ImageJ, and RStudio was used for statistical analysis and data visualization.

5.3.6 Immunohistochemistry

At 1, 2, 3, and 4 months, organoids were pulled for immunohistochemistry. The organoids were fixed in 4% PFA for 20 minutes and washed with PBS. The organoids were incubated for 3 days in 30% (w/v) surcrose at 4°C, embedded in OCT and stored at -80°C overnight. The organoids were cryosectioned with a 50 µm slice thickness. Sections were stored at -80°C until used.

Sections were blocked in PBS solution with 5% donkey serum (Sigma) and 0.3% Triton X-100 (Sigma) for 1 hour. The sections were incubated with primary antibodies overnight and then wased 5x with PBS the next day. The sections were incubated with secondary antibody for 1 hour and then wash 3x with PBS before incubating with DAPI (*vendor*) for 15 minutes. Then the sections were allowed to dry overnight. The slides were stored at 4°C until ready to image. Table 5.1 describes what marker corresponds to each cortical layer, and Table 5.2 provides information on what primary antibodies were used for immunostaining.

Sectioned organoids were imaged with a Zeiss 710 confocal microscope and processed using ImageJ.

5.3.7 CLARITY Tissue Clearing and Imaging

At 1, 2, 3, and 4 months following embedding, organoids were fixed for 20 minutes in 4% PFA. These organoids were then submerged in hydrogel monomer (HM) solution (4% acrylamide, 0.05% bis, and 0.25% VA-044 thermal initiator) overnight at 4°C. The following day, organoids were submerged in fresh HM solution in paraffin molds and placed in a hypoxia chamber where oxygen was displaced with nitrogen gas to allow accelerated crosslinking. The hypoxia chamber was incubated at 45°C for one hour in order to crosslink the HM solution. Embedded organoids were then incubated in an 8% SDS clearing solution at 37°C with agitation for 24-48 hours. Embedded organoids were then washed with PBS 5 times (30 minutes-1 hour per wash) at 37°C with agitation.

Organoids were immunostained using a previously descibed protocol (2). Briefly, the fixed hydrogels were submerged in a blocking buffer solution of 5% goat serum (Thermo Fisher) and 0.03% Triton X-100 in PBS. These hydrogels were then placed on a rocking platform at room temperature overnight. The following day, primary antibodies (Tables 5.1 and 5.2) in blocking buffer were added to the hydrogels and placed on a rocking platform for 2-3 days. The dilution listed in Table 5.2 in order to account for the diffusion through the hydrogel to the organoid and the increased number of cells being stained in 3D. After 2-3 days, the primary

antibody solution was removed, and secondary antibodies and secondary-conjugated primary antibodies in blocking buffer with 4,6-diamidino-2-phenylindole (DAPI) was then added to the hydrogels. These hydrogels were then placed on a rocking platform for another 2-3 days. The hydrogels were then washed 3 times with PBS (1 hour per wash at room temperature). The hydrogels were then imaged using either a Zeiss LSM 710 or LSM 880 confocal microscope, and images were processed using ImageJ.

Cortex Cell Type	Markers
Radial Glia	SOX2, PAX6
Neural Progenitor	PAX6, NESTIN
Neuron	BIII Tubulin
Astrocyte	GFAP
Cortical Layer VI Neurons	TBR1
Cortical Layer V Neurons	CTIP2
Cortical Layer IV	SATB2
Cortical Layer III	CUX1/2
Cortical Layer II	BRN1/2
Cortical Layer I	REELIN

Table 5.1: Markers for cell types found in the human cortex.

Marker	Species	Dilution	Vendor	Catalog Number
488 ZO-1	N/A	1:200	Thermo Fisher	MA3-39100-A488
488 SOX2	N/A	1:200	Thermo Fisher	MA1014D488
555 SOX2	N/A	1:200	Cell Signaling	5179S
650 SOX2	N/A	1:200	Thermo Fisher	MA1-014-D650
Pax6	Rabbit	1:200	Biolegend	901301
647 Pax6	N/A	1:200	abcam	ab215925
βIII Tubulin	Mouse	1:1000	Invitrogen	MA1-19187
555 βIII Tubulin	N/A	1:200	abcam	ab201849
555 βIII Tubulin	N/A	1:200	abcam	ab202519
647 βIII Tubulin	N/A	1:200	abcam	ab190575
GFAP	Rabbit	1:500	Dako	Z0334
TBR1	Rabbit	1:300	abcam	ab31940
CTIP2	Rat	1:200	abcam	ab18465
SATB2	Rabbit	1:200	abcam	ab34735
647 CUX1	N/A	1:250	Santa Cruz	sc-514008 AF647
Reelin	Mouse	1:500	Sigma	MAB5366

Table 5.2: Primary antibodies used to immunostain organoids.

5.3.8 Synaptic Tracing Experiments

One and a half weeks after embedding, an adenoassociated virus (AAV) encoding enhanced green fluorescent protein (EGFP) under the control of the human synapsin promoter, which was a gift from Dr. Bryan Roth (Addgene plasmid 50465), was added to the embedded organoids at an MOI of 500. Medium was replaced after 5 hours in order to remove the virus from the cultures. The formation of synaptic connections was visualized by the spread of the EGFP fluorescence across the neuronal cultures using a Zeiss LSM 710 confocal microscope. Live cells were labeled with calcein in order to visualize the spread of the EGFP signal to live cells within the organoid.

5.4 Results and Discussion

5.4.1 N-cadherin conjugation to gelatin scaffolds and characterization

In a previous study, we demonstrated that methacrylated gelatin (GelMA) can be biofunctionalized with N-cadherin peptides (termed GelMA-Cad), and that GelMA-Cad can improve the functionality of 3D single-cell suspensions of iPSC-derived cortical glutamatergic neurons (2). GelMA hydrogels use photoinitators and UV exposure in order to crosslink, which works well with smaller tissue structures. However, in larger

tissue structures, the UV light not able to penetrate evenly throughout the hydrogel structure. As a result, a stiffness gradient can be created where the hydrogel is stiffer closer to the UV source and softer further away from the UV source. This is not ideal, especially if researchers are interested in creating complex structures such as microchannels within the hydrogels as the softer regions may collapse under the weight of the cells and hydrogel.

As a result, we investigated other crosslinking methods - specifically using transglutaminases (mTG) to enzymatically crosslink the hydrogel structures. With sufficient mixing of the hydrogel and mTG, the hydrogel should form a relatively even stiffness throughout the structure. Because we were not using the mecthacrylic side chains with this crosslinking method, we created a new hydrogel without the methacrylation step. This new hydrogel is termed GelCad as this hydrogel is primarily gelatin conjugated to the N-cadherin peptides. We confirmed this conjugation with ^{1}H NMR, where the peaks around 0.9-1.1, 2.2-2.35, 2.45-2.6, and 2.7-3.0 ppm represent signature N-cadherin peaks (Fig. 5.3A). When we used AFM to measure the stiffness of the hydrogels, there was no significant difference between GelMA-Cad and GelCad (Fig 5.3B).

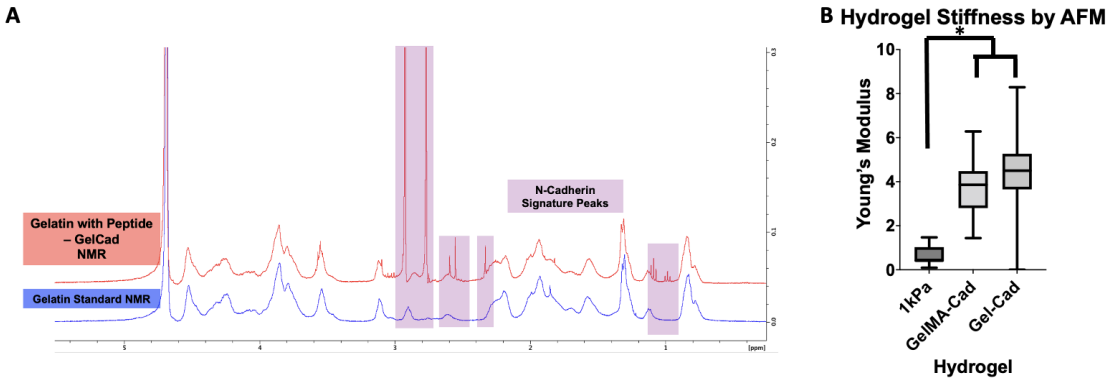

Figure 5.3: Characterization of N-cadherin peptide conjugated to gelatin (GelCad). A) NMR spectra of GelCad. Peaks at 0.9-1.1, 2.2-2.35, 2.45-2.6, and 2.7-3.0 ppm represent signature N-cadherin peaks. B) AFM measurements comparing GelCad and GelMA-Cad. There was no statistical difference between GelMA-Cad and GelCad. Statistical significance was calculated using a one-way ANOVA with posthoc Tukey test (*p $<$0.05).

5.4.2 Organoid reproducibility is improved in scaffolds containing N-cadherin and gelatin

We used a cortical organoid differentiation protocol that combines Dr. Madeline Lancaster's method (8) and Dr. Sergiu Pasca's method (7). We used AggreWells to create the spherical shapes and dual SMAD inhibition (46) to differentiate the stem cells into the epithelium over the first few days of the differentiation protocol. At Day 7 of the differentiation protocol, we removed the dual SMAD inhibition factors and embedded the organoids.

Starting at Day 10 of the differentiation protocol, we took brightfield images every four days in order to

get morphological information about the embedded organoids (Fig. 5.4, 5.5). By Day 14, we observed that organoids embedded in GelMA-Cad and GelCad formed fewer cortical buds when compared to organoids embedded in Matrigel (Fig. 5.4A). Furthermore, by Day 10, all organoids grew significantly, and projections can be seen coming out from organoids embedded in GelMA-Cad (Fig. 5.4A). One month after embedding, the organoids were stained with calcein in order to mark live cells within the structure and imaged (Fig. 5.4B). These images demonstrate that the organoids embedded in GelMA-Cad and GelCad form circular structures with live cells throughout the organoid. These organoids also appear to have a single cortical bud. In contrast, organoids in Matrigel appear to have several cortical buds, and the intensity of the signal was decreased, potentially indicating fewer live cells within the stucture.

One major issue with current cortical organoid protocols is the heterogeneity seen in organoid cultures, especially in organoids embedded in Matrigel. Circularity measurements can represent the reproducibility of an organoid culture, where 1 represents a perfect circle. We found that organoid embedded in a gelatin-based scaffold resulted in significantly more circular structures than organoid embedded in Matrigel at Day 10 of the differentiation protocol (Fig. 5.5A). We traced the circularity measurements over the course of 90 days of culture. We found that there is less variability in the GelMA-Cad organoids than the Matrigel organoids and the organoids in GelMA-Cad stay more circular over time than organoids in Matrigel (Fig. 5.5B). These results imply that gelatin scaffolds biofunctionalized with N-cadherin result in more reproducible organoid structures than traditional methods.

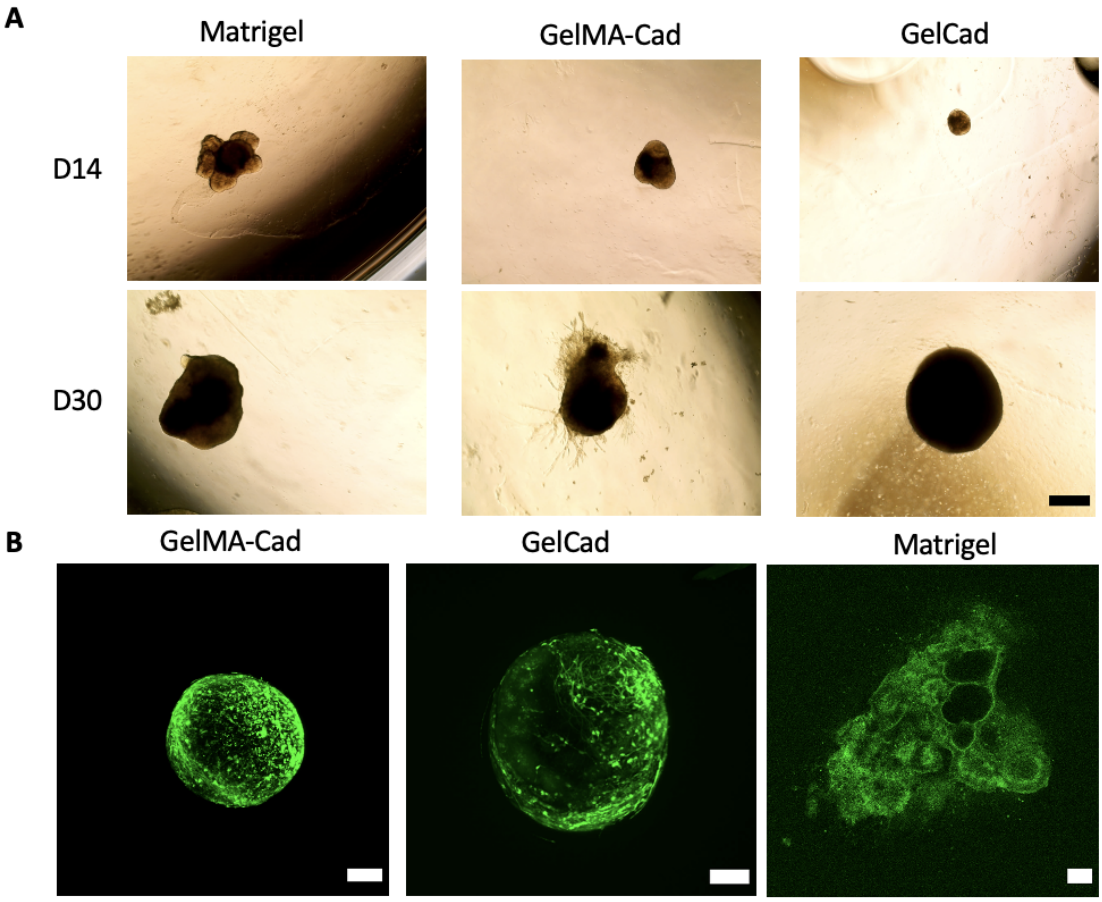

Figure 5.4: Hydrogels with N-cadherin peptides create more circular and reproducible organoid structures than Matrigel. A) Brightfield images of organoids embedded in Matrigel, GelMA-Cad, and GelCad on Days 14 and 30 of the cortical organoid differentiation protocol. All images were taken at the same magnification, and scale bar represents 0.5 mm. B) Organoids stained with calcein to assess live cells. Organoids in GelMA-Cad and GelCad had more circular structures with fewer cortical buds than Matrigel. Scale bars represent 100 μm for all panels.

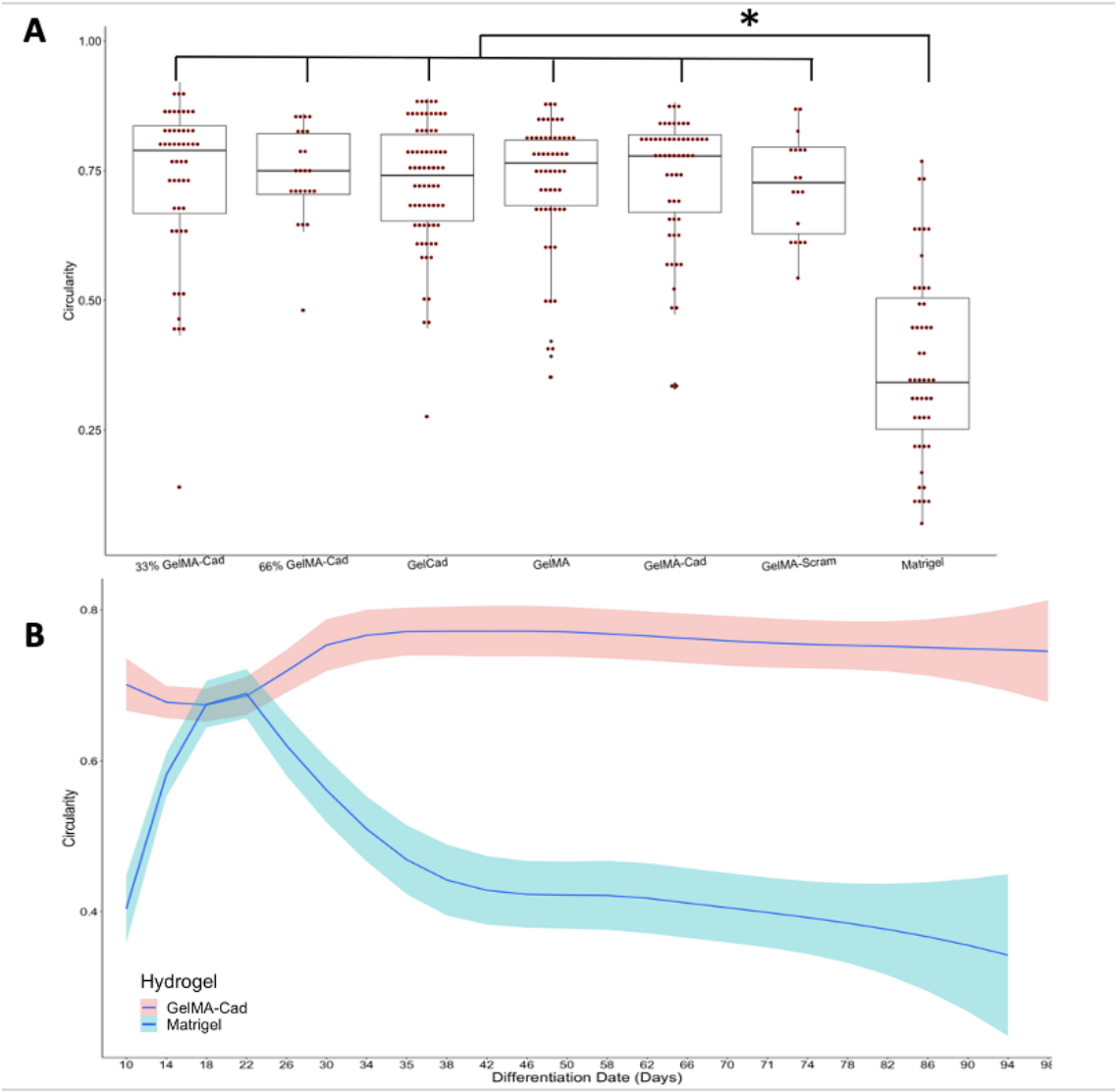

Figure 5.5: Hydrogels with N-cadherin peptides create more circular and reproducible organoid structures than Matrigel. A) Circularity measurements assessed from brightfield images of organoids embedded in hydrogel conditions including GelMA-Cad, GelCad, and Matrigel. 1 represents a perfect circle. Statistical significance was calculated using a one-way ANOVA with posthoc Tukey test (*p $<$0.05). Only organoids embedded in Matrigel had a statistically significant circularity measurement. B) Circularity of organoids embedded in GelMA-Cad and Matrigel over time, where the line represents the mean and the colored regions surrounding the line represent the standard deviation. Organoids in GelMA-Cad were more circular over time and had less variability than organoids in Matrigel.

We also studied how UV crosslinking times might affect organoid circularity and area. We crosslinked GelMA-Cad for 4, 8, or 32 seconds, and took brightfield images 3 days after embedding (Day 10 of the differentiation protocol). Brightfield images showed that organoids in softer hydrogels (4s) result in more projections coming out of the organoids as well as more hetergeneous structures while stiffer hydrogels (8 and 32s) resulted in more homogeneous, circular structures with few to no projections (Fig. 5.6A). Cir-

cularity measurements match these observations where the stiffer hydrogels resulted in higher circularity measurements with less variations (Fig. 5.6B). When the area of the organoids was calculated, softer hydrogels resulted in significantly larger organoid structures (Fig. 5.6C). This data implies that the mechanical properties of the hydrogel also plays a role in the organoid architecture.

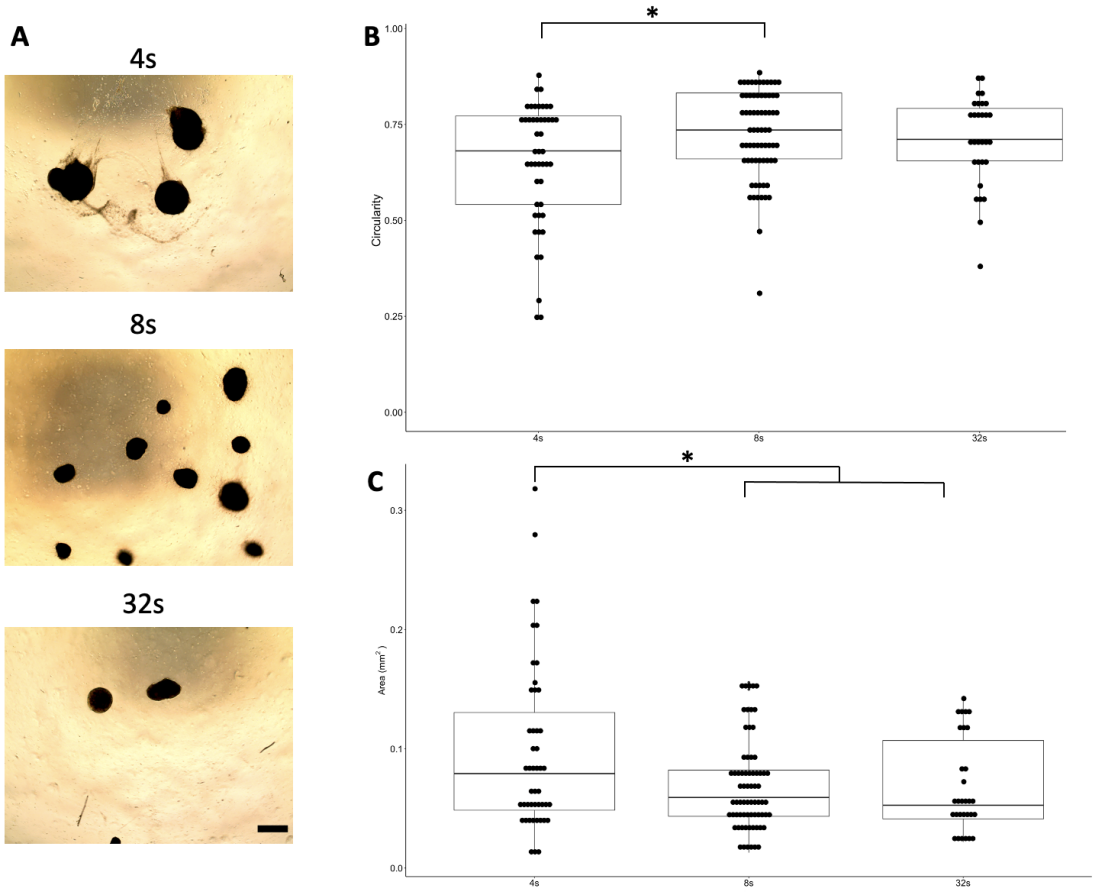

Figure 5.6: Examination of UV crosslinking times on organoid morphology. A) Brightfield images of organoids exposed to UV light for 4, 8, and 32 seconds. Scale is same for all panels, and the scale bar represents 0.5 mm. B) Circularity measurements of organoids with different crosslinking times, where 1 represents a perfect circle. C) Area measurements of organoids with different crosslinking times. Statistical significance was calculated using a one-way ANOVA with posthoc Tukey test (*p $<$0.05).

In the previous chapter (Ch. 4), we studied how N-cadherin presence can affect neuronal differentiation and maturation. Previous studies have shown that reduction of N-cadherin signaling pathways results in increased neurogenesis and neuronal migration during cortical development (179). We were interested in seeing if reducing N-cadherin presence in the hydrogels affected early cortical organoid maturation. We diluted GelMA-Cad with GelMA in order to reduce the N-cadherin density and embedded the organoids at Day 7. We took brightfield images at Day 10 of the differentiation protocol, and the organoids appear larger in lower densities of N-cadherin (Fig. 5.7A). The circularity measurements of the organoids in 33%

GelMA-Cad, 66% GelMA-Cad, and GelMA-Cad were not significantly different (0.73±0.16, 0.74±0.09, and 0.73±0.13, respectively) (Fig. 5.7B). Additionally, the area of the organoids in 33% GelMA-Cad, 66% GelMA-Cad, and GelMA-Cad were not significantly different (0.098±0.077, 0.068±0.046, and 0.090±0.083 mm^2, respectively) (Fig. 5.7C). Longer term cultures may need to be studied in order to see an potential differences in these conditions.

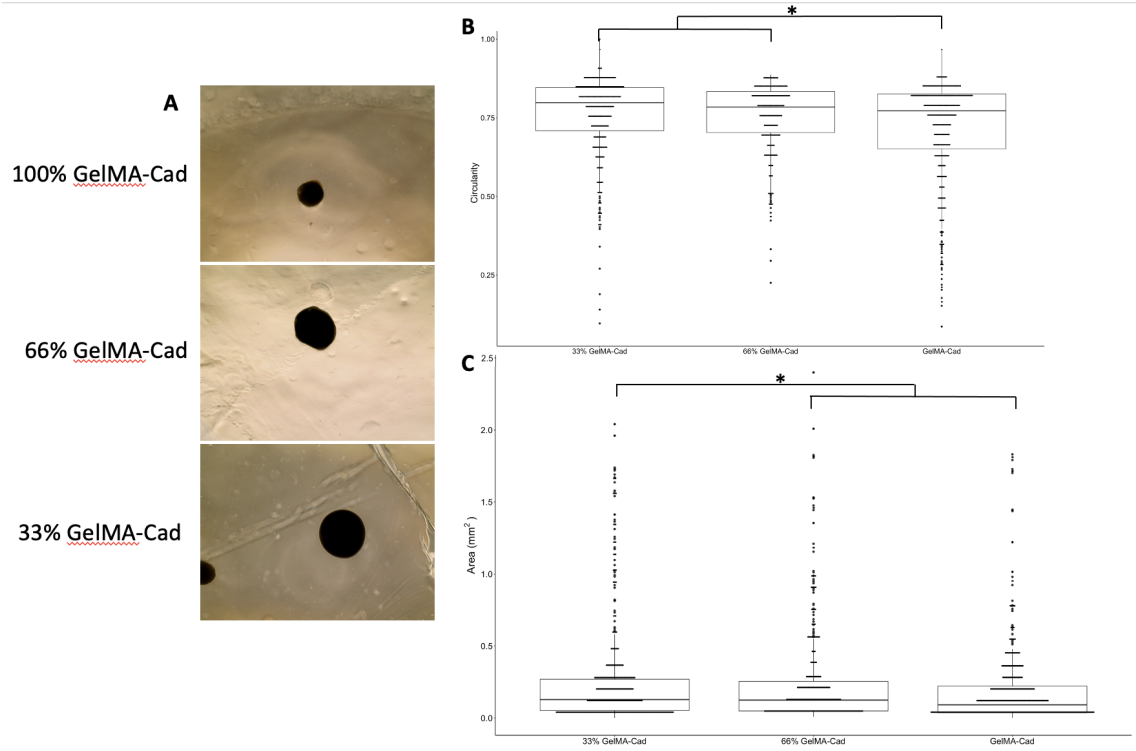

Figure 5.7: Examination of N-cadherin presence on organoid morphology. A) Brightfield images of organoids embedded in 33% GelMA-Cad, 66% GelMA-Cad, and 100% GelMA-Cad. Scale is same for all panels. B) Circularity measurements of organoids with N-cadherin densities, where 1 represents a perfect circle. C) Area measurements of organoids with different N-cadherin densities. Statistical significance was calculated using a one-way ANOVA with posthoc Tukey test (*p $<$0.05).

Finally, we observed that organoids in GelCad were larger than organoid in GelMA-Cad but did not significantly alter the circularity measurement (Fig. 5.8). In order to investigate this further, we crosslinked GelMA with both UV exposure and mTG, and we observed that the GelMA + mTG condition lead to significantly larger organoids than organoids in hydrogels crosslinked with UV. It is possible that this may be due to differences in the degradation properties of the hydrogels, where hydrogels crosslinked with mTG may be easier for the organoids to degrade and remodel. Additionally, transglutaminases are known to be involved in neurite development and synapses function (17). It is possible that this enzymatic crosslinker also affects the cells within the organoids.

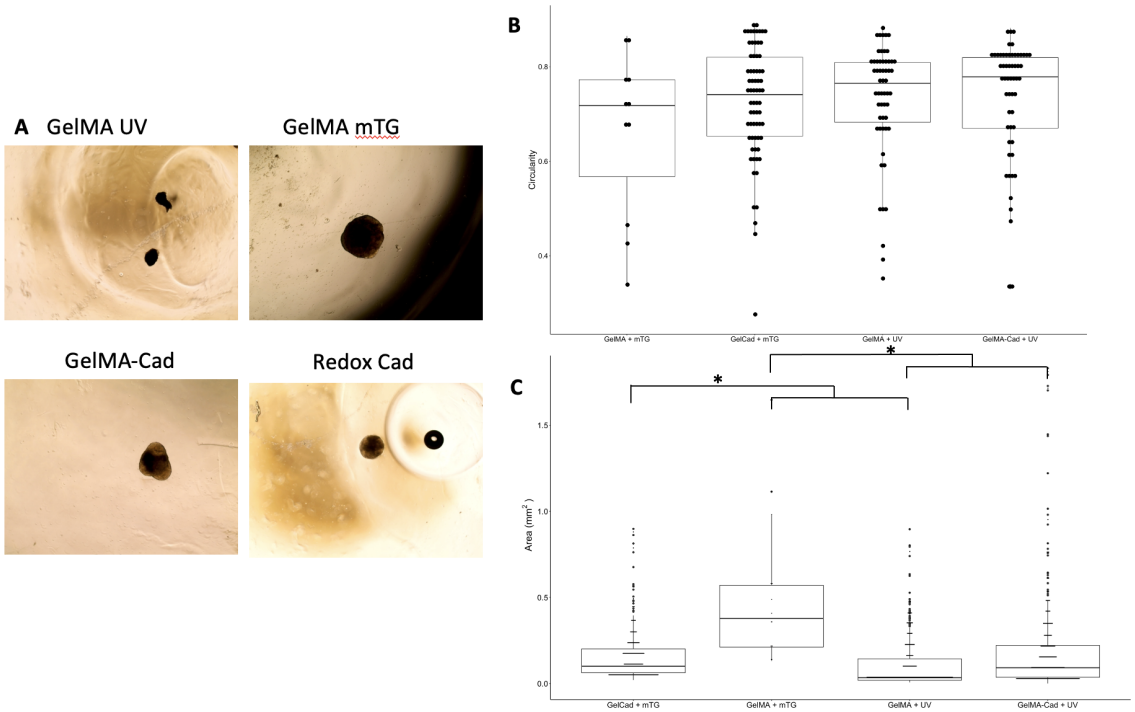

Figure 5.8: Examination of crosslinking method on organoid morphology. A) Brightfield images of Day 10 organoids embedded in GelMA crosslinked with UV, GelMA crosslinked with transglutaminase (mTG), GelMA-Cad crosslinked with UV, and GelCad crosslinked with mTG. B) Circularity measurements of embedded organoids, where a perfect circle is a measurement of 1. C) Area measurements of organoids at Day 10. Statistical significance was calculated using a one-way ANOVA with posthoc Tukey test (*p $<$0.05).

5.4.3 Organoid organization and maturation is improved in scaffolds containing N-cadherin

Based on the brightfield and calcein images, we began to explore whether GelMA-Cad and GelCad reduce the number of cortical buds formed. We used analyzed both organoid sections and tissue cleared organoids in order to look at specific layer architecture. As noted in the Background section, improper cortical laminar organization and heterogeneity of organoid cultures are major limitations to the widespread use of organoid models. A single cortical bud formed within organoid structures would help make organoid models more reproducible. Because organoids are often grown in Matrigel, there is no specific biological cue that directs organoid growth. As a result, there can be a large range of cortical buds formed within the organoids. When we stained cleared organoids that were embedded in GelMA-Cad with the ventricle marker, ZO-1, and the neuron marker, TUJ1, we saw a single, interconnected ventricular zone surrounded by a neuron population (Fig. 5.9A). Furthermore, when we stained a sectioned organoid embedded in GelMA-Cad for the radial glia marker (SOX2) and TUJ1, we did not see multiple cortical buds in the SOX2 stain (Fig. 5.9B) unlike what is normally observed in published cortical organoid protocols (8; 6; 113; 190). We observed similar results with tissue cleared organoids that were embedded in GelCad (Fig. 5.9C). These organoids have a

single population of SOX2+ radial glia cells surrounded by a TUJ1+ neuronal population. These results demonstrate that organoids embedded in hydrogels with N-cadherin cues have a single cortical bud in each organoid, which greatly increases the reproducibility of organoid models. Furthermore, these organoids have correct organization during early time points of the differentiation protocol.

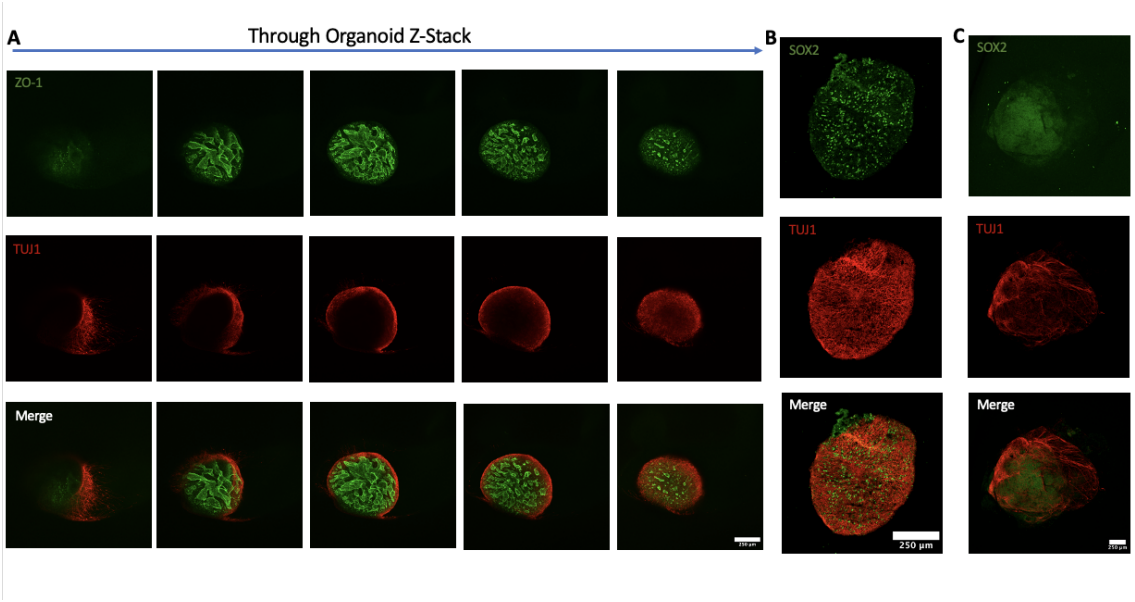

Figure 5.9: Early organoid organization in GelMA-Cad and GelCad appear to form a singular ventricle and cortical bud. A) Tissue cleared organoid that was embedded in GelMA-Cad after 6 weeks of culture. These organoids appear to form a single interconnected ventricle. Note the circularity of the organoid, the inner progenitor zone (ZO-1, green), and outer neuronal layer (TUJ1, red). B) Sectioned organoid that was embedded in GelMA-Cad. There is no obvious formation of multiple cortical buds based on SOX2 (green) expression like what is observed in published images of organoid embedded in Matrigel (8; 6). C Reconstruction of a tissue cleared organoid that was embedded in GelCad. Note the single radial glia population (SOX2, green) surrounded by a larger neuronal population (TUJ1, red). This further supports that organoids embedded in GelMA-Cad and GelCad form a single cortical bud, which would improve the reproducibility of cortical organoid models.

Embedded organoids can be cultured long term (over 150 days) and assessed for more superficial, later born organoid layers. When we sectioned D150 organoids embedded in GelMA-Cad, we found that there is separation between deeper cortical layers (CTIP2) and superficial cortical layers (SATB2) (Fig. 5.10A). Furthermore, the superficial layer observed in the organoids embedded in GelMA-Cad is larger than the superficial layer seen in published organoid protocols (6; 9) (Fig. 5.10A). Additional work is being conducted to look more closely at the separation between individual cortical layers in order to see if N-cadherin cues from the scaffold result in improved cortical laminar organization.

We were also able to conduct synaptic tracing assays in order to further assess the maturation and functionality of the neurons within the organoids. After 1.5 months of culture, an AAV that contains EGFP under the control of human synapsin was added to the organoids for 5 hours. We labeled live cells with calcein

and imaged the organoids immediately after the virus was removed and after 2 days. There was a greater spread of the EGFP signal in the organoids embedded in GelMA-Cad and GelCad than organoids grown in Matrigel (Fig. 5.10B). This suggests that there is greater connectivity among the organoids in the scaffolds with N-cadherin cues, which is an indication of increased model maturity.

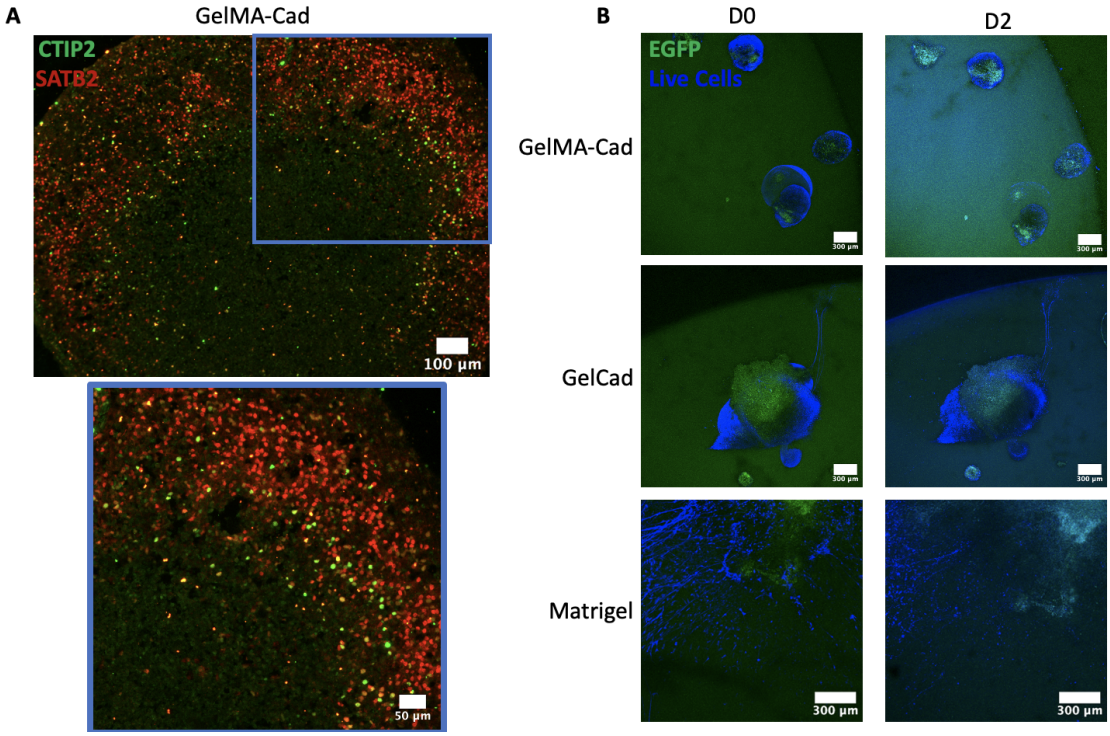

Figure 5.10: Later organoid maturation of organoids grown in GelMA-Cad and GelCad. A) Cortical organoids were grown for 150 days and then pulled for sectioning. This is a representative image of a sectioned organoid embedded in GelMA-Cad stained for a deep cortical layer (CTIP2) and superficial cortical layer (SATB2). The superficial cortical layer is larger than many published cortical organoid protocols (6; 9), which suggests that organoids grown with N-cadherin cues results in more mature organoid structures. B) Synaptic tracing experiments suggest that organoids grown in GelMA-Cad and GelCad are more synaptically connected than organoid grown in Matrigel. After 1.5 months of culture, an AAV that contains EGFP under the control of human synapsin was added to the cultures for 24 hours. The spread of the EGFP signal indicates the formation of synaptic connections.

5.5 Conclusions

This work demonstrates that cortical organoids embedded in gelatin scaffolds biofunctionalized with N-cadherin peptides can result in more homogeneous organoid cultures that have improved cortical structures when compared to existing cortical organoid protocols. Future work involves studying how transglutaminases might affect organoid maturation in 3D. It would be interesting to see if the larger organoids in GelMA crosslinked with mTG also demonstrate the same organization seen in organoids embedded in GelMA-Cad and GelCad. It would also be interesting to conduct RNAseq experiments to see if there are differences in the

cell populations of the organoids embedded in hydrogels crosslinked with mTG and hydrogels crosslinked with UV. Furthermore, more long term cultures of the organoids embedded in hydrogels with different densities of N-cadherin expression. Although we did not observe significant effects after short term culture of these organoids, more long term cultures might reveal differences in neurogenesis in the organoids. Finally, additional organoids modeling different brain regions, such as midbrain organoids and hippocampus organoids, will be embedded in gelatin scaffolds with N-cadherin peptides in order to see these organoid protocols also benefit from hydrogels functionalized with N-cadherin peptides. The improvement of human iPSC-derived brain organoid models will provide more complex *in vitro* modeling tools that researchers can use to study neurodegenerative disease in order to find effective therapeutics.

CHAPTER 6

Conclusions and Future Directions

6.1 Summary

This dissertation described the development of 3D model systems for studying the human brain by combining stem cell technology and biomaterials. A novel bio-functionalized hydrogel, GelMA-Cad, was developed and optimized to support 3D neuronal cultures, in both single cell suspensions and brain cortical organoids. GelMA-Cad solves many of the issues encountered with single cell suspensions of iPSC-derived neurons including the ability to study individual cells within a 3D culture as well as the ability to form functional connections among the neurons in 3D. This hydrogel can also be used to form synaptic connections between different populations of neurons, improving the ability to create more complex models for studying disease. Furthermore, GelMA-Cad improves the reproducibility of cortical organoid structures, which allows for more widespread use of this model. Additionally, the N-cadherin cues help the laminar organization of the organoids, which results in the organoids more closely resembling the architecture of the human brain. These proof of concept models are an exciting step forward in the area of *in vitro* modeling and provide more predictive results that can be translated to *in vivo* animal studies and the human brain.

6.2 Concerns and Limitations

While this work improved many aspects of *in vitro* human models of the brain, there are a few limitations to this work. One such limitation is the absence of a few cell types are important to the function of the human brain and can contribute to disease progression. For example, the models described in this thesis lack a functional blood brain barrier (BBB). The blood brain barrier is a unique system composed of tightly connected endothelial cells that limit the movement of materials both into and out of the brain (193). The presence of the BBB in the model would be highly useful for drug development, as this could provide information about whether treatments are able to get from the blood stream into the brain. The BBB would also be useful for studying methods that the human brain has for clearing aggregates like amyloid beta either by transporting the aggregates out of the brain or by allowing circulating immune cells into the brain to clear the aggregates (194). Additionally, these models can lack glia types that might be of interest to synaptic connectivity and the clearance of toxic species in the brain such as microglia, astrocytes, and oligodendrocytes (194; 195). While the brain organoids described in this thesis have both radial glia and astrocytes, these cell types are more akin to the fetal human brain. Incorporating more mature astrocytes may help support the maturation of iPSC-derived neurons. Additionally, astrocytes contribute to the proper functioning of synapses in the human

brain and can also be affected by protein aggregates during neurodegenerative disease progression (194; 196). Microglia are the resident immune cells of the brain and help clear protein aggregates from the brain (194). In order to be able to fully recapitulate the brain's immune response during disease progression, it is critical to incorporate this cell type. Oligodendrocytes are important to synaptic transmission, especially when connecting neurons over long distances, so as CNS models expand in complexity to model long distance neural communication, it may become necessary to incorporate this cell type in order to fully observe synaptic connectivity. This cell type might also be of particular interest when studying neurodegnerative diseases like multiple sclerosis (MS), where disease pathology involves the specific death of oligodendrocytes in addition to neurons (195). Furthermore, these are very simple models that do not fully recapitulate the complexity of the connectivity among different brain regions. These models have largely focused on the connectivity among cells within a single region, but there are complex neural networks that can contribute to disease progression (197–201). Finally, the size of the models described in this are size limited due to perfusion limitations of UV light through the GelMA-based hydrogels. As the models become more complex, larger hydrogel structures might be required. Other crosslinking methods can lead to a more even stiffness through the hydrogel.

6.3 Future Work

These models are an exciting step forward in the field of neurodegeneration modeling, and the future work for these projects involves addressing the limitations described in the previous section and increasing the complexity of the models in order to form a model that better recapitulates the brain architecture.

6.3.1 Incorporating a Functional Blood Brain Barrier

The decision to use gelatin as the backbone of the scaffolds is partly due to the ability to create more complex architectures within the hydrogel systems, including channels that could be perfused in order to model blood flow in the brain. The stem cell field has developed protocols for creating cell types of interest when it comes to the creation and maintenance of the brain's vascular unit including brain microvascular endothelial cells (BMECs) (43; 104), pericytes (42; 202), and smooth muscle cells (203). Furthermore, additional work has been done in this area to create 3D systems that have a functional perfusable channels that mimic the vascular architecture (204–208), and the BMECs can be seeded into perfusable systems to create a functional barrier (209; 210). This functional BBB model can be incorporated into the 3D neuronal model in order to study how the neurovascular unit functions during disease and how new therapeutics may interact with each cell type in order to treat disease phenotypes.

6.3.2 Adding Additional Glia and Neuron Subtypes into the Model

There are a variety of neuronal subtypes found in the brain in addition to cortical glutamatergic neurons, midbrain dopaminergic neurons, and medium spiny neurons, and these subtypes can contribute to different diseases. In order to expand the capabilities of disease modeling using these 3D neuronal systems, adding additional cell types that may be of importance will also be glia cell types. Addition of multiple neuronal subtypes will also allow researchers to study progression of neurodegenerative disease pathology from one neuronal population to another similar to what is seen in human disease progression (199–201).

For example, currently, there is only one published article where researchers model the interaction between these cell types in 3D (211), and this paper does not show that the 2 cell types form functional synapses with each other. As a result, there is a great need in the field for a 3D synaptically connected model of the connections between the substantia nigra (dopaminergic neurons) and the striatum (medium spiny neurons), which can then be used to study the break down in communication between these two brain regions during Parkinson's disease. Because we have shown that GelMA-Cad can support functional synapses in iPSC-derived glutamatergic neuron monocultures (2), we believe that GelMA-Cad can support functional synapses between iPSC-derived dopaminergic neurons and medium spiny neurons. We are currently differentiating stem cells into midbrain dopaminergic neurons and medium spiny neurons in order to begin creating a model of Parkinson's disease (Fig. 6.1).

Furthermore if neuroinflammation is a research area of interest, it will be important to include astrocytes and microglia, which act as immune cells when activated (194; 212). If multiple sclerosis is the disease of interest, oligodendrocytes will be critical to incorporate into the model (195). With each additional cell type incorporated into the system, the more the model will recapitulate the structure and connectivity of the human brain.

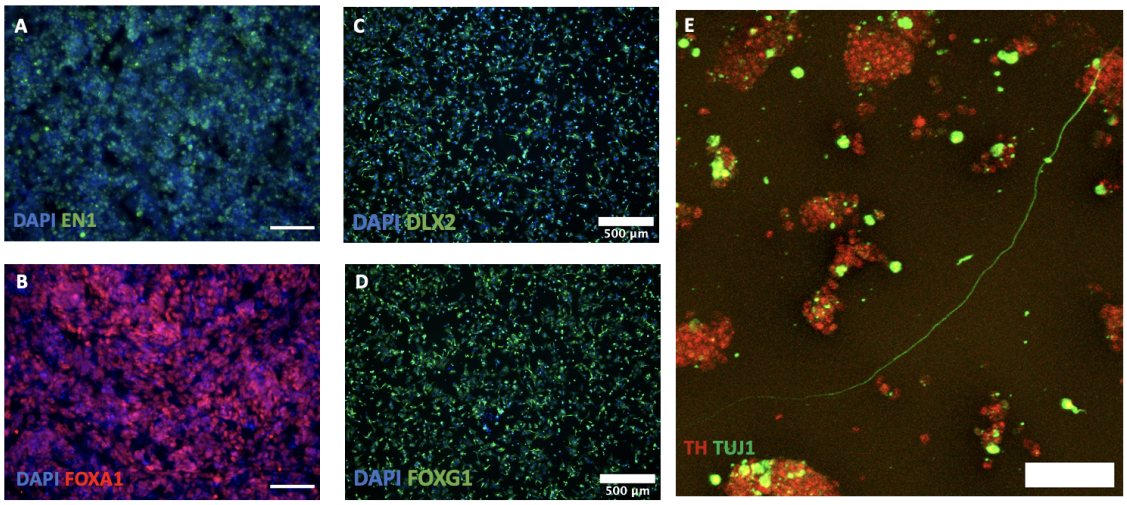

Figure 6.1: Ongoing work to develop a 3D *in vitro* model of Parkinson's disease. A,B) Confirmation that stem cells can be differentiated into midbrain dopaminergic neural progenitors (EN1+, FOXA2+). Scale bars represent 100 µm. C,D) Confirmation that stem cells can be differentiated into medium spiny neural progenitors (DLX2+, FOXG1+). E) Midbrain dopaminergic neural progenitors were embedded into GelMA-Cad and cultured for 2 weeks. The hydrogels were then fixed and stained for the neuronal marker, TUJ1, and the dopaminergic neuron marker, TH. Projections were seen in these cultures after 2 weeks. Scale bar represents 75 µm.

6.3.3 Increasing the Size Potential of the Model

New iterations of GelMA-Cad are being developed where the method of crosslinking the hydrogel are changed in order to allow for larger hydrogel structures. One such method was introduced in Aim 2 with the GelCad hydrogel, which enzymatically crosslinks the hydrogel rather than using a photo initiator and UV light. However, studies need to be conducted to fully understand how the enzyme used to crosslink the hydrogel can contribute to the cellular phenotypes observed. We noted that in the presence of transglutaminase, the organoids grew larger in terms of area when compared to organoids that were exposed to UV. This may be due to the hypothesized role of transglutaminase in brain development (17) It would also be important to understand how incorporation of an enzyme crosslinker might also affect disease progression in our models. For example, transglutaminase is known to contribute to Alzheimer's disease pathology (213–216). Other crosslinking methods that can be explored include using redox initiators or polyethylene glycol (PEG).

6.3.4 Creating Disease Models to Study Disease Pathology

The overall aim of this work is to develop a platform for studying neurodegeneration in human cells, so the future work will focus on the creation and validation of disease models using the systems described in this thesis. There are a variety of methods that can be used to create a disease model including the use of stem cells that have known disease-causing genetic mutations (for example, FAD or PSEN mutations for

modeling Alzheimer's disease) (115; 217; 218) or by incorporating disease-causing protein aggregates (such as embedding amyloid beta aggregates to the cultures for modeling Alzheimer's disease) (112; 219; 215; 220; 221).

We are currently validating an inducible model of Alzheimer's disease with iPSC-derived glutamatergic neurons embedded in GelMA-Cad. We have been able to make synthetic amyloid beta aggregates, which then be added to the 3D neuronal cultures (Fig. 6.2). As soon as 24 hours after adding amyloid beta to the cells, we noticed Alzheimer's disease-like characteristics such as neurite segmentation and swelling. Furthermore, we are able to modulate this response by adjusting the concentration of amyloid beta added to the cultures, where higher concentrations of amyloid beta results in increased neurite segmentation. Ongoing validation includes assessing the presence of phosphorylated tau and vesicular trafficking alterations after addition of amyloid beta. Once validated, we plan on studying the interaction between amyloid beta and neuronal synapses in order to better understand the mechanisms in which amyloid beta causes synaptic dysfunction. We are also making 3D co-cultures of neurons, astrocytes, and microglia in order to study how neuroinflammation in response to amyloid beta aggregates leads to synaptic dysfunction.

Disease models like the one described above can then be used to help uncover mechanisms behind the neuropathology of disease. For example, researchers found that APOEε4 mutations can worsen amyloid beta and tau aggregation when they studied PET images of human patients (222). However, the researchers note that this work was not intended to uncover the mechanisms behind the interactions between APOEε4 and protein aggregation. This is a study that would be possible with the models developed within this dissertation. Researchers can create isogenic iPSC lines with and without the APOEε4 mutation and create 3D neuronal models. These iPSC lines can also be used to generate other cell types that might be of interest such as microglia in order to uncover which cell types might be especially affected by disease-related mutations. The researchers could then induce an Alzheimer's disease-like model by incorporating amyloid beta or tau aggregates in order to determine whether a similar phenotype can be observed as what the researchers observed with PET imaging. Once they have validated the model, researchers can then start studying how APOEε4 interacts with amyloid beta and/or tau and how these interactions can lead to worsening Alzheimer's disease-like characteristics. Similar studies to the one described demonstrate how these 3D iPSC-derived neuronal models can help validate the observations seen in human patients or animal models as well as help uncover the mechanisms behind the phenotypes observed.

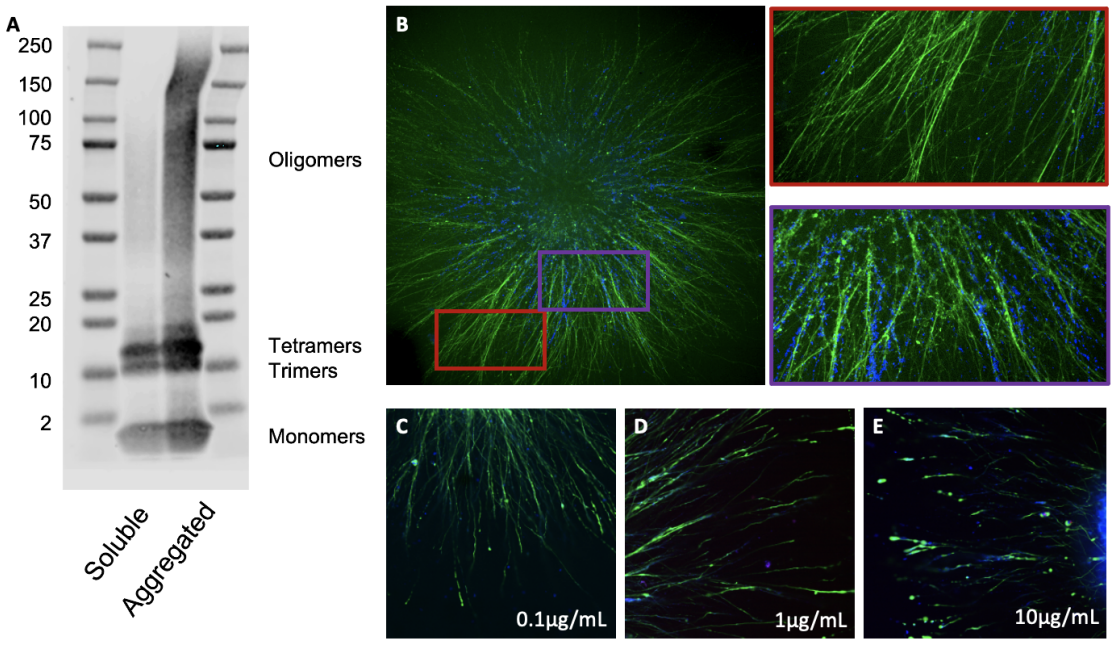

Figure 6.2: Creation and validation of an inducible model of Alzheimer's disease. A) Western blot of monomeric and aggregated synthetic amyloid beta demonstrate that a variety of structures can be formed *in vitro*. B) iPSC-derived neurons were embedded in GelMA-Cad and cultured for 2 weeks prior to the addition of amyloid beta. 24 hours after the addition of 10 µg/mL of aggregated amyloid beta, the neurons were Calcein stained to image live cells. The red insert shows a relatively unaffected region where there is little amyloid beta present, and the neurites remain healthy. The purple insert shows a highly affected region where there is amyloid beta surrounding the neurites, causing them to become swollen and/or disrupted in some regions. These effects can be modulated depending on the concentration of amyloid beta. Low concentrations of amyloid beta (B,C) cause less neurite swelling and segmentation than high concentrations of amyloid beta (D).

6.4 Broader Impacts and Conclusions

The field of neurodegenerative disease research has a great need for new *in vitro* models that can better recapitulate the structure and function of the cell types found in the human brain. This work is a proof of concept that addresses many of the traditional limitations encountered when studying the human brain *in vitro*. The models described in this dissertation can be used to develop disease models that can help uncover the mechanisms of neural connectivity disruption. The single-cell models allow researchers to significantly reduce the number of neurons needed to create synaptic connections in 3D, which increases the resolution of the live neurons. As a result, disease models can be studied while the cells are still alive in addition to studying fixed structures. Furthermore, this work improves the reproducibility of cortical organoids, which improves the potential utility of this emerging model. Additionally, this work provides the framework for creating increasingly complex models that can be used to study co-culture systems of neurodegenerative diseases in 3D. Future work will continue to create 3D *in vitro* models that better recapitulate the human

brain and will potentially bridge the gap between animal models and human patients, which will in turn lead to improved therapeutics for neurodegenerative diseases.

References

[1] Dugger BN, Dickson DW. Pathology of Neurodegenerative Diseases. Cold Spring Harbor Perspectives in Biology. 2017 Jul;9(7):a028035. Available from: https://www.ncbi.nlm.nih.gov/pmc/articles/PMC5495060/.

[2] O'Grady BJ, Balotin KM, Bosworth AM, McClatchey PM, Weinstein RM, Gupta M, et al. Development of an N-Cadherin Biofunctionalized Hydrogel to Support the Formation of Synaptically Connected Neural Networks. ACS Biomaterials Science & Engineering. 2020 Oct;6(10):5811-22. Publisher: American Chemical Society. Available from: https://doi.org/10.1021/acsbiomaterials.0c00885.

[3] Sun T, Hevner RF. Growth and folding of the mammalian cerebral cortex: from molecules to malformations. Nature Reviews Neuroscience. 2014 Apr;15(4):217-32. Number: 4 Publisher: Nature Publishing Group. Available from: https://www.nature.com/articles/nrn3707.

[4] McClatchey PM, Keller AC, Bouchard R, Knaub LA, Reusch JEB. Fully automated software for quantitative measurements of mitochondrial morphology. Mitochondrion. 2016 Jan;26:58-71. Available from: http://www.sciencedirect.com/science/article/pii/S1567724915300404.

[5] Mukhtar T, Taylor V. Untangling Cortical Complexity During Development. Journal of Experimental Neuroscience. 2018 Mar;12. Available from: https://www.ncbi.nlm.nih.gov/pmc/articles/PMC5846925/.

[6] Lancaster MA, Knoblich JA. Generation of Cerebral Organoids from Human Pluripotent Stem Cells. Nature protocols. 2014 Oct;9(10):2329-40. Available from: https://www.ncbi.nlm.nih.gov/pmc/articles/PMC4160653/.

[7] Yoon SJ, Elahi LS, Paşca AM, Marton RM, Gordon A, Revah O, et al. Reliability of human cortical organoid generation. Nature Methods. 2019 Jan;16(1):75-8. Available from: https://www.nature.com/articles/s41592-018-0255-0.

[8] Lancaster MA, Renner M, Martin CA, Wenzel D, Bicknell LS, Hurles ME, et al. Cerebral organoids model human brain development and microcephaly. Nature. 2013 Sep;501(7467):373-9. Available from: http://www.nature.com/articles/nature12517.

[9] Paşca AM, Sloan SA, Clarke LE, Tian Y, Makinson CD, Huber N, et al. Functional cortical neurons and astrocytes from human pluripotent stem cells in 3D culture. Nature methods. 2015 Jul;12(7):671-8. Available from: http://www.ncbi.nlm.nih.gov/pmc/articles/PMC4489980/.

[10] Vanni S, Colini Baldeschi A, Zattoni M, Legname G. Brain aging: A Ianus-faced player between health and neurodegeneration. Journal of Neuroscience Research. 2020;98(2):299-311. _eprint: https://onlinelibrary.wiley.com/doi/pdf/10.1002/jnr.24379. Available from: http://onlinelibrary.wiley.com/doi/abs/10.1002/jnr.24379.

[11] Laurijssens B, Aujard F, Rahman A. Animal models of Alzheimer's disease and drug development. Drug Discovery Today: Technologies. 2013 Sep;10(3):e319-27. Available from: http://www.sciencedirect.com/science/article/pii/S1740674912000182.

[12] Salloway S, Sperling R, Fox NC, Blennow K, Klunk W, Raskind M, et al. Two Phase 3 Trials of Bapineuzumab in Mild-to-Moderate Alzheimer's Disease. New England Journal of Medicine. 2014 Jan;370(4):322-33. Available from: https://doi.org/10.1056/NEJMoa1304839.

[13] Extance A. Alzheimer's failure raises questions about disease-modifying strategies. Nature Reviews Drug Discovery. 2010 Oct;9(10):749-51. Available from: http://www.nature.com/articles/nrd3288.

[14] Check E. Nerve inflammation halts trial for Alzheimer's drug. Nature. 2002 Jan;415(6871):462-2. Available from: http://www.nature.com/articles/415462a.

[15] Turner RS, Stubbs T, Davies DA, Albensi BC. Potential New Approaches for Diagnosis of Alzheimer's Disease and Related Dementias. Frontiers in Neurology. 2020;11. Available from: https://www.frontiersin.org/article/10.3389/fneur.2020.00496.

[16] Ransohoff RM. All (animal) models (of neurodegeneration) are wrong. Are they also useful? Journal of Experimental Medicine. 2018 Nov;215(12):2955-8. Available from: https://doi.org/10.1084/jem.20182042.

[17] Lesort M, Tucholski J, Miller ML, Johnson GVW. Tissue transglutaminase: a possible role in neurodegenerative diseases. Progress in Neurobiology. 2000 Aug;61(5):439-63. Available from: http://www.sciencedirect.com/science/article/pii/S0301008299000520.

[18] Mattson MP. Pathways towards and away from Alzheimer's disease. Nature. 2004 Aug;430(7000):631-9. Number: 7000 Publisher: Nature Publishing Group. Available from: http://www.nature.com/articles/nature02621.

[19] O'Brien RJ, Wong PC. Amyloid Precursor Protein Processing and Alzheimer's Disease. Annual review of neuroscience. 2011;34:185-204. Available from: https://www.ncbi.nlm.nih.gov/pmc/articles/PMC3174086/.

[20] Gowrishankar S, Yuan P, Wu Y, Schrag M, Paradise S, Grutzendler J, et al. Massive accumulation of luminal protease-deficient axonal lysosomes at Alzheimer's disease amyloid plaques. Proceedings of the National Academy of Sciences. 2015 Jul;112(28):E3699-708. Available from: https://www.pnas.org/content/112/28/E3699.

[21] Spires-Jones T, Hyman B. The Intersection of Amyloid Beta and Tau at Synapses in Alzheimer's Disease. Neuron. 2014 May;82(4):756-71. Available from: http://www.sciencedirect.com/science/article/pii/S0896627314003900.

[22] Reddy PH, Beal MF. Amyloid beta, mitochondrial dysfunction and synaptic damage: implications for cognitive decline in aging and Alzheimer's disease. Trends in Molecular Medicine. 2008 Feb;14(2):45-53. Available from: http://www.sciencedirect.com/science/article/pii/S1471491408000038.

[23] Haass C, Selkoe DJ. Soluble protein oligomers in neurodegeneration: lessons from the Alzheimer's amyloid β-peptide. Nature Reviews Molecular Cell Biology. 2007 Feb;8(2):101-12. Number: 2 Publisher: Nature Publishing Group. Available from: http://www.nature.com/articles/nrm2101.

[24] de Calignon A, Polydoro M, Suárez-Calvet M, William C, Adamowicz DH, Kopeikina KJ, et al. Propagation of Tau Pathology in a Model of Early Alzheimer's Disease. Neuron. 2012 Feb;73(4):685-97. Available from: https://www.sciencedirect.com/science/article/pii/S0896627312000384.

[25] Mohandas E, Rajmohan V, Raghunath B. Neurobiology of Alzheimer's disease. Indian Journal of Psychiatry. 2009;51(1):55-61. Available from: https://www.ncbi.nlm.nih.gov/pmc/articles/PMC2738403/.

[26] Iqbal K, Liu F, Gong CX, Grundke-Iqbal I. Tau in Alzheimer Disease and Related Tauopathies. Current Alzheimer research. 2010 Dec;7(8):656-64. Available from: https://www.ncbi.nlm.nih.gov/pmc/articles/PMC3090074/.

[27] Przedborski S. The two-century journey of Parkinson disease research. Nature Reviews Neuroscience. 2017 Apr;18(4):251-9. Number: 4 Publisher: Nature Publishing Group. Available from: http://www.nature.com/articles/nrn.2017.25.

[28] Dauer W, Przedborski S. Parkinson's Disease: Mechanisms and Models. Neuron. 2003 Sep;39(6):889-909. Available from: http://www.sciencedirect.com/science/article/pii/S0896627303005683.

[29] Stefanis L. α-Synuclein in Parkinson's Disease. Cold Spring Harbor Perspectives in Medicine. 2012 Feb;2(2). Available from: https://www.ncbi.nlm.nih.gov/pmc/articles/PMC3281589/.

[30] Kahle PJ, Haass C, Kretzschmar HA, Neumann M. Structure/function of α-synuclein in health and disease: rational development of animal models for Parkinson's and related diseases. Journal of Neurochemistry. 2002;82(3):449-57. _eprint: https://onlinelibrary.wiley.com/doi/pdf/10.1046/j.1471-4159.2002.01020.x. Available from: http://onlinelibrary.wiley.com/doi/abs/10.1046/j.1471-4159.2002.01020.x.

[31] Ghiglieri V, Calabrese V, Calabresi P. Alpha-Synuclein: From Early Synaptic Dysfunction to Neurodegeneration. Frontiers in Neurology. 2018;9. Available from: http://www.frontiersin.org/articles/10.3389/fneur.2018.00295/full.

[32] Younes K, Miller BL. Frontotemporal Dementia: Neuropathology, Genetics, Neuroimaging, and Treatments. The Psychiatric Clinics of North America. 2020 Jun;43(2):331-44.

[33] Cohen TJ, Lee VMY, Trojanowski JQ. TDP-43 functions and pathogenic mechanisms implicated in TDP-43 proteinopathies. Trends in Molecular Medicine. 2011 Nov;17(11):659-67. Available from: https://www.sciencedirect.com/science/article/pii/S1471491411001055.

[34] Ling SC. Synaptic Paths to Neurodegeneration: The Emerging Role of TDP-43 and FUS in Synaptic Functions. Neural Plasticity. 2018 Apr;2018:8413496. Available from: https://www.ncbi.nlm.nih.gov/pmc/articles/PMC5925147/.

[35] Kouri N, Whitwell JL, Josephs KA, Rademakers R, Dickson DW. Corticobasal degeneration: a pathologically distinct 4R tauopathy. Nature Reviews Neurology. 2011 May;7(5):263-72. Number: 5 Publisher: Nature Publishing Group. Available from: https://www.nature.com/articles/nrneurol.2011.43.

[36] Ittner LM, Ke YD, Delerue F, Bi M, Gladbach A, van Eersel J, et al. Dendritic Function of Tau Mediates Amyloid-β Toxicity in Alzheimer's Disease Mouse Models. Cell. 2010 Aug;142(3):387-97. Available from: https://www.sciencedirect.com/science/article/pii/S0092867410007269.

[37] Hoover BR, Reed MN, Su J, Penrod RD, Kotilinek LA, Grant MK, et al. Tau Mislocalization to Dendritic Spines Mediates Synaptic Dysfunction Independently of Neurodegeneration. Neuron. 2010 Dec;68(6):1067-81. Available from: https://www.sciencedirect.com/science/article/pii/S0896627310009724.

[38] Krencik R, Zhang SC. Directed differentiation of functional astroglial subtypes from human pluripotent stem cells. Nature Protocols. 2011 Nov;6(11):1710-7. Available from: https://www.nature.com/articles/nprot.2011.405.

[39] Shaltouki A, Peng J, Liu Q, Rao MS, Zeng X. Efficient Generation of Astrocytes from Human Pluripotent Stem Cells in Defined Conditions. Stem Cells. 2013 May;31(5):941-52. Available from: http://onlinelibrary.wiley.com/doi/10.1002/stem.1334/full.

[40] Orlova Valeria V , Drabsch Yvette, Freund Christian, Petrus-Reurer Sandra, van den Hil Francijna E , Muenthaisong Suchitra, et al. Functionality of Endothelial Cells and Pericytes From Human Pluripotent Stem Cells Demonstrated in Cultured Vascular Plexus and Zebrafish Xenografts. Arteriosclerosis, Thrombosis, and Vascular Biology. 2014 Jan;34(1):177-86. Available from: https://www.ahajournals.org/doi/full/10.1161/ATVBAHA.113.302598.

[41] Wanjare M, Kusuma S, Gerecht S. Perivascular cells in blood vessel regeneration. Biotechnology Journal. 2013;8(4):434-47. Available from: https://onlinelibrary.wiley.com/doi/abs/10.1002/biot.201200199.

[42] Stebbins MJ, Gastfriend BD, Canfield SG, Lee MS, Richards D, Faubion MG, et al. Human pluripotent stem cell–derived brain pericyte–like cells induce blood-brain barrier properties. Science Advances. 2019 Mar;5(3):1-16. Available from: https://advances.sciencemag.org/content/5/3/eaau7375.

[43] Neal EH, Marinelli NA, Shi Y, McClatchey PM, Balotin KM, Gullett DR, et al. A Simplified, Fully Defined Differentiation Scheme for Producing Blood-Brain Barrier Endothelial Cells from Human iPSCs. Stem Cell Reports. 2019 Jun;12(6):1380-8. Available from: http://www.sciencedirect.com/science/article/pii/S2213671119301754.

[44] Abud EM, Ramirez RN, Martinez ES, Healy LM, Nguyen CHH, Newman SA, et al. iPSC-Derived Human Microglia-like Cells to Study Neurological Diseases. Neuron. 2017 Apr;94(2):278-93.e9. Available from: http://www.sciencedirect.com/science/article/pii/S0896627317302866.

[45] Muffat J, Li Y, Yuan B, Mitalipova M, Omer A, Corcoran S, et al. Efficient derivation of microglia-like cells from human pluripotent stem cells. Nature Medicine. 2016 Nov;22(11):1358-67. Available from: https://www.nature.com/articles/nm.4189.

[46] Chambers SM, Fasano CA, Papapetrou EP, Tomishima M, Sadelain M, Studer L. Highly efficient neural conversion of human ES and iPS cells by dual inhibition of SMAD signaling. Nature Biotechnology. 2009 Mar;27(3):275-80. Available from: https://www.nature.com/nbt/journal/v27/n3/full/nbt.1529.html.

[47] Shi Y, Kirwan P, Livesey FJ. Directed differentiation of human pluripotent stem cells to cerebral cortex neurons and neural networks. Nature Protocols. 2012 Oct;7(10):1836-46.

[48] Maroof AM, Keros S, Tyson JA, Ying SW, Ganat YM, Merkle FT, et al. Directed differentiation and functional maturation of cortical interneurons from human embryonic stem cells. Cell Stem Cell. 2013 May;12(5):559-72.

[49] Kriks S, Shim JW, Piao J, Ganat YM, Wakeman DR, Xie Z, et al. Dopamine neurons derived from human ES cells efficiently engraft in animal models of Parkinson's disease. Nature. 2011 Nov;480(7378):547-51.

[50] Nolbrant S, Heuer A, Parmar M, Kirkeby A. Generation of high-purity human ventral midbrain dopaminergic progenitors for in vitro maturation and intracerebral transplantation. Nature Protocols. 2017 Sep;12(9):1962-79. Available from: http://www.nature.com/nprot/journal/v12/n9/full/nprot.2017.078.html.

[51] Kim TW, Piao J, Koo SY, Kriks S, Chung SY, Betel D, et al. Biphasic Activation of WNT Signaling Facilitates the Derivation of Midbrain Dopamine Neurons from hESCs for Translational Use. Cell Stem Cell. 2021 Feb;28(2):343-55.e5. Available from: https://www.sciencedirect.com/science/article/pii/S1934590921000059.

[52] Wu M, Zhang D, Bi C, Mi T, Zhu W, Xia L, et al. A Chemical Recipe for Generation of Clinical-Grade Striatal Neurons from hESCs. Stem Cell Reports. 2018 Sep;11(3):635-50. Available from: http://www.sciencedirect.com/science/article/pii/S2213671118303266.

[53] Moreno H, Morfini G, Buitrago L, Ujlaki G, Choi S, Yu E, et al. Tau pathology-mediated presynaptic dysfunction. Neuroscience. 2016 Jun;325:30-8. Available from: http://www.sciencedirect.com/science/article/pii/S0306452216300239.

[54] Kelava I, Lancaster MA. Dishing out mini-brains: Current progress and future prospects in brain organoid research. Developmental Biology. 2016 Dec;420(2):199-209. Available from: https://www.ncbi.nlm.nih.gov/pmc/articles/PMC5161139/.

[55] Harris KD, Mrsic-Flogel TD. Cortical connectivity and sensory coding. Nature. 2013 Nov;503(7474):51-8. Available from: http://www.nature.com/articles/nature12654.

[56] Kelava I, Lancaster MA. Stem Cell Models of Human Brain Development. Cell Stem Cell. 2016 Jun;18(6):736-48. Available from: https://www.cell.com/cell-stem-cell/abstract/S1934-5909(16)30106-0.

[57] Barros CS, Franco SJ, Müller U. Extracellular Matrix: Functions in the Nervous System. Cold Spring Harbor Perspectives in Biology. 2011 Jan;3(1). Available from: http://www.ncbi.nlm.nih.gov/pmc/articles/PMC3003458/.

[58] Hughes CS, Postovit LM, Lajoie GA. Matrigel: A complex protein mixture required for optimal growth of cell culture. PROTEOMICS. 2010;10(9):1886-90. Available from: http://onlinelibrary.wiley.com/doi/abs/10.1002/pmic.200900758.

[59] Kothapalli CR, Kamm RD. 3D matrix microenvironment for targeted differentiation of embryonic stem cells into neural and glial lineages. Biomaterials. 2013 Aug;34(25):5995-6007. Available from: http://www.sciencedirect.com/science/article/pii/S0142961213005012.

[60] Fatehullah A, Tan SH, Barker N. Organoids as an in vitro model of human development and disease. Nature Cell Biology. 2016 Mar;18(3):246-54. Available from: http://www.nature.com/articles/ncb3312.

[61] Zhang ZN, Freitas BC, Qian H, Lux J, Acab A, Trujillo CA, et al. Layered hydrogels accelerate iPSC-derived neuronal maturation and reveal migration defects caused by MeCP2 dysfunction. Proc Natl Acad Sci U S A. 2016 Mar;113(12):3185-90. Available from: https://www.pnas.org/content/113/12/3185.

[62] Zhuang P, Sun AX, An J, Chua CK, Chew SY. 3D neural tissue models: From spheroids to bioprinting. Biomaterials. 2018 Feb;154:113-33. Available from: https://www.sciencedirect.com/science/article/pii/S0142961217306361.

[63] Ren T, Grosshäuser B, Sridhar K, Nieland TJF, Tocchio A, Schepers U, et al. 3-D geometry and irregular connectivity dictate neuronal firing in frequency domain and synchronization. Biomaterials. 2019 Mar;197:171-81. Available from: http://www.sciencedirect.com/science/article/pii/S0142961219300237.

[64] Bian L, Guvendiren M, Mauck RL, Burdick JA. Hydrogels that mimic developmentally relevant matrix and N-cadherin interactions enhance MSC chondrogenesis. Proc Natl Acad Sci U S A. 2013 Jun;110(25):10117-22. Available from: https://www.ncbi.nlm.nih.gov/pmc/articles/PMC3690835/.

[65] Kadowaki M, Nakamura S, Machon O, Krauss S, Radice GL, Takeichi M. N-cadherin mediates cortical organization in the mouse brain. Developmental Biology. 2007 Apr;304(1):22-33. Available from: http://www.sciencedirect.com/science/article/pii/S0012160606014321.

[66] Matsunaga Y, Noda M, Murakawa H, Hayashi K, Nagasaka A, Inoue S, et al. Reelin transiently promotes N-cadherin–dependent neuronal adhesion during mouse cortical development. Proc Natl Acad Sci. 2017 Feb;114(8):2048-53. Available from: https://www.pnas.org/content/114/8/2048.

[67] Shikanai M, Nakajima K, Kawauchi T. N-Cadherin regulates radial glial fiber-dependent migration of cortical locomoting neurons. Communicative & Integrative Biology. 2011 May;4(3):326-30. Available from: https://doi.org/10.4161/cib.4.3.14886.

[68] Xu C, Funahashi Y, Watanabe T, Takano T, Nakamuta S, Namba T, et al. Radial Glial Cell–Neuron Interaction Directs Axon Formation at the Opposite Side of the Neuron from the Contact Site. Journal of Neuroscience. 2015 Oct;35(43):14517-32. Available from: https://www.jneurosci.org/content/35/43/14517.

[69] Benson DL, Tanaka H. N-Cadherin Redistribution during Synaptogenesis in Hippocampal Neurons. Journal of Neuroscience. 1998 Sep;18(17):6892-904. Available from: http://www.jneurosci.org/content/18/17/6892.

[70] Tan ZJ, Peng Y, Song HL, Zheng JJ, Yu X. N-cadherin-dependent neuron-neuron interaction is required for the maintenance of activity-induced dendrite growth. Proc Natl Acad Sci. 2010 May;107(21):9873-8. Available from: http://europepmc.org/abstract/med/20457910.

[71] Togashi H, Abe K, Mizoguchi A, Takaoka K, Chisaka O, Takeichi M. Cadherin Regulates Dendritic Spine Morphogenesis. Neuron. 2002 Jul;35(1):77-89. Available from: http://www.sciencedirect.com/science/article/pii/S0896627302007481.

[72] Tomaselli KJ, Neugebauer KM, Bixby JL, Lilien J, Reichard LF. N-cadherin and integrins: Two receptor systems that mediate neuronal process outgrowth on astrocyte surfaces. Neuron. 1988 Mar;1(1):33-43. Available from: http://www.sciencedirect.com/science/article/pii/0896627388902073.

[73] Cherry JF, Bennett NK, Schachner M, Moghe PV. Engineered N-cadherin and L1 biomimetic substrates concertedly promote neuronal differentiation, neurite extension and neuroprotection of human neural stem cells. Acta Biomaterialia. 2014 Oct;10(10):4113-26. Available from: http://www.sciencedirect.com/science/article/pii/S1742706114002487.

[74] Lim HJ, Khan Z, Wilems TS, Lu X, Perera TH, Kurosu YE, et al. Human Induced Pluripotent Stem Cell Derived Neural Stem Cell Survival and Neural Differentiation on Polyethylene Glycol Dimethacrylate Hydrogels Containing a Continuous Concentration Gradient of N-Cadherin Derived Peptide His-Ala-Val-Asp-Ile. ACS Biomaterials Science & Engineering. 2017 May;3(5):776-81. Available from: https://doi.org/10.1021/acsbiomaterials.6b00745.

[75] Haque A, Adnan N, Motazedian A, Akter F, Hossain S, Kutsuzawa K, et al. An Engineered N-Cadherin Substrate for Differentiation, Survival, and Selection of Pluripotent Stem Cell-Derived Neural Progenitors. PLOS ONE. 2015 Aug;10(8). Available from: https://journals.plos.org/plosone/article?id=10.1371/journal.pone.0135170.

[76] Miyasaka T, Ding Z, Gengyo-Ando K, Oue M, Yamaguchi H, Mitani S, et al. Progressive neurodegeneration in C. elegans model of tauopathy. Neurobiology of Disease. 2005 Nov;20(2):372-83.

[77] Wittmann CW, Wszolek MF, Shulman JM, Salvaterra PM, Lewis J, Hutton M, et al. Tauopathy in Drosophila: Neurodegeneration Without Neurofibrillary Tangles. Science. 2001 Jul;293(5530):711-4. Publisher: American Association for the Advancement of Science. Available from: http://www.science.org/doi/full/10.1126/science.1062382.

[78] Jackson GR, Wiedau-Pazos M, Sang TK, Wagle N, Brown CA, Massachi S, et al. Human wild-type tau interacts with wingless pathway components and produces neurofibrillary pathology in Drosophila. Neuron. 2002 May;34(4):509-19.

[79] Iijima K, Liu HP, Chiang AS, Hearn SA, Konsolaki M, Zhong Y. Dissecting the pathological effects of human Aβ40 and Aβ42 in Drosophila: A potential model for Alzheimer's disease. Proceedings of the National Academy of Sciences of the United States of America. 2004 Apr;101(17):6623-8. Available from: https://www.ncbi.nlm.nih.gov/pmc/articles/PMC404095/.

[80] Bezard E, Przedborski S. A tale on animal models of Parkinson's disease. Movement Disorders: Official Journal of the Movement Disorder Society. 2011 May;26(6):993-1002.

[81] Razafsha M, Behforuzi H, Harati H, Wafai RA, Khaku A, Mondello S, et al. An updated overview of animal models in neuropsychiatry. Neuroscience. 2013 Jun;240:204-18. Available from: http://www.sciencedirect.com/science/article/pii/S0306452213001863.

[82] Götz J, Ittner LM. Animal models of Alzheimer's disease and frontotemporal dementia. Nature Reviews Neuroscience. 2008 Jul;9(7):532-44.

[83] McGonigle P. Animal models of CNS disorders. Biochemical Pharmacology. 2014 Jan;87(1):140-9. Available from: http://www.sciencedirect.com/science/article/pii/S0006295213003870.

[84] Neha n, Sodhi RK, Jaggi AS, Singh N. Animal models of dementia and cognitive dysfunction. Life Sciences. 2014 Jul;109(2):73-86.

[85] Blandini F, Armentero MT. Animal models of Parkinson's disease. FEBS Journal. 2012 Apr;279(7):1156-66. Available from: http://onlinelibrary.wiley.com/doi/10.1111/j.1742-4658.2012.08491.x/abstract.

[86] Jackson-Lewis V, Blesa J, Przedborski S. Animal models of Parkinson's disease. Parkinsonism & Related Disorders. 2012 Jan;18:S183-5. Available from: http://www.sciencedirect.com/science/article/pii/S1353802011700578.

[87] Gubellini P, Kachidian P. Animal models of Parkinson's disease: An updated overview. Revue Neurologique. 2015 Nov;171(11):750-61.

[88] McDowell K, Chesselet MF. Animal models of the non-motor features of Parkinson's disease. Neurobiology of Disease. 2012 Jun;46(3):597-606.

[89] Vingill S, Connor-Robson N, Wade-Martins R. Are rodent models of Parkinson's disease behaving as they should? Behavioural Brain Research. 2017 Oct.

[90] Link CD. C. elegans models of age-associated neurodegenerative diseases: lessons from transgenic worm models of Alzheimer's disease. Experimental Gerontology. 2006 Oct;41(10):1007-13.

[91] Santana S, Rico EP, Burgos JS. Can zebrafish be used as animal model to study Alzheimer's disease? American Journal of Neurodegenerative Disease. 2012;1(1):32-48.

[92] Colpo GD, Ribeiro FM, Rocha NP, Teixeira AL. Chapter 42 - Animal Models for the Study of Human Neurodegenerative Diseases. In: Conn PM, editor. Animal Models for the Study of Human Disease (Second Edition). Academic Press; 2017. p. 1109-29. Available from: https://www.sciencedirect.com/science/article/pii/B9780128094686000425.

[93] Bezard E, Gross CE, Fournier MC, Dovero S, Bloch B, Jaber M. Absence of MPTP-induced neuronal death in mice lacking the dopamine transporter. Experimental Neurology. 1999 Feb;155(2):268-73.

[94] Purisai MG, McCormack AL, Langston WJ, Johnston LC, Di Monte DA. Alpha-synuclein expression in the substantia nigra of MPTP-lesioned non-human primates. Neurobiology of Disease. 2005 Dec;20(3):898-906.

[95] Porras G, Li Q, Bezard E. Modeling Parkinson's Disease in Primates: The MPTP Model. Cold Spring Harbor Perspectives in Medicine. 2012 Mar;2(3):a009308. Available from: https://www.ncbi.nlm.nih.gov/pmc/articles/PMC3282499/.

[96] Solari N, Bonito-Oliva A, Fisone G, Brambilla R. Understanding cognitive deficits in Parkinson's disease: lessons from preclinical animal models. Learning & Memory (Cold Spring Harbor, NY). 2013 Sep;20(10):592-600.

[97] Dogra N, Mani RJ, Katare DP. The Gut-Brain Axis: Two Ways Signaling in Parkinson's Disease. Cellular and Molecular Neurobiology. 2022 Mar;42(2):315-32. Available from: https://doi.org/10.1007/s10571-021-01066-7.

[98] Deng HX, Siddique T. Transgenic Mouse Models and Human Neurodegenerative Disorders. Archives of Neurology. 2000 Dec;57(12):1695-702. Available from: https://doi.org/10.1001/archneur.57.12.1695.

[99] Zhao X, Bhattacharyya A. Human Models Are Needed for Studying Human Neurodevelopmental Disorders. American Journal of Human Genetics. 2018 Dec;103(6):829-57. Available from: https://www.ncbi.nlm.nih.gov/pmc/articles/PMC6288051/.

[100] Slanzi A, Iannoto G, Rossi B, Zenaro E, Constantin G. In vitro Models of Neurodegenerative Diseases. Frontiers in Cell and Developmental Biology. 2020;8. Available from: https://www.frontiersin.org/article/10.3389/fcell.2020.00328.

[101] Lovett ML, Nieland TJF, Dingle YTL, Kaplan DL. Innovations in 3D Tissue Models of Human Brain Physiology and Diseases. Advanced Functional Materials. 2020;30(44):1909146. _eprint: https://onlinelibrary.wiley.com/doi/pdf/10.1002/adfm.201909146. Available from: http://onlinelibrary.wiley.com/doi/abs/10.1002/adfm.201909146.

[102] Opitz A, Falchier A, Linn GS, Milham MP, Schroeder CE. Limitations of ex vivo measurements for in vivo neuroscience. Proceedings of the National Academy of Sciences. 2017 May;114(20):5243-6. Publisher: Proceedings of the National Academy of Sciences. Available from: https://www.pnas.org/doi/10.1073/pnas.1617024114.

[103] Daviaud N, Garbayo E, Lautram N, Franconi F, Lemaire L, Perez-Pinzon M, et al. Modeling nigrostriatal degeneration in organotypic cultures, a new ex vivo model of Parkinson's disease. Neuroscience. 2014 Jan;256:10-22. Available from: https://www.sciencedirect.com/science/article/pii/S0306452213008749.

[104] Hollmann EK, Bailey AK, Potharazu AV, Neely MD, Bowman AB, Lippmann ES. Accelerated differentiation of human induced pluripotent stem cells to blood-brain barrier endothelial cells. Fluids and barriers of the CNS. 2017 Apr;14(1):9.

[105] Ronaldson-Bouchard K, Vunjak-Novakovic G. Organs-on-a-Chip: A Fast Track for Engineered Human Tissues in Drug Development. Cell Stem Cell. 2018 Mar;22(3):310-24. Available from: https://www.sciencedirect.com/science/article/pii/S1934590918300730.

[106] Raimondi I, Izzo L, Tunesi M, Comar M, Albani D, Giordano C. Organ-On-A-Chip in vitro Models of the Brain and the Blood-Brain Barrier and Their Value to Study the Microbiota-Gut-Brain Axis in Neurodegeneration. Frontiers in Bioengineering and Biotechnology. 2020;7. Available from: https://www.frontiersin.org/article/10.3389/fbioe.2019.00435.

[107] Maoz BM, Herland A, FitzGerald EA, Grevesse T, Vidoudez C, Pacheco AR, et al. A linked organ-on-chip model of the human neurovascular unit reveals the metabolic coupling of endothelial and neuronal cells. Nature Biotechnology. 2018 Oct;36(9):865-74.

[108] Bang S, Jeong S, Choi N, Kim HN. Brain-on-a-chip: A history of development and future perspective. Biomicrofluidics. 2019 Oct;13(5):051301. Available from: https://www.ncbi.nlm.nih.gov/pmc/articles/PMC6783295/.

[109] Lyu Z, Park J, Kim KM, Jin HJ, Wu H, Rajadas J, et al. A neurovascular-unit-on-a-chip for the evaluation of the restorative potential of stem cell therapies for ischaemic stroke. Nature Biomedical Engineering. 2021 Aug;5(8):847-63. Number: 8 Publisher: Nature Publishing Group. Available from: https://www.nature.com/articles/s41551-021-00744-7.

[110] Danku AE, Dulf EH, Braicu C, Jurj A, Berindan-Neagoe I. Organ-On-A-Chip: A Survey of Technical Results and Problems. Frontiers in Bioengineering and Biotechnology. 2022;10. Available from: https://www.frontiersin.org/article/10.3389/fbioe.2022.840674.

[111] O'Grady BJ, Geuy MD, Kim H, Balotin KM, Allchin ER, Florian DC, et al. Rapid prototyping of cell culture microdevices using parylene-coated 3D prints. Lab on a Chip. 2021 Dec;21(24):4814-22. Publisher: The Royal Society of Chemistry. Available from: https://pubs.rsc.org/en/content/articlelanding/2021/lc/d1lc00744k.

[112] Park J, Wetzel I, Marriott I, Dréau D, D'Avanzo C, Kim DY, et al. A 3D Human Tri-Culture System Modeling Neurodegeneration and Neuroinflammation in Alzheimer's Disease. Nature neuroscience. 2018 Jul;21(7):941-51. Available from: https://www.ncbi.nlm.nih.gov/pmc/articles/PMC6800152/.

[113] Qian X, Nguyen HN, Song MM, Hadiono C, Ogden SC, Hammack C, et al. Brain-Region-Specific Organoids Using Mini-bioreactors for Modeling ZIKV Exposure. Cell. 2016 May;165(5):1238-54.

[114] Tan HY, Cho H, Lee LP. Human mini-brain models. Nature Biomedical Engineering. 2021 Jan;5(1):11-25. Number: 1 Publisher: Nature Publishing Group. Available from: http://www.nature.com/articles/s41551-020-00643-3.

[115] Gonzalez C, Armijo E, Bravo-Alegria J, Becerra-Calixto A, Mays CE, Soto C. Modeling amyloid beta and tau pathology in human cerebral organoids. Molecular Psychiatry. 2018 Dec;23(12):2363-74. Number: 12 Publisher: Nature Publishing Group. Available from: https://www.nature.com/articles/s41380-018-0229-8.

[116] Papaspyropoulos A, Tsolaki M, Foroglou N, Pantazaki AA. Modeling and Targeting Alzheimer's Disease With Organoids. Frontiers in Pharmacology. 2020;11. Publisher: Frontiers. Available from: http://www.frontiersin.org/articles/10.3389/fphar.2020.00396/full.

[117] Zhao J, Fu Y, Yamazaki Y, Ren Y, Davis MD, Liu CC, et al. APOE4 exacerbates synapse loss and neurodegeneration in Alzheimer's disease patient iPSC-derived cerebral organoids. Nature Communications. 2020 Nov;11(1):5540. Number: 1 Publisher: Nature Publishing Group. Available from: https://www.nature.com/articles/s41467-020-19264-0.

[118] Fyfe I. Brain organoids shed light on APOE genotype and Alzheimer disease pathology. Nature Reviews Neurology. 2021 Jan;17(1):1-1. Number: 1 Publisher: Nature Publishing Group. Available from: https://www.nature.com/articles/s41582-020-00437-w.

[119] Kang YJ, Cho H. Human brain organoids in Alzheimer's disease. Organoid. 2021 Mar;1. Publisher: The Organoid Society. Available from: http://j-organoid.org/journal/view.php?number=7.

[120] Chen X, Sun G, Tian E, Zhang M, Davtyan H, Beach TG, et al. Modeling Sporadic Alzheimer's Disease in Human Brain Organoids under Serum Exposure. Advanced Science (Weinheim, Baden-Wurttemberg, Germany). 2021 Sep;8(18):e2101462.

[121] Lee SE, Choi H, Shin N, Kong D, Kim NG, Kim HY, et al. Zika virus infection accelerates Alzheimer's disease phenotypes in brain organoids. Cell Death Discovery. 2022 Apr;8(1):1-10. Number: 1 Publisher: Nature Publishing Group. Available from: https://www.nature.com/articles/s41420-022-00958-x.

[122] Bowles KR, Silva MC, Whitney K, Bertucci T, Berlind JE, Lai JD, et al. ELAVL4, splicing, and glutamatergic dysfunction precede neuron loss in MAPT mutation cerebral organoids. Cell. 2021 Aug;184(17):4547-63.e17. Available from: https://www.sciencedirect.com/science/article/pii/S0092867421008291.

[123] Pellegrini L, Lancaster MA. Modeling neurodegeneration with mutant-tau organoids. Cell. 2021 Aug;184(17):4377-9. Available from: https://www.sciencedirect.com/science/article/pii/S0092867421008904.

[124] Kim H, Park HJ, Choi H, Chang Y, Park H, Shin J, et al. Modeling G2019S-LRRK2 Sporadic Parkinson's Disease in 3D Midbrain Organoids. Stem Cell Reports. 2019 Mar;12(3):518-31. Available from: https://www.sciencedirect.com/science/article/pii/S2213671119300220.

[125] Galet B, Cheval H, Ravassard P. Patient-Derived Midbrain Organoids to Explore the Molecular Basis of Parkinson's Disease. Frontiers in Neurology. 2020;11. Available from: https://www.frontiersin.org/article/10.3389/fneur.2020.01005.

[126] Qian X, Nguyen HN, Jacob F, Song H, Ming Gl. Using brain organoids to understand Zika virus-induced microcephaly. Development (Cambridge, England). 2017 Mar;144(6):952-7. Available from: https://www.ncbi.nlm.nih.gov/pmc/articles/PMC5358105/.

[127] Watanabe M, Buth JE, Vishlaghi N, de la Torre-Ubieta L, Taxidis J, Khakh BS, et al. Self-Organized Cerebral Organoids with Human-Specific Features Predict Effective Drugs to Combat Zika Virus Infection. Cell Reports. 2017 Oct;21(2):517-32. Available from: https://www.sciencedirect.com/science/article/pii/S2211124717313372.

[128] Chen A, Guo Z, Fang L, Bian S. Application of Fused Organoid Models to Study Human Brain Development and Neural Disorders. Frontiers in Cellular Neuroscience. 2020;14. Available from: https://www.frontiersin.org/article/10.3389/fncel.2020.00133.

[129] Kornev VA, Grebenik EA, Solovieva AB, Dmitriev RI, Timashev PS. Hydrogel-assisted neuroregeneration approaches towards brain injury therapy: A state-of-the-art review. Computational and Structural Biotechnology Journal. 2018 Jan;16:488-502. Available from: https://www.sciencedirect.com/science/article/pii/S2001037018300977.

[130] Lancaster MA, Corsini NS, Wolfinger S, Gustafson EH, Phillips AW, Burkard TR, et al. Guided self-organization and cortical plate formation in human brain organoids. Nature Biotechnology. 2017 Jul;35(7):659-66. Available from: https://www.nature.com/articles/nbt.3906.

[131] Z Khaing Z, K Seidlits S. Hyaluronic acid and neural stem cells: implications for biomaterial design. Journal of Materials Chemistry B. 2015;3(40):7850-66. Publisher: Royal Society of Chemistry. Available from: http://pubs.rsc.org/en/content/articlelanding/2015/tb/c5tb00974j.

[132] Crapo PM, Medberry CJ, Reing JE, Tottey S, van der Merwe Y, Jones KE, et al. Biologic scaffolds composed of central nervous system extracellular matrix. Biomaterials. 2012 May;33(13):3539-47. Available from: http://www.ncbi.nlm.nih.gov/pmc/articles/PMC3516286/.

[133] DeQuach JA, Yuan SH, Goldstein LSB, Christman KL. Decellularized porcine brain matrix for cell culture and tissue engineering scaffolds. Tissue Engineering Part A. 2011 Nov;17(21-22):2583-92.

[134] Baiguera S, Del Gaudio C, Lucatelli E, Kuevda E, Boieri M, Mazzanti B, et al. Electrospun gelatin scaffolds incorporating rat decellularized brain extracellular matrix for neural tissue engineering. Biomaterials. 2014 Jan;35(4):1205-14. Available from: http://www.sciencedirect.com/science/article/pii/S0142961213013045.

[135] Cho AN, Jin Y, An Y, Kim J, Choi YS, Lee JS, et al. Microfluidic device with brain extracellular matrix promotes structural and functional maturation of human brain organoids. Nature Communications. 2021 Aug;12(1):4730. Number: 1 Publisher: Nature Publishing Group. Available from: https://www.nature.com/articles/s41467-021-24775-5.

[136] Mehta D, Jackson R, Paul G, Shi J, Sabbagh M. Why do trials for Alzheimer's disease drugs keep failing? A discontinued drug perspective for 2010–2015. Expert opinion on investigational drugs. 2017 Jun;26(6):735-9. Available from: https://www.ncbi.nlm.nih.gov/pmc/articles/PMC5576861/.

[137] Denayer T, Stöhr T, Van Roy M. Animal models in translational medicine: Validation and prediction. New Horizons in Translational Medicine. 2014 Sep;2(1):5-11. Available from: https://www.sciencedirect.com/science/article/pii/S2307502314000022.

[138] Bolker JA. Animal Models in Translational Research: Rosetta Stone or Stumbling Block? BioEssays. 2017;39(12):1700089. _eprint: https://onlinelibrary.wiley.com/doi/pdf/10.1002/bies.201700089. Available from: http://onlinelibrary.wiley.com/doi/abs/10.1002/bies.201700089.

[139] Zhang D, Pekkanen-Mattila M, Shahsavani M, Falk A, Teixeira AI, Herland A. A 3D Alzheimer's disease culture model and the induction of P21-activated kinase mediated sensing in iPSC derived neurons. Biomaterials. 2014 Feb;35(5):1420-8. Available from: https://www.sciencedirect.com/science/article/pii/S0142961213013811.

[140] Tian Xeng Be Z, Lu K, Rufaihah AJ, Fan VTt al. Comparison of osteogenesis of human embryonic stem cells within 2D and 3D culture systems. Scandinavian Journal of Clinical and Laboratory Investigation. 2008 Jan;68(1):58-67. Publisher: Taylor & Francis _eprint: https://doi.org/10.1080/00365510701466416. Available from: https://doi.org/10.1080/00365510701466416.

[141] Imamura Y, Mukohara T, Shimono Y, Funakoshi Y, Chayahara N, Toyoda M, et al. Comparison of 2D- and 3D-culture models as drug-testing platforms in breast cancer. Oncology Reports. 2015 Apr;33(4):1837-43. Publisher: Spandidos Publications. Available from: http://www.spandidos-publications.com/10.3892/or.2015.3767.

[142] Di Lullo E, Kriegstein AR. The use of brain organoids to investigate neural development and disease. Nature Reviews Neuroscience. 2017 Oct;18(10):573-84. Available from: https://www.nature.com/articles/nrn.2017.107.

[143] Long KR, Huttner WB. How the extracellular matrix shapes neural development. Open Biology;9(1):180216. Publisher: Royal Society. Available from: http://royalsocietypublishing.org/doi/full/10.1098/rsob.180216.

[144] Zhu J, Marchant RE. Design properties of hydrogel tissue-engineering scaffolds. Expert Review of Medical Devices. 2011 Sep;8(5):607-26. Publisher: Taylor & Francis _eprint: https://doi.org/10.1586/erd.11.27. Available from: https://doi.org/10.1586/erd.11.27.

[145] Zhou X, Cui H, Nowicki M, Miao S, Lee SJ, Masood F, et al. Three-Dimensional-Bioprinted Dopamine-Based Matrix for Promoting Neural Regeneration. ACS Applied Materials & Interfaces. 2018 Mar;10(10):8993-9001. Publisher: American Chemical Society. Available from: https://doi.org/10.1021/acsami.7b18197.

[146] Davey SK, Aung A, Agrawal G, Lim HL, Kar M, Varghese S. Embedded 3D Photopatterning of Hydrogels with Diverse and Complex Architectures for Tissue Engineering and Disease Models. Tissue Engineering Part C: Methods. 2015 Nov;21(11):1188-96. Publisher: Mary Ann Liebert, Inc., publishers. Available from: http://www.liebertpub.com/doi/full/10.1089/ten.tec.2015.0179.

[147] Nichol JW, Koshy S, Bae H, Hwang CM, Yamanlar S, Khademhosseini A. Cell-laden microengineered gelatin methacrylate hydrogels. Biomaterials. 2010 Jul;31(21):5536-44. Available from: https://www.ncbi.nlm.nih.gov/pmc/articles/PMC2878615/.

[148] Kumar KK, Lowe JEW, Aboud AA, Neely MD, Redha R, Bauer JA, et al. Cellular manganese content is developmentally regulated in human dopaminergic neurons. Scientific Reports. 2014 Oct;4:6801. Available from: http://www.nature.com/articles/srep06801.

[149] Lippmann ES, Estevez-Silva MC, Ashton RS. Defined human pluripotent stem cell culture enables highly efficient neuroepithelium derivation without small molecule inhibitors. Stem Cells (Dayton, Ohio). 2014 Apr;32(4):1032-42.

[150] Loessner D, Meinert C, Kaemmerer E, Martine LC, Yue K, Levett PA, et al. Functionalization, preparation and use of cell-laden gelatin methacryloyl–based hydrogels as modular tissue culture platforms. Nature Protocols. 2016 Apr;11(4):727-46. Available from: https://www.nature.com/articles/nprot.2016.037.

[151] Li X, Chen S, Li J, Wang X, Zhang J, Kawazoe N, et al. 3D Culture of Chondrocytes in Gelatin Hydrogels with Different Stiffness. Polymers. 2016 Aug;8(8):269. Available from: https://www.mdpi.com/2073-4360/8/8/269.

[152] Lee BH, Lum N, Seow LY, Lim PQ, Tan LP. Synthesis and Characterization of Types A and B Gelatin Methacryloyl for Bioink Applications. Materials. 2016 Oct;9(10):797. Available from: https://www.mdpi.com/1996-1944/9/10/797.

[153] Stroka KM, Aranda-Espinoza H. Endothelial cell substrate stiffness influences neutrophil transmigration via myosin light chain kinase-dependent cell contraction. Blood. 2011 Aug;118(6):1632-40. Available from: http://www.bloodjournal.org/content/118/6/1632.

[154] McClatchey PM, Mignemi NA, Xu Z, Williams IM, Reusch JEB, McGuinness OP, et al. Automated quantification of microvascular perfusion. Microcirculation (New York, NY: 1994). 2018;25(6).

[155] Jontes JD. The Cadherin Superfamily in Neural Circuit Assembly. Cold Spring Harbor Perspectives in Biology. 2018 Jul;10(7):a029306. Available from: http://cshperspectives.cshlp.org/content/10/7/a029306.

[156] Klotz BJ, Gawlitta D, Rosenberg AJWP, Malda J, Melchels FPW. Gelatin-Methacryloyl Hydrogels: Towards Biofabrication-Based Tissue Repair. Trends in Biotechnology. 2016 May;34(5):394-407. Available from: http://www.sciencedirect.com/science/article/pii/S0167779916000159.

[157] Yue K, Trujillo-de Santiago G, Alvarez MM, Tamayol A, Annabi N, Khademhosseini A. Synthesis, properties, and biomedical applications of gelatin methacryloyl (GelMA) hydrogels. Biomaterials. 2015 Dec;73:254-71. Available from: http://www.sciencedirect.com/science/article/pii/S014296121500719X.

[158] Miller K, Chinzei K, Orssengo G, Bednarz P. Mechanical properties of brain tissue in-vivo: experiment and computer simulation. Journal of Biomechanics. 2000 Nov;33(11):1369-76. Available from: http://www.sciencedirect.com/science/article/pii/S0021929000001202.

[159] Hirakawa K, Hashizume K, Hayashi T. [Viscoelastic property of human brain -for the analysis of impact injury (author's transl)]. No to Shinkei = Brain and Nerve. 1981 Oct;33(10):1057-65.

[160] Bertassoni LE, Cecconi M, Manoharan V, Nikkhah M, Hjortnaes J, Cristino AL, et al. Hydrogel bioprinted microchannel networks for vascularization of tissue engineering constructs. Lab on a Chip. 2014 Jun;14(13):2202-11. Available from: https://pubs.rsc.org/en/content/articlelanding/2014/lc/c4lc00030g.

[161] Meijering E. Neuron tracing in perspective. Cytometry Part A. 2010;77A(7):693-704. Available from: https://onlinelibrary.wiley.com/doi/abs/10.1002/cyto.a.20895.

[162] Ascoli GA. Neuroinformatics Grand Challenges. Neuroinformatics. 2008 Mar;6(1):1-3. Available from: https://search.proquest.com/docview/236486300/citation/B5678628E1AB4706PQ/1.

[163] Radio NM, Mundy WR. Developmental neurotoxicity testing in vitro: Models for assessing chemical effects on neurite outgrowth. NeuroToxicology. 2008 May;29(3):361-76. Available from: http://www.sciencedirect.com/science/article/pii/S0161813X08000223.

[164] Odawara A, Katoh H, Matsuda N, Suzuki I. Physiological maturation and drug responses of human induced pluripotent stem cell-derived cortical neuronal networks in long-term culture. Scientific Reports. 2016 May;6:26181. Available from: https://www.nature.com/articles/srep26181.

[165] Winans AM, Collins SR, Meyer T. Waves of actin and microtubule polymerization drive microtubule-based transport and neurite growth before single axon formation. eLife. 2016 Feb;5:e12387. Available from: https://doi.org/10.7554/eLife.12387.

[166] Muncie JM, Weaver VM. Chapter One - The Physical and Biochemical Properties of the Extracellular Matrix Regulate Cell Fate. In: Litscher ES, Wassarman PM, editors. Current Topics in Developmental Biology. vol. 130 of Extracellular Matrix and Egg Coats. Academic Press; 2018. p. 1-37. Available from: https://www.sciencedirect.com/science/article/pii/S0070215318300346.

[167] Keung AJ, de Juan-Pardo EM, Schaffer DV, Kumar S. Rho GTPases Mediate the Mechanosensitive Lineage Commitment of Neural Stem Cells. Stem Cells. 2011 Nov;29(11):1886-97. Available from: https://doi.org/10.1002/stem.746.

[168] Keung AJ, Dong M, Schaffer DV, Kumar S. Pan-neuronal maturation but not neuronal subtype differentiation of adult neural stem cells is mechanosensitive. Scientific Reports. 2013 May;3(1):1817. Number: 1 Publisher: Nature Publishing Group. Available from: http://www.nature.com/articles/srep01817.

[169] Hedegaard A, Monzón-Sandoval J, Newey SE, Whiteley ES, Webber C, Akerman CJ. Pro-maturational Effects of Human iPSC-Derived Cortical Astrocytes upon iPSC-Derived Cortical Neurons. Stem Cell Reports. 2020 Jul;15(1):38-51. Available from: https://www.sciencedirect.com/science/article/pii/S2213671120301545.

[170] Boni R, Ali A, Shavandi A, Clarkson AN. Current and novel polymeric biomaterials for neural tissue engineering. Journal of Biomedical Science. 2018 Dec;25(1):90. Available from: https://doi.org/10.1186/s12929-018-0491-8.

[171] Chaudhuri O, Koshy ST, Branco da Cunha C, Shin JW, Verbeke CS, Allison KH, et al. Extracellular matrix stiffness and composition jointly regulate the induction of malignant phenotypes in mammary epithelium. Nature Materials. 2014 Oct;13(10):970-8. Number: 10 Publisher: Nature Publishing Group. Available from: http://www.nature.com/articles/nmat4009.

[172] Soofi SS, Last JA, Liliensiek SJ, Nealey PF, Murphy CJ. The elastic modulus of Matrigel™ as determined by atomic force microscopy. Journal of Structural Biology. 2009 Sep;167(3):216-9. Available from: https://www.sciencedirect.com/science/article/pii/S1047847709001385.

[173] Du Bl, Zeng Cg, Zhang W, Quan Dp, Ling Ea, Zeng Ys. A comparative study of gelatin sponge scaffolds and PLGA scaffolds transplanted to completely transected spinal cord of rat. Journal of Biomedical Materials Research Part A. 2014;102(6):1715-25. Available from: https://onlinelibrary.wiley.com/doi/abs/10.1002/jbm.a.34835.

[174] Li G, Che MT, Zhang K, Qin LN, Zhang YT, Chen RQ, et al. Graft of the NT-3 persistent delivery gelatin sponge scaffold promotes axon regeneration, attenuates inflammation, and induces cell migration in rat and canine with spinal cord injury. Biomaterials. 2016 Mar;83:233-48. Available from: http://www.sciencedirect.com/science/article/pii/S0142961215009692.

[175] Liu S, Sun X, Wang T, Chen S, Zeng Cg, Xie G, et al. Nano-fibrous and ladder-like multichannel nerve conduits: Degradation and modification by gelatin. Materials Science and Engineering: C. 2018 Feb;83:130-42. Available from: http://www.sciencedirect.com/science/article/pii/S0928493117328709.

[176] Patel R, Santhosh M, Dash JK, Karpoormath R, Jha A, Kwak J, et al. Ile-Lys-Val-ala-Val (IKVAV) peptide for neuronal tissue engineering. Polymers for Advanced Technologies. 2019;30(1):4-12. _eprint: https://onlinelibrary.wiley.com/doi/pdf/10.1002/pat.4442. Available from: http://onlinelibrary.wiley.com/doi/abs/10.1002/pat.4442.

[177] Even-Ram S, Artym V, Yamada KM. Matrix Control of Stem Cell Fate. Cell. 2006 Aug;126(4):645-7. Publisher: Elsevier. Available from: http://www.cell.com/cell/abstract/S0092-8674(06)01029-4.

[178] Paulson AF, Prasad MS, Thuringer AH, Manzerra P. Regulation of cadherin expression in nervous system development. Cell Adhesion & Migration. 2014 Jan;8(1):19-28. Available from: https://www.ncbi.nlm.nih.gov/pmc/articles/PMC3974789/.

[179] Zhang J, Woodhead GJ, Swaminathan SK, Noles SR, McQuinn ER, Pisarek AJ, et al. Cortical Neural Precursors Inhibit Their Own Differentiation via N-Cadherin Maintenance of β-Catenin Signaling. Developmental Cell. 2010 Mar;18(3):472-9. Available from: http://www.sciencedirect.com/science/article/pii/S1534580710000948.

[180] Zhu M, Wang Y, Ferracci G, Zheng J, Cho NJ, Lee BH. Gelatin methacryloyl and its hydrogels with an exceptional degree of controllability and batch-to-batch consistency. Scientific Reports. 2019 May;9:6863. Available from: https://www.ncbi.nlm.nih.gov/pmc/articles/PMC6499775/.

[181] Ayala R, Shu T, Tsai LH. Trekking across the Brain: The Journey of Neuronal Migration. Cell. 2007 Jan;128(1):29-43. Available from: http://www.sciencedirect.com/science/article/pii/S0092867406016485.

[182] Subramanian L, Calcagnotto ME, Paredes MF. Cortical Malformations: Lessons in Human Brain Development. Frontiers in Cellular Neuroscience. 2020;13. Available from: https://www.frontiersin.org/article/10.3389/fncel.2019.00576.

[183] Budday S, Steinmann PI, Kuhl E. Physical biology of human brain development. Frontiers in Cellular Neuroscience. 2015;9. Publisher: Frontiers. Available from: http://www.frontiersin.org/articles/10.3389/fncel.2015.00257/full.

[184] Amin S, Borrell V. The Extracellular Matrix in the Evolution of Cortical Development and Folding. Frontiers in Cell and Developmental Biology. 2020;0. Publisher: Frontiers. Available from: http://internal.journal.frontiersin.org/articles/10.3389/fcell.2020.604448/full.

[185] Chen ZL, Haegeli V, Yu H, Strickland S. Cortical deficiency of laminin γ1 impairs the AKT/GSK-3β signaling pathway and leads to defects in neurite outgrowth and neuronal migration. Developmental Biology. 2009 Mar;327(1):158-68. Available from: https://www.sciencedirect.com/science/article/pii/S0012160608014164.

[186] Bar I, Lambert de Rouvroit C, Goffinet AM. The evolution of cortical development. An hypothesis based on the role of the Reelin signaling pathway. Trends in Neurosciences. 2000 Dec;23(12):633-8. Available from: https://www.sciencedirect.com/science/article/pii/S0166223600016751.

[187] Veeraval L, O'Leary CJ, Cooper HM. Adherens Junctions: Guardians of Cortical Development. Frontiers in Cell and Developmental Biology. 2020;8. Available from: https://www.frontiersin.org/article/10.3389/fcell.2020.00006.

[188] Ferent J, Zaidi D, Francis F. Extracellular Control of Radial Glia Proliferation and Scaffolding During Cortical Development and Pathology. Frontiers in Cell and Developmental Biology. 2020;0. Publisher: Frontiers. Available from: http://internal.journal.frontiersin.org/articles/10.3389/fcell.2020.578341/full.

[189] Iefremova V, Manikakis G, Krefft O, Jabali A, Weynans K, Wilkens R, et al. An Organoid-Based Model of Cortical Development Identifies Non-Cell-Autonomous Defects in Wnt Signaling Contributing to Miller-Dieker Syndrome. Cell Reports. 2017 Apr;19(1):50-9. Available from: http://www.sciencedirect.com/science/article/pii/S2211124717303935.

[190] Qian X, Jacob F, Song MM, Nguyen HN, Song H, Ming Gl. Generation of human brain region–specific organoids using a miniaturized spinning bioreactor. Nature Protocols. 2018 Mar;13(3):565-80. Available from: https://www.nature.com/articles/nprot.2017.152.

[191] Renner M, Lancaster MA, Bian S, Choi H, Ku T, Peer A, et al. Self-organized developmental patterning and differentiation in cerebral organoids. The EMBO Journal. 2017 May;36(10):1316-29. Available from: https://www.embopress.org/doi/full/10.15252/embj.201694700.

[192] Romero-Morales AI, O'Grady BJ, Balotin KM, Bellan LM, Lippmann ES, Gama V. Spin: an updated miniaturized spinning bioreactor design for the generation of human cerebral organoids from pluripotent stem cells. HardwareX. 2019 Oct;6:e00084. Available from: http://www.sciencedirect.com/science/article/pii/S2468067219300422.

[193] Kadry H, Noorani B, Cucullo L. A blood–brain barrier overview on structure, function, impairment, and biomarkers of integrity. Fluids and Barriers of the CNS. 2020 Dec;17(1):1-24. Number: 1 Publisher: BioMed Central. Available from: http://fluidsbarrierscns.biomedcentral.com/articles/10.1186/s12987-020-00230-3.

[194] Zenaro E, Piacentino G, Constantin G. The blood-brain barrier in Alzheimer's disease. Neurobiology of Disease. 2017 Nov;107:41-56. Available from: https://www.sciencedirect.com/science/article/pii/S0969996116301656.

[195] Ettle B, Schlachetzki JCM, Winkler J. Oligodendroglia and Myelin in Neurodegenerative Diseases: More Than Just Bystanders? Molecular Neurobiology. 2016;53(5):3046-62. Available from: https://www.ncbi.nlm.nih.gov/pmc/articles/PMC4902834/.

[196] Liddelow SA, Barres BA. Reactive Astrocytes: Production, Function, and Therapeutic Potential. Immunity. 2017 Jun;46(6):957-67. Available from: http://www.sciencedirect.com/science/article/pii/S1074761317302340.

[197] Palop JJ, Chin J, Mucke L. A network dysfunction perspective on neurodegenerative diseases. Nature. 2006 Oct;443(7113):768-73. Number: 7113 Publisher: Nature Publishing Group. Available from: http://www.nature.com/articles/nature05289.

[198] Seeley WW, Crawford RK, Zhou J, Miller BL, Greicius MD. Neurodegenerative Diseases Target Large-Scale Human Brain Networks. Neuron. 2009 Apr;62(1):42-52. Available from: https://www.sciencedirect.com/science/article/pii/S0896627309002499.

[199] Braak H, Del Tredici K. Spreading of Tau Pathology in Sporadic Alzheimer's Disease Along Cortico-cortical Top-Down Connections. Cerebral Cortex. 2018 Sep;28(9):3372-84. Publisher: Oxford Academic. Available from: http://academic.oup.com/cercor/article/28/9/3372/5047159.

[200] Braak H, Braak E. Neuropathological stageing of Alzheimer-related changes. Acta Neuropathologica. 1991 Sep;82(4):239-59. Available from: https://doi.org/10.1007/BF00308809.

[201] Visanji NP, Brooks PL, Hazrati LN, Lang AE. The prion hypothesis in Parkinson's disease: Braak to the future. Acta Neuropathologica Communications. 2013 May;1:2. Available from: https://www.ncbi.nlm.nih.gov/pmc/articles/PMC3776210/.

[202] Faal T, Phan DTT, Davtyan H, Scarfone VM, Varady E, Blurton-Jones M, et al. Induction of Mesoderm and Neural Crest-Derived Pericytes from Human Pluripotent Stem Cells to Study Blood-Brain Barrier Interactions. Stem Cell Reports. 2019 Mar;12(3):451-60. Available from: https://www.sciencedirect.com/science/article/pii/S2213671119300062.

[203] Cheung C, Bernardo AS, Pedersen RA, Sinha S. Directed differentiation of embryonic origin–specific vascular smooth muscle subtypes from human pluripotent stem cells. Nature Protocols. 2014 Apr;9(4):929-38. Number: 4 Publisher: Nature Publishing Group. Available from: https://www.nature.com/articles/nprot.2014.059.

[204] Lee VK, Kim DY, Ngo H, Lee Y, Seo L, Yoo SS, et al. Creating Perfused Functional Vascular Channels Using 3D Bio-Printing Technology. Biomaterials. 2014 Sep;35(28):8092-102. Available from: https://www.ncbi.nlm.nih.gov/pmc/articles/PMC4112057/.

[205] O'Grady BJ, Wang JX, Faley SL, Balikov DA, Lippmann ES, Bellan LM. A Customizable, Low-Cost Perfusion System for Sustaining Tissue Constructs. SLAS Technology. 2018 Dec;23(6):592-8. Available from: https://www.sciencedirect.com/science/article/pii/S2472630322012766.

[206] Lee JB, Wang X, Faley S, Baer B, Balikov DA, Sung HJ, et al. Development of 3D Microvascular Networks Within Gelatin Hydrogels Using Thermoresponsive Sacrificial Microfibers. Advanced Healthcare Materials. 2016;5(7):781-5. _eprint: https://onlinelibrary.wiley.com/doi/pdf/10.1002/adhm.201500792. Available from: http://onlinelibrary.wiley.com/doi/abs/10.1002/adhm.201500792.

[207] D'Amico RW, Faley S, Shim Hn, Prosser JR, Agrawal V, Bellan LM, et al. Pulmonary Vascular Platform Models the Effects of Flow and Pressure on Endothelial Dysfunction in BMPR2 Associated Pulmonary Arterial Hypertension. International Journal of Molecular Sciences. 2018 Sep;19(9):2561. Number: 9 Publisher: Multidisciplinary Digital Publishing Institute. Available from: http://www.mdpi.com/1422-0067/19/9/2561.

[208] Mori N, Akagi Y, Imai Y, Takayama Y, Kida YS. Fabrication of Perfusable Vascular Channels and Capillaries in 3D Liver-like Tissue. Scientific Reports. 2020 Apr;10(1):5646. Number: 1 Publisher: Nature Publishing Group. Available from: https://www.nature.com/articles/s41598-020-62286-3.

[209] Campisi M, Shin Y, Osaki T, Hajal C, Chiono V, Kamm RD. 3D self-organized microvascular model of the human blood-brain barrier with endothelial cells, pericytes and astrocytes. Biomaterials. 2018 Oct;180:117-29. Available from: https://www.sciencedirect.com/science/article/pii/S0142961218304915.

[210] Faley SL, Neal EH, Wang JX, Bosworth AM, Weber CM, Balotin KM, et al. iPSC-Derived Brain Endothelium Exhibits Stable, Long-Term Barrier Function in Perfused Hydrogel Scaffolds. Stem Cell Reports. 2019 Mar;12(3):474-87. Available from: https://www.sciencedirect.com/science/article/pii/S2213671119300116.

[211] Struzyna LA, Browne KD, Brodnik ZD, Burrell JC, Harris JP, Chen HI, et al. Tissue engineered nigrostriatal pathway for treatment of Parkinson's disease. Journal of tissue engineering and regenerative medicine. 2018 Jul;12(7):1702-16. Available from: https://www.ncbi.nlm.nih.gov/pmc/articles/PMC6416379/.

[212] Liddelow SA, Guttenplan KA, Clarke LE, Bennett FC, Bohlen CJ, Schirmer L, et al. Neurotoxic reactive astrocytes are induced by activated microglia. Nature. 2017 Jan;541(7638):481-7. Number: 7638 Publisher: Nature Publishing Group. Available from: http://www.nature.com/articles/nature21029.

[213] Torsten M, Aaron L. Microbial Transglutaminase Is Immunogenic and Potentially Pathogenic in Pediatric Celiac Disease. Frontiers in Pediatrics. 2018 Dec;6. Available from: https://www.ncbi.nlm.nih.gov/pmc/articles/PMC6297833/.

[214] Chan SK, Lim TS. Bioengineering of microbial transglutaminase for biomedical applications. Applied Microbiology and Biotechnology. 2019 Apr;103(7):2973-84. Available from: https://doi.org/10.1007/s00253-019-09669-3.

[215] Hartley DM, Zhao C, Speier AC, Woodard GA, Li S, Li Z, et al. Transglutaminase Induces Protofibril-like Amyloid β-Protein Assemblies That Are Protease-resistant and Inhibit Long-term Potentiation. Journal of Biological Chemistry. 2008 Jun;283(24):16790-800. Available from: http://www.jbc.org/content/283/24/16790.

[216] Dudek SM, Johnson GVW. Transglutaminase facilitates the formation of polymers of the β-amyloid peptide. Brain Research. 1994 Jul;651(1):129-33. Available from: http://www.sciencedirect.com/science/article/pii/0006899394906882.

[217] Sproul AA, Jacob S, Pre D, Kim SH, Nestor MW, Navarro-Sobrino M, et al. Characterization and Molecular Profiling of PSEN1 Familial Alzheimer's Disease iPSC-Derived Neural Progenitors. PLoS ONE. 2014 Jan;9(1). Available from: https://www.ncbi.nlm.nih.gov/pmc/articles/PMC3885572/.

[218] Raja WK, Mungenast AE, Lin YT, Ko T, Abdurrob F, Seo J, et al. Self-Organizing 3D Human Neural Tissue Derived from Induced Pluripotent Stem Cells Recapitulate Alzheimer's Disease Phenotypes. PLOS ONE. 2016 Sep;11(9):e0161969. Publisher: Public Library of Science. Available from: https://journals.plos.org/plosone/article?id=10.1371/journal.pone.0161969.

[219] Bilousova T, Miller CA, Poon WW, Vinters HV, Corrada M, Kawas C, et al. Synaptic Amyloid-β Oligomers Precede p-Tau and Differentiate High Pathology Control Cases. The American Journal of Pathology. 2016 Jan;186(1):185-98. Available from: http://www.sciencedirect.com/science/article/pii/S0002944015005805.

[220] Kuperstein I, Broersen K, Benilova I, Rozenski J, Jonckheere W, Debulpaep M, et al. Neurotoxicity of Alzheimer's disease Aβ peptides is induced by small changes in the Aβ42 to Aβ40 ratio. The EMBO Journal. 2010 Oct;29(19):3408-20. Available from: https://www.embopress.org/doi/full/10.1038/emboj.2010.211.

[221] Stine WB, Jungbauer L, Yu C, LaDu MJ. Preparing Synthetic Aβ in Different Aggregation States. In: Roberson ED, editor. Alzheimer's Disease and Frontotemporal Dementia: Methods and Protocols. Methods in Molecular Biology. Totowa, NJ: Humana Press; 2011. p. 13-32. Available from: https://doi.org/10.1007/978-1-60761-744-0_2.

[222] Therriault J, Benedet AL, Pascoal TA, Mathotaarachchi S, Savard M, Chamoun M, et al. APOEε4 potentiates the relationship between amyloid-β and tau pathologies. Molecular Psychiatry. 2020 Mar:1-12. Publisher: Nature Publishing Group. Available from: https://www.nature.com/articles/s41380-020-0688-6.